MODULATING LOCAL IMMUNE ENVIRONMENT TO DETER TUBERCULOSIS PROGRESSION

A Dissertation

Presented to the Faculty of the Graduate School

of Cornell University

In Partial Fulfillment of the Requirements for the Degree of

Doctor of Philosophy

by

Yitian Xu

May 2018

MODULATING LOCAL IMMUNE ENVIRONMENT TO DETER TUBERCULOSIS PROGRESION

Yitian Xu, Ph. D.

Cornell University 2018

Mycobacterium tuberculosis (Mtb) remains a grave threat to world health with emerging drug resistant strains. One prominent feature of Mtb infection is the extensive reprogramming of host environment at the site of infection. In this dissertation, we have taken two different approaches to target immune environment, with the hope to perturb Mtb infection. First, we report that inhibition of matrix metalloproteinases (MMPs) enhances the *in vivo* potency of the frontline TB drugs isoniazid and rifampicin. MMPs expression is markedly upregulated in human tuberculosis (TB) granulomas and murine infection models. Inhibition of MMP activity leads to an increase in pericyte-covered blood vessel numbers and appears to stabilize the integrity of the infected lung tissue. In treated mice, we observe an increased delivery and/or retention of Evans Blue dye and frontline TB drugs in the infected lungs, resulting in enhanced drug efficacy. These findings indicate that targeting Mtb-induced host tissue remodeling can increase therapeutic efficacy and could enhance the effectiveness of current drug regimens. Second, we show that synthetic mRNA encoding CCL2 or CCL3 are able to recruit certain populations of monocyte in a non-inflammatory manner. These recruited monocytes stay in a neutral, non-programmed state, exhibiting neither bactericidal nor tissue-repairing phenotypes. Additional *Ifn-γ* mRNA or *Il-4* mRNA can polarize these cells to different phenotypes. Furthermore, the monocytes recruited by *Ccl3* and *Ifn-γ* mRNA were able to launch

the most rapid and strongest superoxide burst compared to other mRNA combinations. These findings demonstrate a synthetic mRNA based immune-modulation scheme that allows recruitment and modification of specific immune cell populations *in vivo*, which can impact tuberculosis progression.

BIOGRAPHICAL SKETCH

Yitian Xu obtained his bachelor degree in Biological Science from Sun Yet-sen University in 2012 and Master of Engineering from Cornell University in 2013. He then joined the Ph.D. program of Cornell University and became a member of Dr. Shen's lab. His research projects were collaborated with and conducted in Dr. David Russell's lab. As co-chairs of Yitian's committee, Dr. Shen and Dr. Russell supervised Yitian's dissertation research.

To my families, Jianfa Xu and Shaohui Chen, Weidan Xu,

and my girlfriend, Danmeng Huang

ACKNOWLEDGMENTS

I would like to thank my advisors, Dr. Xiling Shen and Dr. David G. Russell, for his guidance and support through my Ph. D. They taught me how to be a good scientist and pave the way of my future career. I would like to thank my committee member, Dr. Paul Soloway, for his helpful discussion and guidance on my thesis studies. Dr. Soloway instructed me in several classes and stimulated my interest in life science. I would like to thank Dr. Lu Huang, Dr. Shumin Tan, Dr. Saikat Boliar, Dr. Davide Pisu and Dr. Brian Vanderven for technical guidance and critical discussion, and everyone else in the Shen lab and Russell lab for generous help.

I would like to thank my families, Jianfa Xu, Shaohui Chen and Weidan Xu, for their unlimited support to pursuing my Ph. D abroad. I would like to thank my girlfriend, Danmeng Huang, for her heartwarming encouragement when I am frustrated and her unconditional support when I am over-occupied.

I am truly grateful to everyone who helped me in this journey!

TABLE OF CONTENTS

LIST OF FIGURES

LIST OF TABLES

LIST OF ABBREVIATIONS

α-SMA	Alpha smooth muscle actin
ATG5	Autophagy protein 5
BCG	Bacillus camette-guerin
BMDM	Bone marrow-derived macrophage
CDC	Center of Disease Control
DC	Dendritic cell
ECM	Extracellular matrix
EF5	2-nitroimidazole structure
ESAT-6	Secreted antigenic target-6
GFP	Green fluorescent protein
HFBA	Heptafluorobutyric acid
HIV	Human immunodeficiency virus
HPLC	High-pressure liquid chromatography
IFN-γ	Interferon gamma
INH	Isoniazid
LAMP	Lysosome-associated membrane proteins
LC-MS/MS	Liquid chromatography coupled to tandem mass spectrometry
LDL	Low density lipoprotein
LPLA2	Lysosomal phospholipase A2
LPM	Large peritoneal macrophages
MBL	Mannose-binding lectin
MFI	Mean fluorescence index
MDR	Macrophage disappearance reaction
MDR-TB	Multidrug-resistant TB
MGC	Multinucleated giant cell

MMP	Matrix metalloproteinase
Mtb	*Mycobacterium tuberculosis*
NET	Neutrophil extracellular traps
NK cell	Natural killer cells
NO	Nitric oxide
NOS2	Nitric oxide synthase 2
NOX2	NADPH oxidase 2
NP	Nanoparticle
PDIM	Phthiocerol dimycocerosate
PIMO	Pimonidazole hydrochloride
PRR	Pattern recognition receptor
RIF	Rifampicin
RNS	Reactive nitrogen species
ROS	Reactive oxygen species
SPM	Small peritoneal macrophage
TAG	Triacylglycerol
TB	Tuberculosis
TDM	Trehalose dimycolate
TNF-α	Tumor necrotic factor alpha
vATPase	Vesicular atpase
VEGF	Vascular epithelial growth factor
WHO	World health organization
XDR-TB	Extensively drug-resistant TB

CHAPTER ONE

Introduction

1.1 Tuberculosis, the disease

Tuberculosis (TB) continues to present as a grave threat to the global health. According to the 2016 global tuberculosis report from World Health Organization (WHO), more than 10 million people were newly infected in 2015, and one third of the global population have latent TB [1, 2]. More than 60% of these new cases happened in Asia and more than a quarter in Africa. New cases in 30 high TB burden countries consisted of 87% of total new cases. 60% of new cases occurred in six countries (in order of highest to lowest): India, Indonesia, China, Nigeria, Pakistan, and South Africa [1]. Moreover, 1.8 million people died due to the disease in 2015, making TB one of the top 10 causes of death worldwide [2]. Among these death, 0.4 million people were patients co-infected with human immunodeficiency virus (HIV), which accounted for 35% of all HIV deaths, making TB a leading killer of HIV patients. More than one third of HIV patients were ill from TB in 2015, with 1.2 million new cases of co-infection of TB and HIV in 2015 [1]. On the other hand, the problem of drug resistance has become more and more challenging, with about half-a-million people developing multidrug-resistant TB (MDR-TB) and unresponsive to the two most powerful frontline TB drugs, isoniazid (INH) and rifampicin (RIF) [1-3]. Although second-line TB drugs are available for treating MDR-TB, extensive chemotherapy is required and these costly chemo-drugs have serious side effects [1-3]. Unfortunately, some of these patients will continue to develop a more severe type of drug resistance, called extensively drug-resistant TB (XDR-TB), which doesn't

respond to most second-line TB drugs [1-3]. Only 52% of MDR-TB and 28% of XDR-TB patients were successfully treated.

To cope with this TB epidemics, the "End TB strategy" was proposed in 2014 to set a new serial of goals between from 2016-2035 [1]. The ultimate goal is to reduce the new TB cases to around 10 cases per 100,000 people every year. The two main indicators of achieving "End TB strategy" are a 95% reduction of deaths caused by TB and a 90% reduction of TB incidence rate in 2035, compared to those in 2015 [1]. A milestone is set for 2020 to achieve a 35% reduction in deaths caused by TB and a 20% reduction rate in TB incidence rate, compared to those in 2015 [1]. However, the average percentage of reduction for TB incident rate between 2000 to 2015 is about 1.5%, which needs to be improved to a 4%-5% reduction percentage, in order to fulfill the 2020 milestone [1].

Tuberculosis is caused by the infection of *Mycobacterium tuberculosis* (Mtb) bacillus. *M. tuberculosis* is a rod-shaped bacterium and was first identified by Robert Koch in 1882 [4]. It requires high level of oxygen to grow with a replication time of 16-24 hours *in vitro*, and much more time *in vivo* during chronic infection [5]. *M. tuberculosis* has a complex, waxy outer membrane mainly consisting of a unique long chain fatty acid called mycolic acid, which prevents the Gram staining since the dye cannot penetrate this hydrophobic coating [6]. Therefore, *M. tuberculosis* is classified as neither a Gram-positive or Gram-negative bacterium. However, the mycolic acid is subjected to acid-fast staining such as Ziehl-Neelsen staining, which will stain the

bacteria to bright red and is used for diagnosis with patients' sputum samples [7]. Similarly, this lipid coating of *M. tuberculosis* prevents penetration of a variety of antibiotics, hindering the development of new anti-TB drugs. Around 8% of *M. tuberculosis*'s genome is dedicated to fatty acid metabolism, indicating the importance of lipid metabolism to Mtb's survival during evolution [8]. Many anti-TB drugs target the biosynthesis pathways of these lipids to achieve bactericidal effect, exampled by one of the most effective frontline TB drug, isoniazid (INH). It targets the synthesis of mycolic acid, therefore inhibiting the cell wall synthesis. Furthermore, these lipids on Mtb's outer membrane can act as virulent factors to induce granulomatous response in the host. During Mtb infection, the bacteria are able to release mycobacterial lipids, such as phosphatidylinositol dimannosides, cardiolipin, phosphatidylglycerol, phosphatidylethanolamine, trehalose monomycolate, trehalose dimycolate, and mycoside B to surrounding environment and uninfected neighboring cells [9-11]. Among these lipids, trehalose dimycolate (TDM) is able to induce IL-1β, IL-6, and TNF-α within macrophage *in vitro* [11]. We previously demonstrated that TDM coated polystyrene beads mixed within a gel matrix, matrigel, injected into mice can induce a granulomatous response exampled by recruitment of leukocytes to the beads and secretion of inflammatory cytokines [12-14].

M. tuberculosis belongs to the order of *Actinomycetales*, which is usually closely related to Gram-positive bacteria such as *Staphylococci* and *Streptococci*. Recent evident suggested that Mtb is more close to Gram-negative bacteria according to their shared conserved genes. It is believed that the common ancestor of *M. tuberculosis*

complex, including *M. tuberculosis*, *M. africanum*, *M. bovis*, *M. canetii* and *M. microti*, evolved in East Africa about 40,000 years ago [15]. Since this common ancestor of *M. tuberculosis* complex infected ancestry human, this organism has not only evolved to become a well-adapted human pathogen under survival pressure, but also shaped the evolution of human species. Evident suggested that human species was under selection pressure of *M. tuberculosis* infection long before human migrated out of Africa [15]. Collectively, human and *M. tuberculosis* have co-evolved, migrating and expanding together in the world.

When exposed to *M. tuberculosis*, 5-10% people develop active disease, while the remaining 90-95% develop latent disease [16]. Although the majority don't develop active disease, they remain a vast reservoir for bacteria that can be reactivated. About 5% of the latent-infected people will develop active disease, while the risk will boost significantly to around 13% of reactivation when the patients' immune system is comprised due to aging, HIV infection, or immune-suppressive drugs taken after organ transplant [16]. The active tuberculosis disease is characterized by symptoms including persistent coughing for more than 3 months, chest pain, blood or sputum from coughing, loss of appetite and weight, night sweat, fatigue, recurring fever. Latent disease may not show any symptom [1, 2].

Nowadays, two most common methods are used to detect the presence of *M. tuberculosis* infection in people: TB skin test and TB blood test [1, 2]. The rationale behind a TB skin test is that if one has/had an active or latent tuberculosis disease, a

subcutaneously injection of *M. tuberculosis* antigens will trigger an immune response, revealed as a large bump at the site of injection. The bump is measured after 48-72 hours injection and an induration size over 15mm is considered positive for the skin test. Less than 5mm is considered negative while a bump between 5mm to 15mm can be positive depending on the patients' condition. A further diagnosis may be needed to confirm the result. However, people who have previously vaccinated with *M. bovis* Bacillus Camette-Guerin (BCG) may develop a false positive reaction to the TB antigens, making the TB skin test unreliable for these people. The other method, TB blood test is not affected by previous vaccination of BCG. The assay uses an ELISA to detect interferon gamma (IFN-γ) released from T cells stimulated by specific *M. tuberculosis* antigens (ESAT-6, CFP-10, and TB 7.7), which are not found in BCG or other common environmental mycobacteria. As a result, a positive detection of IFN-γ indicates the patient has been exposed to *M. tuberculosis*. However, both the TB skin test and blood test cannot differentiate between active and latent disease. Further in-depth diagnosis methods are required to determine the status of the disease including a posterior-anterior chest radiograph and an acid-fast staining on patients' sputum smear sample [7]. A chest X-ray exam can reveal area of shadow in the lung, which are lesions caused by *M. tuberculosis* infection. Acid-fast staining can identify *M. tuberculosis*'s presence in the sputum sample. A subsequent culture of original sputum sample will finally confirm the presence of *M. tuberculosis*. However, treatment of tuberculosis can begin before the positive culture of the sputum sample, if all the other indicators show a positive infection.

The current treatment regimen uses 4 frontline drugs, isoniazid, rifampin, ethambutol, pyrazinamide, which were first synthesized half a century ago [1, 2]. Treatment of tuberculosis recommended by Center of Disease Control (CDC) will start with a 2-month intensive phase, then followed by a 4-7 months continuation phase. It is not surprising that within this total of 6-9 months treatment, failure through patients not following the whole treatment, drugs not available in underdeveloped areas, and non-responsiveness can happen, and all these situations contribute to emergence of drug-resistant TB strains. Conventional treatment of MDR-TB can last for more than 18 months using a different combination of second-line TB drugs, including fluoroquinolone, ethionamide, cycloserine and para-aminosalicylic acid [1, 2]. However, some of these second-line TB drugs are highly toxic and responsible for severe adverse effects, which lead to restricted usage of these drugs. In 2016, WHO revised its guideline for MDR-TB treatment to an inexpensive and standardized regimen with shorter (9-12 months) treatment period, based on a few studies that showed promising results using this regimen for MDR-TB patients without resistance to any second-line TB drug [1]. Patients with XDR-TB or resistance to second-line TB drugs cannot use this regimen. However, this advancement significantly reduces the treatment duration and cost for MDR-TB patients.

1.2 Immune response to Mtb infection

1.2.1 Overview

The infection of *M. tuberculosis* can occur with as low as one single bacterium [15, 17]. Aerosol droplets containing the bacteria, coughed out by active TB patients, can

be inhaled by healthy individuals. The bacteria are usually phagocytosed by alveolar macrophages, the resident macrophage in the lung patrolling for pathogen invasion. Some studies indicated the bacteria can also be engulfed by alveolar epithelial pneumocytes or dendritic cells in the lung [18, 19]. The infected macrophage will migrate inwards to the interstitial space and initiate production of pro-inflammatory cytokines and chemokines, including tumor necrotic factor alpha (TNF-α), CCL2 and CXCL10, to recruit more innate immune cells to the infection site. Neutrophils are indicated as first responders in murine infection models, however, it is unclear that whether neutrophil is important in a natural infection with a much lower infection dose [15]. Monocytes are also recruited following the CCL2 signal, maturing into macrophages as they reach the infection site. More recent data suggested that local interstitial macrophage can also proliferate in the lung and migrate to the infection site [20]. These uninfected macrophages can phagocytose the apoptotic infected macrophages and release more TNF-α signal, amplifying the inflammation. Until this point, the bacteria can resist the killing of these innate cells and expand exponentially. During this time, dendritic cells are also recruited to the infected site and take up the bacteria. Infected dendritic cells then migrate to the neighboring lymph nodes and present the processed antigen to T cells, which results in differentiation and recruitment of T cells to the infection site. The presence of T cells at the infection site marks the beginning of the adaptive immune response phase. The production of IFN-γ by CD4 T cells will activate the macrophage to produce reactive oxygen and nitrogen species to kill the bacteria within. Moreover, the presence of IFN-γ can inhibit the production of TNF-α to dampen the inflammation, in order to prevent fatal pathology

by destructive inflammation. At this point, the tissue is greatly remodeled by these cells and this cell aggregate begins to form a granuloma structure.

The human TB granuloma consists a variety of immune cells with highly organized structure (Figure 1.1). The infected macrophages locate at the center of the granuloma, surrounded by a layer of uninfected macrophages including macrophage-derived giant cells, epithelioid cells and foamy macrophages [15, 17]. Outside of this macrophage layer is a layer rich of lymphocytes. The granuloma will develop a fibrotic cuff around the structure to further contain the bacteria. This contained structure can last for one's lifetime without developing an active disease, until his immune system is comprised. Compromise of immune system can result from aging, HIV infection or taking immune suppressive drugs after organ transplant. At this point, the granuloma structure can no longer contain the bacteria, and will rupture and release the bacteria into the airway. Patients who experience this re-activation process will release the bacteria into the atmosphere by coughing.

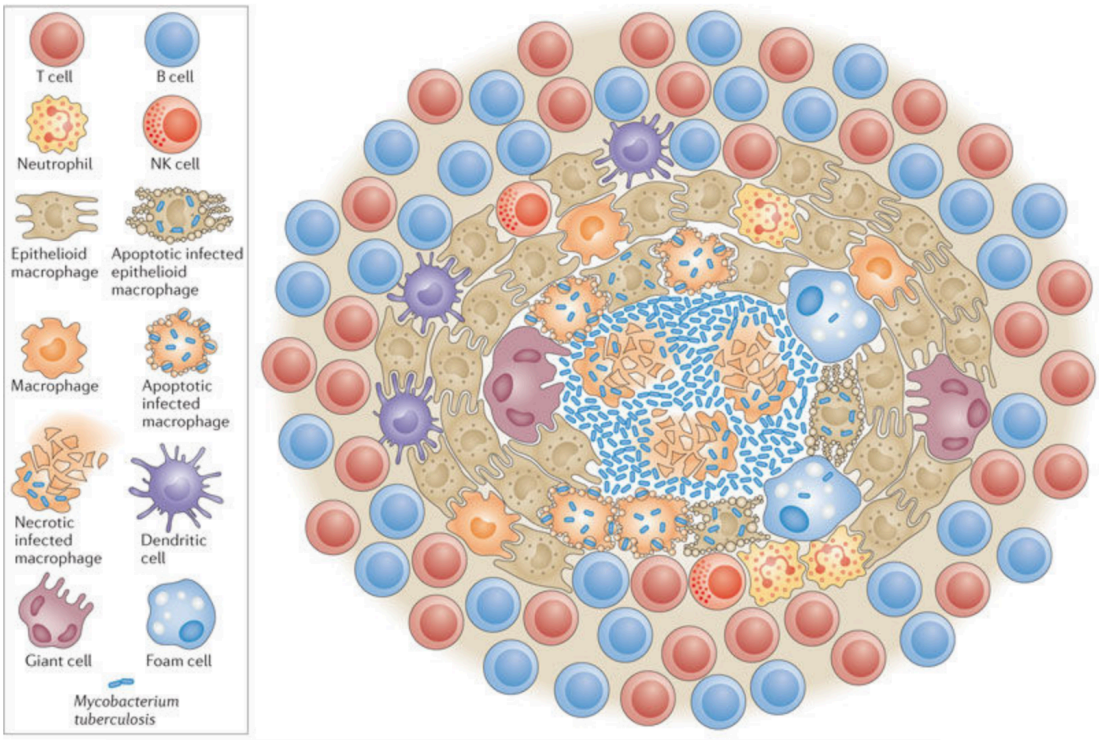

Figure 1.1 Different immune cells present in TB granuloma and their arrangement. Adapted from Ramakrishnan et al. [21].

1.2.2 Host immune response by Macrophage and Adaptation by *M. tuberculosis*

Macrophage is the primary host cell in which *M. tuberculosis* resides [15, 22, 23]. Although *M. tuberculosis* can infect all myeloid cells including neutrophils and dendritic cells, the majority of *M. tuberculosis* are within macrophages. It is therefore important to understand the interaction between macrophage and *M. tuberculosis*.

Upon encounter, various surface lipids of *M. tuberculosis* can be recognized by pattern recognition receptors (PRRs) of macrophage, which will initiate phagocytosis [23]. This process can be enhanced by opsonization of the bacteria with molecules such as surfactants, mannose-binding lectin (MBL) and complement components. After phagocytosis, macrophage employs several methods trying to eliminate the bacteria including phagosome-lysosome fusion, production of reactive oxygen and nitrogen species (ROS and RNS), and starvation [24].

The bacteria are within vesicles called phagosomes after being phagocytosed [24]. Phagosome maturation through continuous fusion and fission with trans-Golgi transporter vesicles, endosomes, lysosomes, and autophagosomes, lowers the pH in the phagosomal lumen for optimal enzymatic activity of anti-bacterial hydrolases and peptides. The proton pumping vesicular ATPase (vATPase) is required for phagosomal acidification and present at low copy number in the early phagosome, which has a mildly acidic pH of 6 to 6.5 [25]. As the phagosome maturates, vATPase is assembled to facilitate phagosomal acidification. The late phagosomal stage fuses

with lysosomes, which are marked with lysosome-associated membrane proteins (LAMP1 and LAMP2) as well as newly synthesized lysosomal enzymes. Some of these enzymes target the bacteria membrane for degradation. For example, lysosomal phospholipase A2 (LPLA2) functions to degrade exogenous and endogenous membranes, including membrane of engulfed bacteria [26]. After fusion of phagosome and lysosome, the final product, the phagolysosome has a pH of 4 to 4.5, which is essential for high hydrolase activity and mycobacterial killing [15, 25]. The acidic environment in the phagolysosome limits mycobacterial metabolism, and eventually leads to growth arrest if carbon sources are not available [27].

However, *M. tuberculosis* has developed many methods to survive this hostile environment. Firstly, the bacteria can use their surface-associated phthiocerol dimycocerosate (PDIM) lipids to avoid recognition by phagocytes [24]. Secondly, mycobacterial cell wall lipids, including man-LAM or PIMs, can delay maturation of the early phagosome [28]. Similarly, beads coated with the mycobacterial cord factor TDM can delay phagosome maturation [13], which can be rescued by IFN-γ treatment [29]. Phagosome arrested by *M. tuberculosis* shares early phagosomal features including low vATPase expression and an almost neutral pH. Third, *M. tuberculosis* can inhibit phagosome-lysosome fusion by activating the calcium-dependent phosphatase calcineurin in the phagosome, which can be reversed by calcineurin-inhibitors cyclosporine or FK506 [30]. Lastly, *M. tuberculosis* virulent factors, including Rv3671c, can help the bacteria survive at pH of 4.5 [31, 32]. Even though the metabolism of *M. tuberculosis* is tremendously limited in phagolysosome, the

bacteria can still replicate slowly if specific carbon sources such as pyruvate, acetate, or cholesterol, are available [32].

After phagocytosis, the macrophage can release TNF-α and stimulate ROS production in mitochondria [15]. However, *M. tuberculosis* can resist DNA damage-dependent radicals stress and only die from overwhelming level of ROS [33, 34]. This resistance of ROS can be conferred by Mtb gene locus, *mel2*, which share similarity with bioluminescent genes in other organisms to resist ROS-induced DNA damage [33]. The *mel2* mutant is susceptible to H_2O_2 treatment in broth and has impaired growth in macrophage. Mice infected with the *mel2* mutant have a reduced bacterial burden and better pathology in the persistent stage. Another study used transposon mutant library to screen for genes that involve in ROS resistant in Mtb, and identified *mmpL9* and *moaD1* mutants are susceptible to H_2O_2 treatment and have growth defect in human macrophages [35]. Excessive TNF-α and ROS are suggested to contribute to necrosis of infected cells, which will release the bacteria to the extracellular environment and further facilitate their growth [36]. The bacteria experience an exponential growth until T cells are recruited to the infection site and secrete IFN-γ, which will fully activate the infected macrophage for killing. Upon activation, macrophage recruits NADPH oxidase 2 (NOX2) to the phagosomal membrane, to generate ROS inside the bacteria-containing phagosomes [37]. Reactive nitrogen species (RNS), on the other hand, are another kind of very effective Mtb-killing agent [24]. Nitric oxide (NO), produced by nitric oxide synthase 2 (NOS2) using arginine, will diffuse through the phagosomal membrane and react with ROS to generate different RNS, including

nitrogen dioxide, peroxynitrite, dinitrigen trioxide [37]. These RNS and ROS can damage bacterial DNA, membrane lipids, tyrosine and thiol residues through oxidation. People sharing mutations or polymorphisms in NOS2 or NOX2 have a defect on RNS or ROS production and are more susceptible to the disease [37, 38].

There are different subsets of macrophages in the lung. Macrophages occupying the alveolar space in the lung are alveolar macrophages, while macrophages located within the interstitial space (alveolar interstitium, the bronchiolar submucosa, and the vascular adventitia) are interstitial macrophages [39]. It is only recently that people have realized that these macrophages have different origins and behaviors upon inflammation or infection. Alveolar macrophages originate from precursors in yolk sac or fetal liver while interstitial macrophages derive from hematopoietic stem cells [39]. Recently published work from our lab showed that upon Mtb infection, the number of interstitial macrophages increased rapidly [20]. This increase of interstitial macrophages was due to local proliferation in addition to their differentiation from monocytes. Moreover, interstitial macrophages are able to generate reactive nitrogen species to damage engulfed bacteria, while alveolar macrophages were less active. This difference appear due, in part at least, to their different metabolic status: interstitial macrophages employ anaerobic respiration predominately, while alveolar macrophages use aerobic respiration [20].

During Mtb infection, macrophages can transform into different types of macrophage, including foamy macrophages and multinucleated giant cells (Figure 1.2), which are

present in the human granuloma [15, 17]. It is still debated whether the epithelioid cells, also present in human granuloma, are transformed from macrophages. *In vitro* studies showed co-culture of monocytes with platelets can drive transformation of monocytes into epithelioid cells [40]. However, epithelioid cells found in human granuloma were identified as more biosynthetic than phagocytic [41], which questions the origin of these epithelioid cells. Therefore, we will focus on discussing foamy macrophages and multinucleated giant cells.

Macrophages can transform into foamy macrophage loaded with lipid droplets. These lipid droplets are mostly cholesterol, cholesterol esters and triacylglycerol (TAG). The formation of foam cells is a result of imbalance between influx and efflux of low density lipoprotein (LDL) [17, 42]. This imbalance can be induced by Mtb cell wall lipid including TDM and oxidized mycolic acid [17, 43]. Within Mtb infected foamy macrophages, the bacteria were found closely located near the lipid droplets, suggesting that these lipid droplets may serve as a nutrient source for the bacteria [17, 43]. Moreover, these foamy macrophages were found surrounding the necrotic center of granuloma in TB patients, suggesting these foamy cells could contribute to tissue necrosis and caseum formation. Indeed, lipid components from human TB granuloma caseum were shown to be mostly cholesterol, cholesteryl ester and triacylglycerol (TAG), which is consistent with the lipids found in the foamy macrophages [17, 44]. This implies that the caseation might be formed by accumulation of lipid debris released from dead foamy macrophages.

Another distinct feature of human TB granuloma, is the presence of multinucleated giant cells (MGCs), which are formed by cell fusion of macrophages/monocytes [45]. These cells are morphologically conspicuous for their multiple nuclei arrangement. MGCs with central aggregated or randomly distributed nuclei are foreign body type MGCs, which are induced by consistent foreign body stimulation. MGCs with arcuate or semicircular nuclei locating at the periphery of the cytoplasm, are Langhans type MGCs, which are usually found in TB granuloma [46]. These Langhans type MGCs can be induced by poorly digestible pathogen factors or persistent pathogens such as mycobacteria [45, 46]. Avirulent mycobacteria, however, cannot stimulate MGC formation, possibly because of their lack of virulent cell wall components and secreted products [47]. Several studies showed cytokines such as IFN-γ induced MGC formation [48]. However, since MGCs are absent in Mtb infected mouse, there is no animal evidence for these *in vitro* studies, yet. MGCs' functions are also poorly understood. *In vitro* studies showed that MGCs from human granuloma secreted different cytokines including and IL-10, IFN-γ, TNF-α, TGF-β, and chemokines including CXCL10, CCL2, as well as matrix metalloproteinases-9 [48, 49]. Another study showed MGCs failed to phagocytose bacteria *in vitro*, but were able to present antigen [50].

1.2.3 Host immune response by neutrophils

Upon recognition of pathogen invasion by resident or patrolling immune cells, neutrophils are recruited to the infection site with the goal to rapidly phagocyte and eliminate the pathogen [24]. Unlike phagosome maturation in macrophage,

phagosome maturation in neutrophils occurs within seconds (vs minutes in macrophage), almost simultaneously with phagocytosis event [24]. During phagosome maturation in neutrophils, primary azurophilic and secondary specific granules fuse with the phagosome and facilitate pathogen killing. Secondary specific and tertiary gelatinase granules can fuse with the plasma membrane to release the granules content to extracellular environment. Neutrophils can also release their DNA extracellularly, forming neutrophil extracellular traps (NET), to restrain pathogens and further eliminate them.

However, neutrophil phagocytosis, neutrophil granules and NET are unable to control mycobacterial growth [51]. Indeed, many studies suggested that neutrophils failed to eliminate *M. tuberculosis in vitro* after rapid phagocytosis. Corleis et al. showed neutrophils released cytosolic component, DNA and free bacteria into extracellular environment after necrotic cell death within 10h after infection, which was induced by Mtb virulent factors encoded by RD1 [52]. Moreover, excessive ROS produced by neutrophils are released into the extracellular environment, causing tissue inflammation. Latent TB patients with mutations in the NADP oxidase gene had reduced ROS production, and did not develop necrotic neutrophil death.

In vivo, there are increasing evidence indicating that neutrophils contribute to TB granuloma necrosis. Mice infection with Mtb stains of increased virulence (Erdman strain vs H37Rv, H37Ra or ΔphoPR strains) was associated with increased neutrophils in the lung [53]. Mtb infected resistant mouse strains such as DO and C57BL/6 mice

had reduced neutrophil number and necrotic lesions compared to susceptible mouse strains [24]. Depletion of neutrophils led to reduced tissue pathology and mycobacterial burden, as well as improved survival in I/St but not C57BL/6 mice [54, 55]. $Atg5^{fl/fl\text{-}Lysm\text{-}cre}$ mice which lack autophagy protein 5 (ATG5) expression in all myeloid cells, harbored high number of neutrophils in the lung, leading to early animal death between day 30-40 post infection [56]. Depletion of neutrophils in these mice reduced bacterial burden and lung pathology, as well as improved survival [56]. Some earlier studies showed a protective role of neutrophils *in vivo*, by depleting neutrophils with anti-Gr-1 antibody, which also depleted other myeloid origin cells [57]. In active TB patients, neutrophil is the predominate immune cell population in the sputum and broncho-alveolar lavage fluid [58]. Moreover, these neutrophils contain most of the viable mycobacteria. Therefore, neutrophil's presence in the lung seem to be beneficial for TB progression.

1.2.4 Host immune response by dendritic cells

Dendritic cells (DCs) are proved to be vital to mediate adaptive immune response by antigen presentation. DCs are specialized antigen presenting cells that can activate naïve T cells. Upon infection by Mtb, immature DCs can take up the bacteria or bacteria-containing apoptotic bodies [59]. Then they migrate to the neighboring draining lymph nodes, while they are maturating. At the same time they are processing and presenting bacterial antigens on their surface MHC I, MHC II and CD1 molecules. Mature DCs will prime the naïve T cells, and stimulate T cell differentiation and expansion. These effector T cells will migrate back to the infection site to launch the

adaptive immune response and control bacterial growth. Depletion of DCs in mice leads to an excessive bacterial load in the lung, due to inefficient CD4 T cell response [59, 60]. Contradictory results have been reported regarding how Mtb infection alters DCs' functions, including cell migration, antigen processing and presentation [59]. Some studies showed Mtb infection increased DCs' MHC II presentation and ability to stimulate IFN-γ secretion from T cells [61, 62]. Other studies, on the other hand, showed Mtb induced IL-10 production, which inhibited DC maturation [63]. Moreover, infected DCs expressed lower level of surface integrin, which limited their migration to lymph nodes. *In vivo* studies showed impaired ability to present antigen and stimulate CD4 T cell in Mtb infected DCs [64].

1.2.5 Host immune response by lymphocytes

Adaptive immunity is crucial to limit bacterial growth and prevent reactivation, which can be demonstrated by the increased susceptibility to Mtb in HIV patients with reduced number of CD4 T cells. IFN-γ released from both CD4 and CD8 T cells can activate macrophage for more effective killing, as discussed previously. In addition to the ability to secrete IFN-γ, CD4 T cells have other important functions to control infection [22]. Depletion of CD4 T cells drove early death of infected animals with high level of bacterial burden, despite the similar levels of IFN-γ and NOS2 in infected animals with or without depletion [22, 65]. This implies that there is other important function of CD4 T cells in controlling infection besides producing IFN-γ. CD8 T cells, on the other hand, are also important in controlling infection due to their ability to produce IFN-γ and lyse infected cells/bacteria [22]. Depletion of CD4 T cells

didn't alter the level of IFN-γ, mainly due to CD8 T cells' compensatory production of IFN-γ. Most importantly, CD8 T cells can mediate direct lysis of infected cells to release intracellular bacteria, which will be further lysed by cytotoxic proteins including perforin and granulysin [66, 67]. Other possible mechanisms of controlling infection by lysing infected cells hypothesized that some infected cells such as foamy macrophages or MGCs, cannot be activated to eliminate the bacteria within. Lysing these cells to release the bacteria could allow the activated macrophages to destroy the bacteria more effectively [68].

B cells during Mtb infection were considered irrelevant until a decade ago, when studies found B cell deficiency led to increased number of pulmonary neutrophils and bacterial burden, as well as worsened pathology and survival rate [69]. Moreover, antibodies are able to recognize the bacteria, enhancing animal survival [70]. These suggest an important role of B cells in Mtb infection.

1.3 Important environmental factors during tuberculosis progression

1.3.1 Overview

The formation of granuloma is a distinct hallmark of human tuberculosis. A rich body of literature focuses on the cellular components in this particular structure, neglecting the roles of environmental factors in this process. Mtb taken-up by macrophages have to cope with the hostile environment of low pH [71]. The bacteria sense the pH level in the environment, which impacts their replication status. When the macrophages fail to eliminate the bacteria and the granuloma begins to form, uninfected immune cells

are recruited to the infected area and surround the infected cells, forming scattered cell aggregates [15]. Activated macrophages can secrete vascular epithelial growth factor (VEGF), induced by Mtb, to promote formation of new blood vessels [72, 73]. These newly-grown blood vessels can provide nutrient as well as uninfected host cells for the bacteria. During the formation of granuloma, the matrix of infected area is dramatically remodeled, to expand interstitial space for cell infiltration and provide the extracellular matrix scaffold for blood vessels. Expression of matrix metalloproteinases (MMPs) is up-regulated in infected macrophages and neighboring epithelial cells, induced by Mtb virulent factor ESAT-6 [74]. Fibrotic tissue is deposited at the edge of granuloma and eventually a fibrotic wall is generated around the periphery of the granuloma. If the disease progresses into later stage, blood vessels will start to shrink within the granuloma, limiting the oxygen supply at the center of granuloma. This hypoxic environment facilitates cell necrosis, which leads to further caseation. Finally, if the disease develops into the active transmission phase, the fibrotic wall of the granuloma cavitates to allow free bacteria to enter the airway, which is correlates with high level of MMP-9 protein detected in patient serum [15].

1.3.2 Angiogenesis during *M. tuberculosis* infection

During early granuloma formation, VEGF is induced by Mtb and secreted by activated macrophage, stimulating new blood vessel growth [15, 75]. Zebrafish infected *M. marinum* promoted angiogenesis during early granuloma formation around four days post infection, accompanied with VEGFA production by macrophages [76]. Elevated level of VEGF was also found in the sera from active pulmonary TB patients,

compared to inactive TB patients or healthy individuals [73, 77]. New blood vessels are able to penetrate the cell aggregates to provide nutrient and oxygen. As the fibrotic wall is built around the granuloma, the blood vessels within the granuloma begin to shrink, leaving the core of the granuloma with reducing nutrient and oxygen supply. Histological analysis of human granuloma showed that significantly reduced vasculature in active cavitary lesions, compared to non-progressive lesions [78].

One potential treatment is to restore normal vasculature within the granuloma. Restoring blood supply in the granuloma can improve access of frontline TB drugs to the persistent, non-replicating bacteria in the core. Moreover, oxygen concentrations can be restored by normalized vasculature in the granuloma, preventing further cell necrosis and tissue caseation [75]. However, in the absence of antimicrobial drug treatment, re-establishing lesion perfusion could be detrimental by facilitating bacilli dissemination [79]. Therefore, granuloma-targeted therapy aiming at restoring vascular perfusion is a possible adjunctive treatment along with bactericidal or bacteriostatic drugs.

VEGF is not only a potent inducer of angiogenesis, but also able to increase endothelial cell vascular permeability. Over-production of proangiogenic factors, including VEGF, will recruit excessive endothelial cells with abnormalities [80]. These abnormal endothelial cells have a different gene expression profile, require growth factors for survival and fail to function as a barrier for plasma proteins [80]. Moreover, excessive VEGF results in the reduction and dysfunction of pericytes,

which are important cells covering the endothelial cells and proving nutrient and support [80]. Abnormal pericytes have irregular shapes and extend their cytoplasmic processes away from blood vessel. These abnormalities of pericytes could result in endothelial cells malnutrition and ultimately death. Lastly, basement membrane is also affected by excessive proangiogenic factors [80]. Basement membrane is a layer of matrix specifically wrapping around the endothelial cells and associated peritype and providing a scaffold within the tissue. Abnormal basement membrane covers the blood vessel unevenly and dissociates with the endothelial cells. Taken together, these abnormalities of endothelial cell, pericyte and basement membrane, induced by excessive proangiogenic factors, result in blood vessels leakage. Leaked blood vessels have a reduced blood flow and impaired delivery of oxygen and nutrients. Similarly, drug delivery is compromised by blood vessel leakage. Inhibiting VEGF by a VEGF receptor tyrosine kinase inhibitor reduced vascular leakage, and improved oxygen availability for mycobacteria-residing tissue in zebrafish infection model [81]. Reduction of bacterial burden and tissue dissemination were observed in zebrafish treated with VEGF inhibitors. In rabbit TB granuloma model, Datta et al. showed anti-VEGF antibody were able to normalize vasculature in the granuloma and reduce tissue hypoxia, which eventually improved small molecule delivery [82].

1.3.3 Extracellular matrix (ECM) remodeling during *M. tuberculosis* infection

Tissue remodeling is another important feature during granuloma formation [15]. The interstitial space is greatly remodeled at the beginning of granuloma formation, allowing infiltration of different immune cells. Both cell migration and blood vessel

formation need matrix scaffold to initiate cell deposition. As the granuloma develops, fibrotic tissue is deposited around the cell aggregates, to "wall off" the infection, which requires extensive matrix remodeling. Finally, when the disease progresses to active state, the fibrotic wall around the granuloma is broken down to release the bacteria. Taken together, matrix remodeling is a continuous progress throughout the formation of granuloma, exhibiting different outcomes at different stages. In addition to providing scaffold for the tissue, extracellular matrix also actively interacts with and regulates immune and stromal cells. For example, matrix modulated immune and epithelial cell survival [83], activation [84], autophagy[85], phago-lysosomal fusion [86] and cytokine secretion [87].

The matrix metalloproteinase (MMP) enzymes are major contributors to this remodeling process due to their ability to degrade ECM such as collagen and proteoglycans. MMPs belong to a family of zinc-dependent endopeptidases with 24 members in mammals, many of which are indicated to play important roles during granuloma formation [88, 89]. MMP-2 and MMP-9 are known to degrade type IV collagen, a major component of the basement membrane in the lung, and were found markedly up-regulated in expression in human tuberculosis granulomas [90, 91]. MMP-1 was identified as one of most highly upregulated gene in a transcriptional profiling of patients with pulmonary tuberculosis and latent infection [89, 92, 93]. These studies demonstrated that MMP-1 upregulation led to initial collagen destruction and reduced cell survival within the granuloma. MMP-8, one of pre-synthesized collagenases by neutrophils, was the main driver of tissue destruction and

lung pathology in the active stage of human tuberculosis [58, 94]. Other MMPs have been studied extensively in human tuberculosis tissue, including MMP-8 [94] and MMP-14 [95], whose expression were significantly up-regulated.

Different types of immune cells (e.g. macrophages and neutrophils) and stromal cells (e.g. fibroblasts and epithelial cells) can produce different types of MMP. Different MMPs have different matrix substrates including collagen, elastin, fibronectin. Moreover, this production of MMPs can be induced by Mtb virulent factors. For example, early secreted antigenic target-6 (ESAT-6) induced MMP-9 production in neighboring epithelial cells [74] and MMP-10 production in primary human macrophages [96]. Besides extracellular matrix, some vital chemokines and cytokines are proteolytic targets of MMPs [97-106]. For instant, CCL2 and CCL7, the chemokines that recruit monocytes, were able to be digested by MMPs including MMP-2 and MMP-9 [98, 106]. CCL8, CCL13 and CXCL10 were also subject to MMP cleavage *in vivo* [98, 106]. The mannose binding lectin (MBL), a key component of the lectin pathway in innate immunity, has a collagen-like domain that can be cleaved by MMP-2, MMP-9 and MMP-14 [97].

Stabilization the extracellular matrix can potentially control the active progress of Mtb infection, considering tuberculosis treatment preventing cavity collapse had a cure rate of up to 70% [107] before antibiotic was discovered. Specific MMP inhibitors have been developed originally for treating cancer metastasis [101]. However, studies using MMP inhibitors for tuberculosis treatment in different animal models have generated

conflicting data. Walker et al. used doxycycline, a FDA-approved MMP inhibitor, in a guinea pig infection model and observed a reduced pulmonary bacterial burden after 8-week treatment [108]. Hernandez-Pando et al. observed a type-2 cytokine response profile and a delayed granuloma formation in murine pulmonary tuberculosis after treatment with MMP inhibitors [109]. In contrast, Izzo et al. observed increased collagen deposition in early granuloma formation after MMP inhibition, as well as a reduced bacterial burden in the lung at early phase [110]. However, a subsequent study from the same group did not observed a reduced bacterial burden in the lung following MMP inhibition [91]. These studies argue that there is value in determining the impact of MMP inhibition on disease progression and on granuloma architecture.

1.3.4 pH change during *M. tuberculosis* infection

During phagosome maturation, the phagosome continuously fused with other intracellular vehicles, lowering the pH level inside between 6-6.5 [111]. Further fusion of phagosome and lysosome lowers the pH level around 4-4.5. This hostile environment drives Mtb to change its transcriptional profile significantly [71]. Treatment with concanamycin A arrested phagosome maturation and stopped Mtb's transcriptional response, indicating Mtb possesses a sensing mechanism that detects pH change [71]. Tan et. al. showed Mtb can also sense increased level of [Cl^-], which is a counter-ion to balance the increased level of [H^+] during phagosome maturation [112]. Mtb then developed a shifted transcriptional profile, dominated by the phoPR regulatory system. Vanda et. al. demonstrated that Mtb can maintain intra-bacterial pH in acidic environment both in broth and within activated macrophage [31]. However,

mutation of membrane-bound protein Rv3671c rendered Mtb's resistance to acid in broth and in activated macrophage. Moreover, disruption of Rv3671c severely impaired Mtb's resistance *in vivo*, and complementation by Rv3671c restored Mtb's virulence. These studies indicate that resistance to acidic environment is vital to Mtb both *in vitro* and *in vivo*.

1.3.5 Hypoxic environment formation during *M. tuberculosis* infection

The necrotic center of the granuloma is usually hypoxic, due to limited blood vessel access [15]. It has been hypothesized that hypoxic environment will induce dormant state of the bacteria. This hypothesis is based on *in vitro* studies showing that bacterial growth was arrested in low oxygen environment [113]. Recent studies have confirmed that hypoxia can induce around 50 genes known as the dormancy regulon *in vitro* [114, 115]. These non-replicating bacteria were resistant to isoniazid and ethambutol and less susceptible to rifampicin [116]. Furthermore, the bacteria in the necrotic center of the granuloma may lower its metabolic activities and stay in a non-replicating state, because of limited oxygen and nutrient supply [116]. These bacteria are often responsible for disease reactivation when immune system is compromised.

Hypoxia-imaging agents, such as pimonidazole hydrochloride (PIMO), have been used to probe the hypoxic state in different Mtb infection models [117, 118]. C57BL/6 mice infected with Mtb, which is known for lack of highly stratified granuloma, had low PIMO signal within the lung tissue [117]. On the other hand, C57BL/6 mice infected with *Mycobacterium avium* strain TMC724, showed positive PIMO signal in

the lung tissue, suggesting hypoxic pulmonary lesions can be developed in this infection model [117]. Moreover, guinea pigs infected with Mtb, which usually develops necrotic center in the granuloma, also stained positive for PIMO, indicating the hypoxic nature of the necrotic center of granuloma [119]. In another comprehensive study, 4 different Mtb infection animal models, including mouse, guinea pig, rabbit and non-human primate Mtb infection models, were used to identify the hypoxic nature of caseous lesions in the granuloma [119]. PIMO staining showed discrete area surrounding the necrotic lesions of granuloma from guinea pig, rabbit and non-human primate infection were hypoxic, while no positive staining observed in murine lesions. Using another hypoxia-sensing compound, 2-nitroimidazole structure (EF5), Tsai et. al. demonstrated that C57BL/6J mouse Mtb infection did not develop hypoxic lesions like human patients did [120]. Lastly, an effective drug against Mtb in a hypoxic environment *in vitro*, metronidazole, was effective in reducing bacterial burden in rabbit *M. bovis* infection but not mouse *M. bovis* infection [121].

Under hypoxic environment, immune cells undergo several metabolic shifts within the TB granuloma, including employing glycolysis and limiting glutamate's entry into TCA cycle [122, 123]. Macrophages are shown to accumulate triacylglycerol (TAG) under hypoxic condition, leading to formation of foamy macrophages in the granuloma [124]. This TAG can be utilized by Mtb to synthesize its cell wall lipids [125]. Moreover, disrupting TAG synthesis pathway in the bacteria results in sensitivity to antibiotics, indicating the importance of TAG synthesis pathway in developing Mtb drug tolerance.

1.4 Aims of this study

The aims of this dissertation are to modulate host environment *in vivo*, in order to perturb Mtb infection. Chapter Two details the use of specific MMP inhibitors to limit MMP activities *in vivo* during Mtb infection, in order to explore potential benefit of targeting host environmental factors. Chapter Three utilizes synthetic mRNA to recruit and modulate host immune cells *in vivo*, in order to explore the potential of gene therapy in future tuberculosis treatment.

1.5 Reference

1. World Health Organization. Global tuberculosis report 2016. World Health Organization, 2016.

2. Centers for Disease Control and Prevention. Drug Resistant Tuberculosis: The Next Global Health Crisis? Centers for Disease Control and Prevention, 2015.

3. Manjelievskaia J, Erck D, Piracha S, Schrager L. Drug-resistant TB: deadly, costly and in need of a vaccine. Trans R Soc Trop Med Hyg. 2016;110(3):186-91. doi: 10.1093/trstmh/trw006. PubMed PMID: 26884499; PubMed Central PMCID: PMCPMC4755426.

4. Parham P. The immune system. 3rd ed: Garland Science, Taylor & Francis Group; 2009.

5. Munoz-Elias EJ, Timm J, Botha T, Chan WT, Gomez JE, McKinney JD. Replication dynamics of Mycobacterium tuberculosis in chronically infected mice. Infect Immun. 2005;73(1):546-51. Epub 2004/12/25. doi: 10.1128/IAI.73.1.546-551.2005. PubMed PMID: 15618194; PubMed Central PMCID: PMCPMC538940.

6. Fu LM, Fu-Liu CS. Is Mycobacterium tuberculosis a closer relative to Gram-positive or Gram-negative bacterial pathogens? Tuberculosis (Edinb). 2002;82(2-3):85-90. Epub 2002/10/03. PubMed PMID: 12356459.

7. Cudahy P, Shenoi SV. Diagnostics for pulmonary tuberculosis. Postgrad Med J. 2016;92(1086):187-93. Epub 2016/03/24. doi: 10.1136/postgradmedj-2015-133278. PubMed PMID: 27005271; PubMed Central PMCID: PMCPMC4854647.

8. Cole ST, Brosch R, Parkhill J, Garnier T, Churcher C, Harris D, et al.

Deciphering the biology of Mycobacterium tuberculosis from the complete genome sequence. Nature. 1998;393(6685):537-44. Epub 1998/06/20. doi: 10.1038/31159. PubMed PMID: 9634230.

9. Beatty WL, Rhoades ER, Ullrich HJ, Chatterjee D, Heuser JE, Russell DG. Trafficking and release of mycobacterial lipids from infected macrophages. Traffic. 2000;1(3):235-47. PubMed PMID: 11208107.

10. Geisel RE, Sakamoto K, Russell DG, Rhoades ER. In vivo activity of released cell wall lipids of Mycobacterium bovis bacillus Calmette-Guerin is due principally to trehalose mycolates. J Immunol. 2005;174(8):5007-15. PubMed PMID: 15814731.

11. Rhoades E, Hsu F, Torrelles JB, Turk J, Chatterjee D, Russell DG. Identification and macrophage-activating activity of glycolipids released from intracellular Mycobacterium bovis BCG. Mol Microbiol. 2003;48(4):875-88. PubMed PMID: 12753183.

12. Rhoades ER, Geisel RE, Butcher BA, McDonough S, Russell DG. Cell wall lipids from Mycobacterium bovis BCG are inflammatory when inoculated within a gel matrix: characterization of a new model of the granulomatous response to mycobacterial components. Tuberculosis (Edinb). 2005;85(3):159-76. doi: 10.1016/j.tube.2004.10.001. PubMed PMID: 15850754.

13. Sakamoto K, Geisel RE, Kim MJ, Wyatt BT, Sellers LB, Smiley ST, et al. Fibrinogen regulates the cytotoxicity of mycobacterial trehalose dimycolate but is not required for cell recruitment, cytokine response, or control of mycobacterial infection. Infect Immun. 2010;78(3):1004-11. doi: 10.1128/IAI.00451-09. PubMed PMID: 20028811; PubMed Central PMCID: PMCPMC2825938.

14. Sakamoto K, Kim MJ, Rhoades ER, Allavena RE, Ehrt S, Wainwright HC, et al. Mycobacterial trehalose dimycolate reprograms macrophage global gene expression and activates matrix metalloproteinases. Infect Immun. 2013;81(3):764-76. doi: 10.1128/IAI.00906-12. PubMed PMID: 23264051; PubMed Central PMCID: PMCPMC3584883.

15. Russell DG. Who puts the tubercle in tuberculosis? Nat Rev Microbiol. 2007;5(1):39-47. doi: 10.1038/nrmicro1538. PubMed PMID: 17160001.

16. Rook GA, Dheda K, Zumla A. Immune responses to tuberculosis in developing countries: implications for new vaccines. Nat Rev Immunol. 2005;5(8):661-7. Epub 2005/08/02. doi: 10.1038/nri1666. PubMed PMID: 16056257.

17. Russell DG, Cardona PJ, Kim MJ, Allain S, Altare F. Foamy macrophages and the progression of the human tuberculosis granuloma. Nat Immunol. 2009;10(9):943-8. doi: 10.1038/ni.1781. PubMed PMID: 19692995; PubMed Central PMCID: PMCPMC2759071.

18. Bermudez LE, Goodman J. Mycobacterium tuberculosis invades and replicates within type II alveolar cells. Infect Immun. 1996;64(4):1400-6. Epub 1996/04/01. PubMed PMID: 8606107; PubMed Central PMCID: PMCPMC173932.

19. Bermudez LE, Sangari FJ, Kolonoski P, Petrofsky M, Goodman J. The efficiency of the translocation of Mycobacterium tuberculosis across a bilayer of epithelial and endothelial cells as a model of the alveolar wall is a consequence of transport within mononuclear phagocytes and invasion of alveolar epithelial cells. Infect Immun. 2002;70(1):140-6. Epub 2001/12/19. PubMed PMID: 11748175; PubMed Central PMCID: PMCPMC127600.

20. Huang L, Nazarova EV, Tan S, Liu Y, Russell DG. Growth of Mycobacterium tuberculosis in vivo segregates with host macrophage metabolism and ontogeny. J Exp Med. 2018. Epub 2018/03/04. doi: 10.1084/jem.20172020. PubMed PMID: 29500179.

21. Ramakrishnan L. Revisiting the role of the granuloma in tuberculosis. Nat Rev Immunol. 2012;12(5):352-66. Epub 2012/04/21. doi: 10.1038/nri3211. PubMed PMID: 22517424.

22. Flynn JL, Chan J. Immunology of tuberculosis. Annu Rev Immunol. 2001;19:93-129. doi: 10.1146/annurev.immunol.19.1.93. PubMed PMID: 11244032.

23. Russell DG, VanderVen BC, Lee W, Abramovitch RB, Kim MJ, Homolka S, et al. Mycobacterium tuberculosis wears what it eats. Cell Host Microbe. 2010;8(1):68-76. doi: 10.1016/j.chom.2010.06.002. PubMed PMID: 20638643; PubMed Central PMCID: PMCPMC2929656.

24. Weiss G, Schaible UE. Macrophage defense mechanisms against intracellular bacteria. Immunol Rev. 2015;264(1):182-203. Epub 2015/02/24. doi: 10.1111/imr.12266. PubMed PMID: 25703560; PubMed Central PMCID: PMCPMC4368383.

25. Sturgill-Koszycki S, Schlesinger PH, Chakraborty P, Haddix PL, Collins HL, Fok AK, et al. Lack of acidification in Mycobacterium phagosomes produced by exclusion of the vesicular proton-ATPase. Science. 1994;263(5147):678-81. Epub 1994/02/04. PubMed PMID: 8303277.

26. Schneider BE, Behrends J, Hagens K, Harmel N, Shayman JA, Schaible UE. Lysosomal phospholipase A2: a novel player in host immunity to Mycobacterium tuberculosis. Eur J Immunol. 2014;44(8):2394-404. Epub 2014/05/16. doi:

10.1002/eji.201344383. PubMed PMID: 24825529.

27. Abramovitch RB, Rohde KH, Hsu FF, Russell DG. aprABC: a Mycobacterium tuberculosis complex-specific locus that modulates pH-driven adaptation to the macrophage phagosome. Mol Microbiol. 2011;80(3):678-94. Epub 2011/03/16. doi: 10.1111/j.1365-2958.2011.07601.x. PubMed PMID: 21401735; PubMed Central PMCID: PMCPMC3138066.

28. Kang PB, Azad AK, Torrelles JB, Kaufman TM, Beharka A, Tibesar E, et al. The human macrophage mannose receptor directs Mycobacterium tuberculosis lipoarabinomannan-mediated phagosome biogenesis. J Exp Med. 2005;202(7):987-99. Epub 2005/10/06. doi: 10.1084/jem.20051239. PubMed PMID: 16203868; PubMed Central PMCID: PMCPMC2213176.

29. Schaible UE, Sturgill-Koszycki S, Schlesinger PH, Russell DG. Cytokine activation leads to acidification and increases maturation of Mycobacterium avium-containing phagosomes in murine macrophages. J Immunol. 1998;160(3):1290-6. Epub 1998/05/07. PubMed PMID: 9570546.

30. Jayachandran R, Sundaramurthy V, Combaluzier B, Mueller P, Korf H, Huygen K, et al. Survival of mycobacteria in macrophages is mediated by coronin 1-dependent activation of calcineurin. Cell. 2007;130(1):37-50. Epub 2007/07/17. doi: 10.1016/j.cell.2007.04.043. PubMed PMID: 17632055.

31. Vandal OH, Pierini LM, Schnappinger D, Nathan CF, Ehrt S. A membrane protein preserves intrabacterial pH in intraphagosomal Mycobacterium tuberculosis. Nat Med. 2008;14(8):849-54. Epub 2008/07/22. doi: 10.1038/nm.1795. PubMed PMID: 18641659; PubMed Central PMCID: PMCPMC2538620.

32. Baker JJ, Johnson BK, Abramovitch RB. Slow growth of Mycobacterium tuberculosis at acidic pH is regulated by phoPR and host-associated carbon sources. Mol Microbiol. 2014;94(1):56-69. Epub 2014/07/01. doi: 10.1111/mmi.12688. PubMed PMID: 24975990; PubMed Central PMCID: PMCPMC4177513.

33. Cirillo SL, Subbian S, Chen B, Weisbrod TR, Jacobs WR, Jr., Cirillo JD. Protection of Mycobacterium tuberculosis from reactive oxygen species conferred by the mel2 locus impacts persistence and dissemination. Infect Immun. 2009;77(6):2557-67. Epub 2009/04/08. doi: 10.1128/IAI.01481-08. PubMed PMID: 19349422; PubMed Central PMCID: PMCPMC2687327.

34. Voskuil MI, Bartek IL, Visconti K, Schoolnik GK. The response of mycobacterium tuberculosis to reactive oxygen and nitrogen species. Front Microbiol. 2011;2:105. Epub 2011/07/08. doi: 10.3389/fmicb.2011.00105. PubMed PMID: 21734908; PubMed Central PMCID: PMCPMC3119406.

35. Mestre O, Hurtado-Ortiz R, Dos Vultos T, Namouchi A, Cimino M, Pimentel M, et al. High throughput phenotypic selection of Mycobacterium tuberculosis mutants with impaired resistance to reactive oxygen species identifies genes important for intracellular growth. PLoS One. 2013;8(1):e53486. Epub 2013/01/16. doi: 10.1371/journal.pone.0053486. PubMed PMID: 23320090; PubMed Central PMCID: PMCPMC3540035.

36. Roca FJ, Ramakrishnan L. TNF dually mediates resistance and susceptibility to mycobacteria via mitochondrial reactive oxygen species. Cell. 2013;153(3):521-34. Epub 2013/04/16. doi: 10.1016/j.cell.2013.03.022. PubMed PMID: 23582643; PubMed Central PMCID: PMCPMC3790588.

37. Fang FC. Antimicrobial reactive oxygen and nitrogen species: concepts and controversies. Nat Rev Microbiol. 2004;2(10):820-32. Epub 2004/09/21. doi: 10.1038/nrmicro1004. PubMed PMID: 15378046.

38. Nathan CF, Hibbs JB, Jr. Role of nitric oxide synthesis in macrophage antimicrobial activity. Curr Opin Immunol. 1991;3(1):65-70. Epub 1991/02/11. PubMed PMID: 1711326.

39. Garbi N, Lambrecht BN. Location, function, and ontogeny of pulmonary macrophages during the steady state. Pflugers Arch. 2017;469(3-4):561-72. Epub 2017/03/16. doi: 10.1007/s00424-017-1965-3. PubMed PMID: 28289977.

40. Feng Y, Dorhoi A, Mollenkopf HJ, Yin H, Dong Z, Mao L, et al. Platelets direct monocyte differentiation into epithelioid-like multinucleated giant foam cells with suppressive capacity upon mycobacterial stimulation. J Infect Dis. 2014;210(11):1700-10. Epub 2014/07/06. doi: 10.1093/infdis/jiu355. PubMed PMID: 24987031; PubMed Central PMCID: PMCPMC4224136.

41. Crawford CL. The Epithelioid Cell in Tuberculosis is Secretory and Not a Macrophage. J Infect Dis. 2015;212(7):1172-3. Epub 2015/03/25. doi: 10.1093/infdis/jiv155. PubMed PMID: 25801654.

42. Galkina E, Ley K. Immune and inflammatory mechanisms of atherosclerosis (*). Annu Rev Immunol. 2009;27:165-97. Epub 2009/03/24. doi: 10.1146/annurev.immunol.021908.132620. PubMed PMID: 19302038; PubMed Central PMCID: PMCPMC2734407.

43. Peyron P, Vaubourgeix J, Poquet Y, Levillain F, Botanch C, Bardou F, et al. Foamy macrophages from tuberculous patients' granulomas constitute a nutrient-rich

reservoir for M. tuberculosis persistence. PLoS Pathog. 2008;4(11):e1000204. Epub 2008/11/13. doi: 10.1371/journal.ppat.1000204. PubMed PMID: 19002241; PubMed Central PMCID: PMCPMC2575403.

44. Kim MJ, Wainwright HC, Locketz M, Bekker LG, Walther GB, Dittrich C, et al. Caseation of human tuberculosis granulomas correlates with elevated host lipid metabolism. EMBO Mol Med. 2010;2(7):258-74. doi: 10.1002/emmm.201000079. PubMed PMID: 20597103; PubMed Central PMCID: PMCPMC2913288.

45. Palmer MV, Thacker TC, Waters WR. Multinucleated giant cell cytokine expression in pulmonary granulomas of cattle experimentally infected with Mycobacterium bovis. Vet Immunol Immunopathol. 2016;180:34-9. Epub 2016/10/04. doi: 10.1016/j.vetimm.2016.08.015. PubMed PMID: 27692093.

46. Okamoto H, Mizuno K, Horio T. Langhans-type and foreign-body-type multinucleated giant cells in cutaneous lesions of sarcoidosis. Acta Derm Venereol. 2003;83(3):171-4. Epub 2003/06/21. doi: 10.1080/00015550310007148. PubMed PMID: 12816149.

47. Torrelles JB, Sieling PA, Arcos J, Knaup R, Bartling C, Rajaram MV, et al. Structural differences in lipomannans from pathogenic and nonpathogenic mycobacteria that impact CD1b-restricted T cell responses. J Biol Chem. 2011;286(41):35438-46. Epub 2011/08/24. doi: 10.1074/jbc.M111.232587. PubMed PMID: 21859718; PubMed Central PMCID: PMCPMC3195570.

48. Zhu XW, Friedland JS. Multinucleate giant cells and the control of chemokine secretion in response to Mycobacterium tuberculosis. Clin Immunol. 2006;120(1):10-20. Epub 2006/03/01. doi: 10.1016/j.clim.2006.01.009. PubMed PMID: 16504587.

49. Mustafa T, Mogga SJ, Mfinanga SG, Morkve O, Sviland L. Immunohistochemical analysis of cytokines and apoptosis in tuberculous lymphadenitis. Immunology. 2006;117(4):454-62. Epub 2006/03/25. doi: 10.1111/j.1365-2567.2005.02318.x. PubMed PMID: 16556259; PubMed Central PMCID: PMCPMC1782255.

50. Lay G, Poquet Y, Salek-Peyron P, Puissegur MP, Botanch C, Bon H, et al. Langhans giant cells from M. tuberculosis-induced human granulomas cannot mediate mycobacterial uptake. J Pathol. 2007;211(1):76-85. Epub 2006/11/23. doi: 10.1002/path.2092. PubMed PMID: 17115379.

51. Dallenga T, Schaible UE. Neutrophils in tuberculosis--first line of defence or booster of disease and targets for host-directed therapy? Pathog Dis. 2016;74(3). Epub 2016/02/24. doi: 10.1093/femspd/ftw012. PubMed PMID: 26903072.

52. Corleis B, Korbel D, Wilson R, Bylund J, Chee R, Schaible UE. Escape of Mycobacterium tuberculosis from oxidative killing by neutrophils. Cell Microbiol. 2012;14(7):1109-21. Epub 2012/03/13. doi: 10.1111/j.1462-5822.2012.01783.x. PubMed PMID: 22405091.

53. Repasy T, Martinez N, Lee J, West K, Li W, Kornfeld H. Bacillary replication and macrophage necrosis are determinants of neutrophil recruitment in tuberculosis. Microbes Infect. 2015;17(8):564-74. Epub 2015/04/12. doi: 10.1016/j.micinf.2015.03.013. PubMed PMID: 25862076; PubMed Central PMCID: PMCPMC4508221.

54. Logunova N, Korotetskaya M, Polshakov V, Apt A. The QTL within the H2 Complex Involved in the Control of Tuberculosis Infection in Mice Is the Classical

Class II H2-Ab1 Gene. PLoS Genet. 2015;11(11):e1005672. Epub 2015/12/01. doi: 10.1371/journal.pgen.1005672. PubMed PMID: 26618355; PubMed Central PMCID: PMCPMC4664271.

55. Seiler P, Aichele P, Raupach B, Odermatt B, Steinhoff U, Kaufmann SH. Rapid neutrophil response controls fast-replicating intracellular bacteria but not slow-replicating Mycobacterium tuberculosis. J Infect Dis. 2000;181(2):671-80. Epub 2000/02/11. doi: 10.1086/315278. PubMed PMID: 10669354.

56. Kimmey JM, Huynh JP, Weiss LA, Park S, Kambal A, Debnath J, et al. Unique role for ATG5 in neutrophil-mediated immunopathology during M. tuberculosis infection. Nature. 2015;528(7583):565-9. Epub 2015/12/10. doi: 10.1038/nature16451. PubMed PMID: 26649827; PubMed Central PMCID: PMCPMC4842313.

57. Daley JM, Thomay AA, Connolly MD, Reichner JS, Albina JE. Use of Ly6G-specific monoclonal antibody to deplete neutrophils in mice. J Leukoc Biol. 2008;83(1):64-70. Epub 2007/09/22. doi: 10.1189/jlb.0407247. PubMed PMID: 17884993.

58. Eum SY, Kong JH, Hong MS, Lee YJ, Kim JH, Hwang SH, et al. Neutrophils are the predominant infected phagocytic cells in the airways of patients with active pulmonary TB. Chest. 2010;137(1):122-8. Epub 2009/09/15. doi: 10.1378/chest.09-0903. PubMed PMID: 19749004; PubMed Central PMCID: PMCPMC2803122.

59. Mihret A. The role of dendritic cells in Mycobacterium tuberculosis infection. Virulence. 2012;3(7):654-9. Epub 2012/11/17. doi: 10.4161/viru.22586. PubMed PMID: 23154283; PubMed Central PMCID: PMCPMC3545947.

60. Tian T, Woodworth J, Skold M, Behar SM. In vivo depletion of CD11c+ cells delays the CD4+ T cell response to Mycobacterium tuberculosis and exacerbates the outcome of infection. J Immunol. 2005;175(5):3268-72. Epub 2005/08/24. PubMed PMID: 16116218.

61. Fortsch D, Rollinghoff M, Stenger S. IL-10 converts human dendritic cells into macrophage-like cells with increased antibacterial activity against virulent Mycobacterium tuberculosis. J Immunol. 2000;165(2):978-87. Epub 2000/07/06. PubMed PMID: 10878374.

62. Tascon RE, Soares CS, Ragno S, Stavropoulos E, Hirst EM, Colston MJ. Mycobacterium tuberculosis-activated dendritic cells induce protective immunity in mice. Immunology. 2000;99(3):473-80. Epub 2000/03/11. PubMed PMID: 10712679; PubMed Central PMCID: PMCPMC2327172.

63. Demangel C, Garnier T, Rosenkrands I, Cole ST. Differential effects of prior exposure to environmental mycobacteria on vaccination with Mycobacterium bovis BCG or a recombinant BCG strain expressing RD1 antigens. Infect Immun. 2005;73(4):2190-6. Epub 2005/03/24. doi: 10.1128/IAI.73.4.2190-2196.2005. PubMed PMID: 15784562; PubMed Central PMCID: PMCPMC1087454.

64. Wolf AJ, Linas B, Trevejo-Nunez GJ, Kincaid E, Tamura T, Takatsu K, et al. Mycobacterium tuberculosis infects dendritic cells with high frequency and impairs their function in vivo. J Immunol. 2007;179(4):2509-19. Epub 2007/08/07. PubMed PMID: 17675513.

65. Scanga CA, Mohan VP, Yu K, Joseph H, Tanaka K, Chan J, et al. Depletion of CD4(+) T cells causes reactivation of murine persistent tuberculosis despite continued

expression of interferon gamma and nitric oxide synthase 2. J Exp Med. 2000;192(3):347-58. Epub 2000/08/10. PubMed PMID: 10934223; PubMed Central PMCID: PMCPMC2193220.

66. Stenger S, Hanson DA, Teitelbaum R, Dewan P, Niazi KR, Froelich CJ, et al. An antimicrobial activity of cytolytic T cells mediated by granulysin. Science. 1998;282(5386):121-5. Epub 1998/10/02. PubMed PMID: 9756476.

67. Stenger S, Mazzaccaro RJ, Uyemura K, Cho S, Barnes PF, Rosat JP, et al. Differential effects of cytolytic T cell subsets on intracellular infection. Science. 1997;276(5319):1684-7. Epub 1997/06/13. PubMed PMID: 9180075.

68. Kaufmann SH. Immunity to intracellular bacteria. Annu Rev Immunol. 1993;11:129-63. Epub 1993/01/01. doi: 10.1146/annurev.iy.11.040193.001021. PubMed PMID: 8476559.

69. Maglione PJ, Xu J, Chan J. B cells moderate inflammatory progression and enhance bacterial containment upon pulmonary challenge with Mycobacterium tuberculosis. J Immunol. 2007;178(11):7222-34. Epub 2007/05/22. PubMed PMID: 17513771.

70. Teitelbaum R, Glatman-Freedman A, Chen B, Robbins JB, Unanue E, Casadevall A, et al. A mAb recognizing a surface antigen of Mycobacterium tuberculosis enhances host survival. Proc Natl Acad Sci U S A. 1998;95(26):15688-93. Epub 1998/12/23. PubMed PMID: 9861031; PubMed Central PMCID: PMCPMC28105.

71. Rohde KH, Abramovitch RB, Russell DG. Mycobacterium tuberculosis invasion of macrophages: linking bacterial gene expression to environmental cues.

Cell Host Microbe. 2007;2(5):352-64. doi: 10.1016/j.chom.2007.09.006. PubMed PMID: 18005756.

72. Ragno S, Romano M, Howell S, Pappin DJ, Jenner PJ, Colston MJ. Changes in gene expression in macrophages infected with Mycobacterium tuberculosis: a combined transcriptomic and proteomic approach. Immunology. 2001;104(1):99-108. Epub 2001/09/29. PubMed PMID: 11576227; PubMed Central PMCID: PMCPMC1783284.

73. Alatas F, Alatas O, Metintas M, Ozarslan A, Erginel S, Yildirim H. Vascular endothelial growth factor levels in active pulmonary tuberculosis. Chest. 2004;125(6):2156-9. Epub 2004/06/11. PubMed PMID: 15189936.

74. Volkman HE, Pozos TC, Zheng J, Davis JM, Rawls JF, Ramakrishnan L. Tuberculous granuloma induction via interaction of a bacterial secreted protein with host epithelium. Science. 2010;327(5964):466-9. doi: 10.1126/science.1179663. PubMed PMID: 20007864; PubMed Central PMCID: PMCPMC3125975.

75. Kiran D, Podell BK, Chambers M, Basaraba RJ. Host-directed therapy targeting the Mycobacterium tuberculosis granuloma: a review. Semin Immunopathol. 2016;38(2):167-83. Epub 2015/10/30. doi: 10.1007/s00281-015-0537-x. PubMed PMID: 26510950; PubMed Central PMCID: PMCPMC4779125.

76. Polotsky VY, Belisle JT, Mikusova K, Ezekowitz RA, Joiner KA. Interaction of human mannose-binding protein with Mycobacterium avium. J Infect Dis. 1997;175(5):1159-68. PubMed PMID: 9129080.

77. Matsuyama W, Hashiguchi T, Matsumuro K, Iwami F, Hirotsu Y, Kawabata M, et al. Increased serum level of vascular endothelial growth factor in pulmonary

tuberculosis. Am J Respir Crit Care Med. 2000;162(3 Pt 1):1120-2. doi: 10.1164/ajrccm.162.3.9911010. PubMed PMID: 10988140.

78. Ulrichs T, Kosmiadi GA, Jorg S, Pradl L, Titukhina M, Mishenko V, et al. Differential organization of the local immune response in patients with active cavitary tuberculosis or with nonprogressive tuberculoma. J Infect Dis. 2005;192(1):89-97. Epub 2005/06/09. doi: 10.1086/430621. PubMed PMID: 15942898.

79. Dartois V. The path of anti-tuberculosis drugs: from blood to lesions to mycobacterial cells. Nat Rev Microbiol. 2014;12(3):159-67. Epub 2014/02/04. doi: 10.1038/nrmicro3200. PubMed PMID: 24487820; PubMed Central PMCID: PMCPMC4341982.

80. Baluk P, Hashizume H, McDonald DM. Cellular abnormalities of blood vessels as targets in cancer. Curr Opin Genet Dev. 2005;15(1):102-11. Epub 2005/01/22. doi: 10.1016/j.gde.2004.12.005. PubMed PMID: 15661540.

81. Oehlers SH, Cronan MR, Scott NR, Thomas MI, Okuda KS, Walton EM, et al. Interception of host angiogenic signalling limits mycobacterial growth. Nature. 2015;517(7536):612-5. doi: 10.1038/nature13967. PubMed PMID: 25470057; PubMed Central PMCID: PMCPMC4312197.

82. Datta M, Via LE, Kamoun WS, Liu C, Chen W, Seano G, et al. Anti-vascular endothelial growth factor treatment normalizes tuberculosis granuloma vasculature and improves small molecule delivery. Proc Natl Acad Sci U S A. 2015;112(6):1827-32. doi: 10.1073/pnas.1424563112. PubMed PMID: 25624495; PubMed Central PMCID: PMCPMC4330784.

83. Buchheit CL, Rayavarapu RR, Schafer ZT. The regulation of cancer cell death

and metabolism by extracellular matrix attachment. Semin Cell Dev Biol. 2012;23(4):402-11. Epub 2012/05/15. doi: 10.1016/j.semcdb.2012.04.007. PubMed PMID: 22579674.

84. Sorokin L. The impact of the extracellular matrix on inflammation. Nat Rev Immunol. 2010;10(10):712-23. Epub 2010/09/25. doi: 10.1038/nri2852. PubMed PMID: 20865019.

85. Lock R, Debnath J. Extracellular matrix regulation of autophagy. Curr Opin Cell Biol. 2008;20(5):583-8. Epub 2008/06/25. doi: 10.1016/j.ceb.2008.05.002. PubMed PMID: 18573652; PubMed Central PMCID: PMCPMC2613490.

86. Newman SL, Gootee L, Kidd C, Ciraolo GM, Morris R. Activation of human macrophage fungistatic activity against Histoplasma capsulatum upon adherence to type 1 collagen matrices. J Immunol. 1997;158(4):1779-86. Epub 1997/02/15. PubMed PMID: 9029116.

87. Merline R, Moreth K, Beckmann J, Nastase MV, Zeng-Brouwers J, Tralhao JG, et al. Signaling by the matrix proteoglycan decorin controls inflammation and cancer through PDCD4 and MicroRNA-21. Sci Signal. 2011;4(199):ra75. Epub 2011/11/17. doi: 10.1126/scisignal.2001868. PubMed PMID: 22087031; PubMed Central PMCID: PMCPMC5029092.

88. Al Shammari B, Shiomi T, Tezera L, Bielecka MK, Workman V, Sathyamoorthy T, et al. The Extracellular Matrix Regulates Granuloma Necrosis in Tuberculosis. J Infect Dis. 2015;212(3):463-73. doi: 10.1093/infdis/jiv076. PubMed PMID: 25676469; PubMed Central PMCID: PMCPMC4539912.

89. Ong CW, Elkington PT, Friedland JS. Tuberculosis, pulmonary cavitation, and

matrix metalloproteinases. Am J Respir Crit Care Med. 2014;190(1):9-18. doi: 10.1164/rccm.201311-2106PP. PubMed PMID: 24713029; PubMed Central PMCID: PMCPMC4226026.

90. Parks WC, Shapiro SD. Matrix metalloproteinases in lung biology. Respir Res. 2001;2(1):10-9. doi: 10.1186/rr33. PubMed PMID: 11686860; PubMed Central PMCID: PMCPMC59564.

91. Taylor JL, Hattle JM, Dreitz SA, Troudt JM, Izzo LS, Basaraba RJ, et al. Role for matrix metalloproteinase 9 in granuloma formation during pulmonary Mycobacterium tuberculosis infection. Infect Immun. 2006;74(11):6135-44. doi: 10.1128/IAI.02048-05. PubMed PMID: 16982845; PubMed Central PMCID: PMCPMC1695484.

92. Rand L, Green JA, Saraiva L, Friedland JS, Elkington PT. Matrix metalloproteinase-1 is regulated in tuberculosis by a p38 MAPK-dependent, p-aminosalicylic acid-sensitive signaling cascade. J Immunol. 2009;182(9):5865-72. doi: 10.4049/jimmunol.0801935. PubMed PMID: 19380835.

93. Elkington PT, Emerson JE, Lopez-Pascua LD, O'Kane CM, Horncastle DE, Boyle JJ, et al. Mycobacterium tuberculosis up-regulates matrix metalloproteinase-1 secretion from human airway epithelial cells via a p38 MAPK switch. J Immunol. 2005;175(8):5333-40. PubMed PMID: 16210639.

94. Ong CW, Elkington PT, Brilha S, Ugarte-Gil C, Tome-Esteban MT, Tezera LB, et al. Neutrophil-Derived MMP-8 Drives AMPK-Dependent Matrix Destruction in Human Pulmonary Tuberculosis. PLoS Pathog. 2015;11(5):e1004917. doi: 10.1371/journal.ppat.1004917. PubMed PMID: 25996154; PubMed Central PMCID:

PMCPMC4440706.

95. Sathyamoorthy T, Tezera LB, Walker NF, Brilha S, Saraiva L, Mauri FA, et al. Membrane Type 1 Matrix Metalloproteinase Regulates Monocyte Migration and Collagen Destruction in Tuberculosis. J Immunol. 2015;195(3):882-91. doi: 10.4049/jimmunol.1403110. PubMed PMID: 26091717; PubMed Central PMCID: PMCPMC4505956.

96. Brilha S, Sathyamoorthy T, Stuttaford LH, Walker NF, Wilkinson RJ, Singh S, et al. Early Secretory Antigenic Target-6 Drives Matrix Metalloproteinase-10 Gene Expression and Secretion in Tuberculosis. Am J Respir Cell Mol Biol. 2017;56(2):223-32. doi: 10.1165/rcmb.2016-0162OC. PubMed PMID: 27654284; PubMed Central PMCID: PMCPMC5359650.

97. Butler GS, Sim D, Tam E, Devine D, Overall CM. Mannose-binding lectin (MBL) mutants are susceptible to matrix metalloproteinase proteolysis: potential role in human MBL deficiency. J Biol Chem. 2002;277(20):17511-9. doi: 10.1074/jbc.M201461200. PubMed PMID: 11891230.

98. Denney H, Clench MR, Woodroofe MN. Cleavage of chemokines CCL2 and CXCL10 by matrix metalloproteinases-2 and -9: implications for chemotaxis. Biochem Biophys Res Commun. 2009;382(2):341-7. doi: 10.1016/j.bbrc.2009.02.164. PubMed PMID: 19281798.

99. Cauwe B, Martens E, Proost P, Opdenakker G. Multidimensional degradomics identifies systemic autoantigens and intracellular matrix proteins as novel gelatinase B/MMP-9 substrates. Integr Biol (Camb). 2009;1(5-6):404-26. doi: 10.1039/b904701h. PubMed PMID: 20023747.

100. Rozanov DV, Savinov AY, Golubkov VS, Postnova TI, Remacle A, Tomlinson S, et al. Cellular membrane type-1 matrix metalloproteinase (MT1-MMP) cleaves C3b, an essential component of the complement system. J Biol Chem. 2004;279(45):46551-7. doi: 10.1074/jbc.M405284200. PubMed PMID: 15381670.

101. Vandenbroucke RE, Libert C. Is there new hope for therapeutic matrix metalloproteinase inhibition? Nat Rev Drug Discov. 2014;13(12):904-27. doi: 10.1038/nrd4390. PubMed PMID: 25376097.

102. Vanlaere I, Libert C. Matrix metalloproteinases as drug targets in infections caused by gram-negative bacteria and in septic shock. Clin Microbiol Rev. 2009;22(2):224-39, Table of Contents. doi: 10.1128/CMR.00047-08. PubMed PMID: 19366913; PubMed Central PMCID: PMCPMC2668236.

103. Khokha R, Murthy A, Weiss A. Metalloproteinases and their natural inhibitors in inflammation and immunity. Nat Rev Immunol. 2013;13(9):649-65. doi: 10.1038/nri3499. PubMed PMID: 23969736.

104. Cauwe B, Van den Steen PE, Opdenakker G. The biochemical, biological, and pathological kaleidoscope of cell surface substrates processed by matrix metalloproteinases. Crit Rev Biochem Mol Biol. 2007;42(3):113-85. doi: 10.1080/10409230701340019. PubMed PMID: 17562450.

105. Wuthrich M, Ersland K, Sullivan T, Galles K, Klein BS. Fungi subvert vaccine T cell priming at the respiratory mucosa by preventing chemokine-induced influx of inflammatory monocytes. Immunity. 2012;36(4):680-92. doi: 10.1016/j.immuni.2012.02.015. PubMed PMID: 22483803; PubMed Central PMCID: PMCPMC3334432.

106. McQuibban GA, Gong JH, Wong JP, Wallace JL, Clark-Lewis I, Overall CM. Matrix metalloproteinase processing of monocyte chemoattractant proteins generates CC chemokine receptor antagonists with anti-inflammatory properties in vivo. Blood. 2002;100(4):1160-7. PubMed PMID: 12149192.

107. Sellors TH. The results of thoracoplasty in pulmonary tuberculosis. Thorax. 1947;2(4):216-23. Epub 1947/12/01. PubMed PMID: 18896485; PubMed Central PMCID: PMCPMC1018249.

108. Walker NF, Clark SO, Oni T, Andreu N, Tezera L, Singh S, et al. Doxycycline and HIV infection suppress tuberculosis-induced matrix metalloproteinases. Am J Respir Crit Care Med. 2012;185(9):989-97. doi: 10.1164/rccm.201110-1769OC. PubMed PMID: 22345579; PubMed Central PMCID: PMCPMC3359940.

109. Hernandez-Pando R, Orozco H, Arriaga K, Pavon L, Rook G. Treatment with BB-94, a broad spectrum inhibitor of zinc-dependent metalloproteinases, causes deviation of the cytokine profile towards type-2 in experimental pulmonary tuberculosis in Balb/c mice. Int J Exp Pathol. 2000;81(3):199-209. PubMed PMID: 10971741; PubMed Central PMCID: PMCPMC2517727.

110. Izzo AA, Izzo LS, Kasimos J, Majka S. A matrix metalloproteinase inhibitor promotes granuloma formation during the early phase of Mycobacterium tuberculosis pulmonary infection. Tuberculosis (Edinb). 2004;84(6):387-96. doi: 10.1016/j.tube.2004.07.001. PubMed PMID: 15525562.

111. Yates RM, Hermetter A, Russell DG. Recording phagosome maturation through the real-time, spectrofluorometric measurement of hydrolytic activities. Methods Mol Biol. 2009;531:157-71. Epub 2009/04/07. doi: 10.1007/978-1-59745-

396-7_11. PubMed PMID: 19347317; PubMed Central PMCID: PMCPMC2756812.

112. Tan S, Sukumar N, Abramovitch RB, Parish T, Russell DG. Mycobacterium tuberculosis responds to chloride and pH as synergistic cues to the immune status of its host cell. PLoS Pathog. 2013;9(4):e1003282. doi: 10.1371/journal.ppat.1003282. PubMed PMID: 23592993; PubMed Central PMCID: PMCPMC3616970.

113. Shiloh MU, Manzanillo P, Cox JS. Mycobacterium tuberculosis senses host-derived carbon monoxide during macrophage infection. Cell Host Microbe. 2008;3(5):323-30. Epub 2008/05/14. doi: 10.1016/j.chom.2008.03.007. PubMed PMID: 18474359; PubMed Central PMCID: PMCPMC2873178.

114. Florczyk MA, McCue LA, Stack RF, Hauer CR, McDonough KA. Identification and characterization of mycobacterial proteins differentially expressed under standing and shaking culture conditions, including Rv2623 from a novel class of putative ATP-binding proteins. Infect Immun. 2001;69(9):5777-85. Epub 2001/08/14. PubMed PMID: 11500455; PubMed Central PMCID: PMCPMC98695.

115. Voskuil MI, Visconti KC, Schoolnik GK. Mycobacterium tuberculosis gene expression during adaptation to stationary phase and low-oxygen dormancy. Tuberculosis (Edinb). 2004;84(3-4):218-27. Epub 2004/06/23. doi: 10.1016/j.tube.2004.02.003. PubMed PMID: 15207491.

116. Gomez JE, McKinney JD. M. tuberculosis persistence, latency, and drug tolerance. Tuberculosis (Edinb). 2004;84(1-2):29-44. Epub 2003/12/13. PubMed PMID: 14670344.

117. Aly S, Wagner K, Keller C, Malm S, Malzan A, Brandau S, et al. Oxygen status of lung granulomas in Mycobacterium tuberculosis-infected mice. J Pathol.

2006;210(3):298-305. Epub 2006/09/27. doi: 10.1002/path.2055. PubMed PMID: 17001607.

118. Via LE, Lin PL, Ray SM, Carrillo J, Allen SS, Eum SY, et al. Tuberculous granulomas are hypoxic in guinea pigs, rabbits, and nonhuman primates. Infect Immun. 2008;76(6):2333-40. Epub 2008/03/19. doi: 10.1128/IAI.01515-07. PubMed PMID: 18347040; PubMed Central PMCID: PMCPMC2423064.

119. Lenaerts AJ, Hoff D, Aly S, Ehlers S, Andries K, Cantarero L, et al. Location of persisting mycobacteria in a Guinea pig model of tuberculosis revealed by r207910. Antimicrob Agents Chemother. 2007;51(9):3338-45. Epub 2007/05/23. doi: 10.1128/AAC.00276-07. PubMed PMID: 17517834; PubMed Central PMCID: PMCPMC2043239.

120. Tsai MC, Chakravarty S, Zhu G, Xu J, Tanaka K, Koch C, et al. Characterization of the tuberculous granuloma in murine and human lungs: cellular composition and relative tissue oxygen tension. Cell Microbiol. 2006;8(2):218-32. doi: 10.1111/j.1462-5822.2005.00612.x. PubMed PMID: 16441433.

121. Wayne LG, Sramek HA. Metronidazole is bactericidal to dormant cells of Mycobacterium tuberculosis. Antimicrob Agents Chemother. 1994;38(9):2054-8. Epub 1994/09/01. PubMed PMID: 7811018; PubMed Central PMCID: PMCPMC284683.

122. Wallis RS, Hafner R. Advancing host-directed therapy for tuberculosis. Nat Rev Immunol. 2015;15(4):255-63. Epub 2015/03/15. doi: 10.1038/nri3813. PubMed PMID: 25765201.

123. Delmastro-Greenwood MM, Piganelli JD. Changing the energy of an immune

response. Am J Clin Exp Immunol. 2013;2(1):30-54. Epub 2013/07/26. PubMed PMID: 23885324; PubMed Central PMCID: PMCPMC3714201.

124. Daniel J, Maamar H, Deb C, Sirakova TD, Kolattukudy PE. Mycobacterium tuberculosis uses host triacylglycerol to accumulate lipid droplets and acquires a dormancy-like phenotype in lipid-loaded macrophages. PLoS Pathog. 2011;7(6):e1002093. Epub 2011/07/07. doi: 10.1371/journal.ppat.1002093. PubMed PMID: 21731490; PubMed Central PMCID: PMCPMC3121879.

125. Garton NJ, Waddell SJ, Sherratt AL, Lee SM, Smith RJ, Senner C, et al. Cytological and transcript analyses reveal fat and lazy persister-like bacilli in tuberculous sputum. PLoS Med. 2008;5(4):e75. Epub 2008/04/04. doi: 10.1371/journal.pmed.0050075. PubMed PMID: 18384229; PubMed Central PMCID: PMCPMC2276522.

Chapter 2

Matrix Metalloproteinase inhibitors enhance the efficacy of frontline drugs against *Mycobacterium tuberculosis*

Abstract

Mycobacterium tuberculosis (Mtb) remains a grave threat to world health with emerging drug resistant strains. One prominent feature of Mtb infection is the extensive reprogramming of host tissue at the site of infection. Here we report that inhibition of matrix metalloproteinase (MMP) activity by a panel of small molecule inhibitors enhances the *in vivo* potency of the frontline TB drugs isoniazid (INH) and rifampicin (RIF). Inhibition of MMP activity leads to an increase in pericyte-covered blood vessel numbers and appears to stabilize the integrity of the infected lung tissue. In treated mice, we observe an increased delivery and/or retention of frontline TB drugs in the infected lungs, resulting in enhanced drug efficacy. These findings indicate that targeting Mtb-induced host tissue remodeling can increase therapeutic efficacy and could enhance the effectiveness of current drug regimens.

2.1 Introduction

Mycobacterium tuberculosis (Mtb) continues to pose a threat to global health. In 2015, 10.4 million people were estimated to have become infected with Mtb and 1.8 million people died because of TB (0.4 million deaths within from TB/HIV co-infection), making Mtb the leading cause of death worldwide from a single infectious agent, ranking above HIV/AIDS[1-3]. TB/HIV co-infection is responsible for about one fourth of all TB deaths and one third of all HIV/AIDS deaths[1, 4]. Furthermore, the incidence of drug resistant TB increased significantly in 2015 compared to previous years[1-3]. Development of new or re-purposed drugs for TB treatment is needed to accomplish the Sustainable Development Goals, which aims to reduce 90% of TB incidence rate by 2030 [1, 5].

Mtb's success as a pathogen depends upon its ability to reprogram its host environment at both the cellular and tissue levels [6, 7]. The tuberculosis granuloma is characterized by extensive tissue remodeling, extracellular matrix (ECM) deposition and angiogenesis, and ultimately tissue destruction in those granulomas progressing to active disease[8]. The matrix metalloproteinase (MMP) enzymes are major contributors to this remodeling process due to their ability to degrade ECM such as collagen and proteoglycans[9-11]. Among the MMP family, MMP-2 and MMP-9 are known to degrade type IV collagen, fibronectin and elastin in the lung[10, 12, 13], and are markedly up-regulated in expression in human tuberculosis granulomas[14, 15]. Other MMPs have been studied in human tuberculosis tissue and the expression of MMP-1[16-18], MMP-8[19] and MMP-14[20] are significantly up-regulated. Many

studies suggested that this up-regulation of MMPs is induced by Mtb infection, and eventually leads to collagen destruction and granuloma necrosis[16-25]. Studies using MMP inhibitors in Mtb infected animal models have generated conflicting data. Hernandez-Pando et al. observed a type-2 cytokine response profile and a delayed granuloma formation in murine pulmonary tuberculosis after treatment with MMP inhibitors[26]. In contrast, Izzo et al. observed increased collagen deposition in early granuloma formation after MMP inhibition, as well as a reduced bacterial burden in the lung at early phase[27]. However, a subsequent study from the same group did not observe a reduced bacterial burden in the lung following MMP inhibition[10]. These studies argue that there is value in further analysis of the impact of MMP inhibition on disease progression and on granuloma architecture.

Most current TB regimens involve a combination of the four drugs (isoniazid, rifampicin, ethambutol, pyrazinamide) as the first-line of treatment. However, the duration of treatment required to generate an enduring cure is usually 6-9 months. Not surprisingly, issues of non-compliance and failure occur frequently, and lead to the ongoing emergence of drug-resistant strains. Selection for drug resistant Mtb happens independently at multiple different geographic locations and is a widespread problem. Therefore, effective strategies to shorten the treatment duration and reduce the incidence of drug resistance are critically important.

In this study, we examined existing human TB granuloma datasets [14] in combination with infectious and non-infectious granuloma models to probe the increased

expression of MMP-2 and MMP-9 in Mtb granulomas. Treatment of Mtb-infected mice with a panel of small molecule MMP inhibitors alone had no effect on bacterial burden, but markedly enhanced bacterial killing by the frontline TB drugs INH and RIF approximately 10-fold. We verified the *in vivo* activity of these inhibitors through demonstrating that they block MMP-mediated cleavage of collagen and the mannose binding lectin (MBL). Treatment with these inhibitors also impacted granuloma morphology and appeared to stabilize the blood vessels that irrigated the infection site. Consistent with the improved blood vessel health, we found that MMP inhibition enhanced drug penetrance/retention in the infected tissue, which explains the enhanced efficacy of the anti-TB compounds used in combination with MMP inhibitors.

2.2 Methods

Ethics statement

All animal experiments were performed in strict accordance with the National Institutes of Health "Guide for the Care and Use of Laboratory Animals", and approved by Cornell University Institutional Animal Care and Use Committee under protocols 2006-0019, 2011-0086, 2010-0100, 2013-0003. All animal experiments performed inside Biosafety Level 3 facility were approved under protocol 2011-0086. All efforts were made to minimize suffering.

Mouse and Bone marrow-derived macrophage

C57BL/6J mice, MBL knockout mice (B6.129S4-Mbl1^{tm1Kata} Mbl2^{tm1Kata}/J) were obtained from the Jackson Laboratory and housed under pathogen-free conditions.

Bone marrow-derived macrophages (BMDMs) were isolated from bone marrow of C57BL/6J wild type mice, and maintained in DMEM (Corning Cellgro) containing 10% FBS (Thermo Scientific), 10% L929-cell conditioned media, 2mM L-glutamine, 1mM sodium pyruvate and antibiotics (penicillin/streptomycin) (Corning cellgro), at 37ºC in a 5% CO2 incubator[28, 29].

Reporter cell line, plasmid construction, IVIS imaging

To validate the up-regulation of MMP-2 and MMP-9 during Mtb infection, we constructed reporter cell lines that have promoters of *Mmp-2* and *Mmp-9* upstream of GFP and luciferase encoding cassettes. The luminescent signal was detected and

quantified by the IVIS imaging instrument. The primers sequences for *Mmp-2* and *Mmp-9* promoter's region were designed using PrimerPremier5 (Table1).

	Primer sequence
Mmp-2	F: CCATCGATGCAAAGGTGACAACCGTGA R: GGACTAGTGGCTGGAAGAGTGCTGGC
Mmp-9	F: CCATCGATTAGAAGCAGGAGGACCCGA R: GGACTAGTTGGCTAACGCTGCCTTTG

Table 1. Primer sequence of *Mmp-2* and *Mmp-9*

Mouse genome DNA was used as template to amplify the sequences, which were inserted into plasmid pGreen-Fire. Vectors with genes of interest were transferred into RAW 264.7 macrophage cell line (ATCC® TIB-71™) using a lentivirus infection system. Single colonies were picked and validated for expression levels of GFP and luciferase. We used a non-infectious Mtb trehalose dimycolate (TDM) granuloma model to test whether these stable cell lines can express GFP and luciferase [30, 31]. TDM coated beads were suspended in Matrigel, mixed with the reporter RAW cell lines, and inoculated subcutaneously in the scruff of a mouse. The mice were anesthetized at certain time points, injected with luciferase substrate and imaged with a IVIS machine (Caliper Lifescience).

TDM granuloma model and the Mtb/Matrigel granuloma model

TDM matrigel injection method has been described previously[14, 31, 32]. Briefly, 1mg TDM (Enzo life science) was dissolved in 100μl chloroform/methanol mixture (2:1). 4μl of the dissolved TDM (40μg) was transferred to a glass tube and dried under nitrogen gas. 150μl polystyrene microspheres (approximately 10^4 particles 79.4±0.5μm Duke Scientific) were washed with 1ml PBS and added to the tube. The tube was sonicated in 55℃ water bath for 1h, in order to coat the TDM onto the beads. 5×10^6 BMDMs or reporter RAW cells were harvested and mixed with TDM-coated beads in 400μl cold Matrigel (Corning). 27G syringe was used to inject the mixture subcutaneously in the mouse scruff. After 7 days, mice were sacrificed and matrigel tissue was extracted for histology or collagen content measurement.

For Mtb/Matrigel granulomas, Mtb Erdman from frozen titered stocks was passaged through 25G syringe 8 times to dissociate clumps. The stock was diluted 1000 times in PBS containing 0.05% Tween 80 and 10^3 bacteria in 25μl were mixed with 400μl matrigel containing 5×10^6 BMDMs, and injected subcutaneously into the mouse scruff. After 28 days, mice were sacrificed and matrigel tissue was extracted for histology or collagen content measurement.

Lung infection and drug treatment

In order to investigate drug effects on pulmonary Mtb infection, we infected mice intranasally as described previously[33, 34]. Mice were anesthetized with isoflurane and then 25μl of PBS+0.5% Tween 80 containing 10^3 bacteria was delivered into the nares of the mice. Erdman WT and the fluorescent reporter strains Erdman

(*smyc'*::mCherry) were used for infection experiments as described previously[33]. After mice were euthanized, the left lobe and the accessory lobe were used for CFU plating, while the right lobes were either fixed in 4% paraformaldehyde for confocal microscopy or histological analysis, or used for protein extraction and collagen content measurement.

Marimastat (10mg/kg/day) and other MMP inhibitors were delivered via intra-peritoneal injection every other day starting 7 days post infection. INH (12.5mg/kg/day) and RIF (5mg/kg/day) were added to the drinking water starting 14 days post infection and replenished every week.

Tissue Collagen Quantitation

Method is adapted from C. Kliment et al[35]. Briefly, tissue samples were weighed and put into glass tubes, which were placed in 100℃ heat blocks inside a fume hood until the tissue were completely dry[35]. 2ml of 6M HCl was added to each tube, which was sealed under inert gas and incubated on the heat block for 24h. 2ml of PBS was added to each tube to reconstitute the sample and incubated at 60℃ for 1h. The samples were centrifuged at 14,000rpm to remove the undissolved substance and analyzed for hydroxyproline content. 400µl sample was incubated with 200µl chloramine-T solution (50mM chloramine-T, 30% v/v 2-methoxyethnol and 50% v/v hydroxyproline buffer) for 20 min at room temperature. Then 200µl perchloric acid (BioVision) was added and tubes were incubated 5min at room temperature. Finally, 200µl p-dimethylamino-benzaldehyde solution (1.34M p- dimethylamino-

benzaldehyde dissolved in 2-methoxyethnol) was added to each tube and tubes were incubated at 60℃ for 20min. Absorbance measurements were read in a 96-well plate at 557nm on Envision plate reader (PerkinElmer).

Confocal immunofluorescence microscopy

Confocal analysis was conducted as detailed previously[33]. Briefly, lung tissue was sectioned in to 1 mm thick slices with a razor blade. Then tissue was blocked and permeabilized in PBS + 3% BSA + 0.1% Triton X-100 at room temperature for 1h in the dark. Samples were incubated with primary antibody (CD31, 1:100, BD; α-SMA, 1:200, Abcam) overnight at 4℃ and corresponding secondary antibodies, in the presence of DAPI (1:500) and Alexa fluor 647 conjugated Phalloidin (1:50) at room temperature for 2h in the dark. Samples were washed 3 times with PBS and mounted with mounting medium (Vectorshield). Imaging was conducted using a Leica SP5 confocal microscope and signal was quantified by Volocity software[33].

Immunohistochemistry and quantitative image analysis

Infected lung tissues were fixed and sectioned by the Histology lab of Animal Health Diagnostic Center in Cornell University. Briefly, unstained slides were hydrated and stained with primary antibodies (CD31, 1:1000, BD; α-SMA, 1:500, Abcam) overnight at 4℃. Slides were washed and stained with secondary antibodies (1:200, biotinylated goat anti-rabbit IgG antibody, Vector lab) and ABC kit at room temperature for 2h. Sections were developed with DAB and mounted for digital

scanning (Scanscope, Aperio Technologies). Blind quantitative analysis of IHC images were performed with the Imagescope (Aperio Technologies) software.

Western blot

The middle lobe of the right lung from mice infected with Erdman strain Mtb was homogenized within cold RIPA buffer supplemented with protease inhibitor (Roche) to extract protein. Proteins were run on 10% SDS-PAGE gel and later transferred to PVDF membrane (Millipore). The membrane was incubated with primary antibody (MBL 1:100 Hycult; MMP-2 and MMP-9, 1:2000 Abgent) overnight at 4℃ and with secondary antibodies at room temperature for 2h. The membranes were incubated with Super Pico Chemiluminescent Solution kit for 5min and developed with Amersham Hyperfilm™ ECL films (GE Healcare).

Evans Blue dye quantitation in infected mouse lung

Mice infected with Erdman Mtb were treated with Marimastat as described above. At 4 weeks post infection, mice received a retro-orbital injection of 25mg/kg Evans blue dye and sacrificed 30min after injection. The left lobe and accessary lobe were used for CFU plating and the right lobes were homogenized and incubated in formamide at 55℃ for 20h to extract the dye. The homogenate was centrifuged and the supernatant was read for absorbance at 620nm and 740nm. The following formula was used to correct for contamination with heme pigment[36-38]:

$$E620_{corrected} = E620_{raw} - (1.426 \times E740_{raw} + 0.030)$$

A standard curve was used to calculate the amount of dye in the lung, which was

further normalized to tissue weight.

Frontline TB drugs measurement in infected animals by high-pressure liquid chromatography coupled to tandem mass spectrometry (LC-MS/MS) analysis

Methods were adapted from previous studies measuring ethambutol in pulmonary TB lesion [39]. Briefly, mice were infected with Erdman Mtb and treated with Marimastat as described above. At 4 weeks, infected animals received a single retro-orbital injection of RIF 2mg/kg and INH 5mg/kg, and sacrificed 1h, 2h and 4h after injection. Lung tissue was collected and homogenized by adding 3 parts of PBS buffer. Samples were shaken using a SPEX Sample Prep Geno/Grinder 2010 for 5 minutes at 1500 rpm with steel beads. Blood samples were collected in tubes coated with K_2EDTA and centrifuged at 4000 rpm for 10 min to collect plasma. Standards and QCs were created by adding 10 μL of spiking stock (neat 1 mg/mL DMSO stocks of RIF, INH, and Acetyl-INH diluted in 50/50 (Acetonitrile/water)) to 90 μL of drug free plasma (Bioreclamation) or control lung tissue homogenate. 20 μL of control, standards, QCs, or study samples were added to 200 μL of Acetonitrile/Methanol 50/50 protein precipitation solvent containing 20 ng/mL RIF-d8, INH-d4, and Ac-INH-d4 (Toronto Research Chemicals). Extracts were vortexed for 5 minutes and centrifuged at 4000 rpm for 5 minutes. 100 μL of supernatant was combined with 100 μL of 2% cinnamaldehyde in methanol to derivatize INH. Mixture was vortexed for 30 minutes to complete reaction. 100 μL of mixture was combined with 100 μL of Milli-Q water prior to HPLC-MS/MS analysis.

High-pressure liquid chromatography (HPLC) coupled to tandem mass spectrometry (LC/MS/MS) analysis was performed on a Sciex Applied Biosystems Qtrap 4000 triple-quadrupole mass spectrometer coupled to an Agilent 1260 HPLC system to quantify the biological samples. Chromatography for RIF, INH, and Acetyl-INH was performed on an Thermo Hypersil Betasil C8 (2.1x50 mm; particle size, 5 μm) using a reverse phase gradient elution. The gradient used 0.1% formic acid and 0.01% Heptafluorobutyric Acid (HFBA) in Milli-Q deionized water for the aqueous mobile phase and 0.1% formic acid 0.01% HFBA in acetonitrile for the organic mobile phase. RIF-d8, INH-d4, and Acetyl-INH-d4 were used as internal standards (IS). The compounds were ionized using ESI positive mode ionization and monitored using masses RIF (823.50/791.60), RIF-d8 (831.50/799.60), INH (252.20/80.30), INH-d4 (256.20/84.30), Ac-INH (180.40/121.00), and Ac-INH-d4 (184.40/142.10).

Statistics

Two-tailed Unpaired Student *t* test with Welch-correction, 1-way and 2-way ANOVA with Šidák multiple comparison tests were conducted in Prism (GraphPad). All experiments were repeated at least twice. Number of mice used in each experiment is indicated in Figure legends.

2.3 Results

2.3.1 Induction of expression of MMPs in non-infectious and infectious TB granuloma models.

Previously we had performed transcriptional analysis on material acquired from cryosections from human pulmonary tuberculosis granulomas[14]. We re-analyzed the datasets from 5 caseous human pulmonary TB granuloma and 2 normal lung parenchyma (GSE20050)[14]. Differential analysis was performed using GEO2R to investigate the differential transcriptomic signature in TB granuloma tissue compared to the uninvolved tissue (Figure 2.1A). Among the differentially-expressed genes, transcripts for both MMP-9 and MMP-2 were significantly more abundant, over 190 fold ($\log_2$(FC)=7.6, p value, adjust p value < 0.001), and over 40 fold ($\log_2$(FC)=5.35, p value=0.001, adjusted p value = 0.016), respectively (Figure 2.1B). This is consistent with previous measurements of MMP expression in human tuberculosis granulomas[11, 16-21, 23, 24].

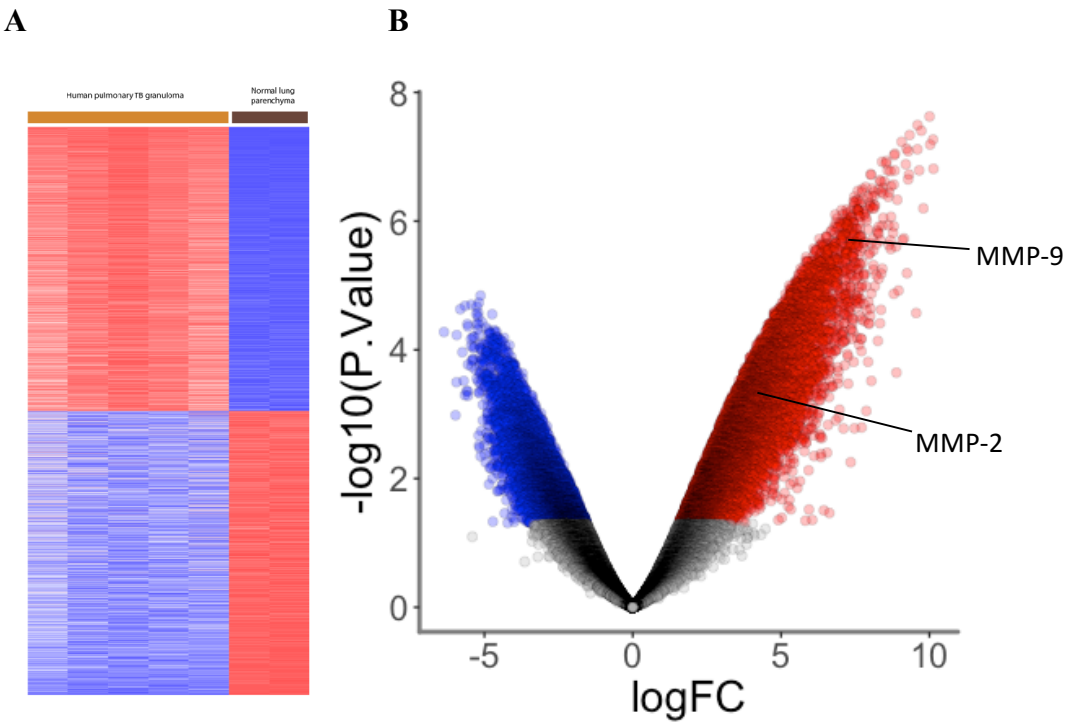

Figure 2.1 MMP-9 and MMP-2 level are up-regulated in human TB granuloma. **(A):** Heatmap showing gene expression profile generated from microarray dataset [34] analysis comparing 5 caseous human pulmonary TB granuloma and 2 normal lung parenchyma (GSE20050). **(B):** Volcano plot showed 12878 up-regulated genes (red dots, p.value < 0.05, Fold change >2) and 8062 down-regulated genes (blue dots, p.value < 0.05, Fold change <0.5) in TB granuloma. MMP-9 and MMP-2 were labeled among the up-regulated genes.

To examine the induction and expression of MMP-2 and MMP-9 in experimental infectious and non-infectious murine TB granuloma models we used both a subcutaneous granuloma model [14, 31, 32] for *in vivo* imaging in parallel with the more conventional, intranasal Mtb challenge. Western blot analysis of equivalent amounts of tissue from Mtb-infected and uninfected mouse lungs confirmed the increased expression of MMP-2 and MMP-9 in the Mtb-infected tissue (Figure 2.2A). In order to visualize the up-regulation in transcription of MMP-2 and MMP-9 genes we used reporter RAW cell lines that expressed luciferase under regulation of the MMP-2 and MMP-9 promoter regions. These cells were mixed with a Matrigel suspension containing polystyrene beads coated with the mycobacterial lipid TDM. TDM, or cord factor, is known to have granuloma-inducing properties and has been used previously in non-infectious granuloma models [30, 32, 40, 41]. The suspension was inoculated subcutaneously into the mouse scruff, and the tissue response to the challenge was imaged at days 3 and 7 post-inoculation. Quantification of the level of luciferase expression (Figure 2.2B and C) demonstrated the up-regulation of MMP promoter activity in the TDM-bead containing granulomas in comparison to those containing uncoated beads. These data confirm previous reports of up-regulated expression on MMPs in both human TB granulomas and the murine experimental granuloma models used in the current study[16-25].

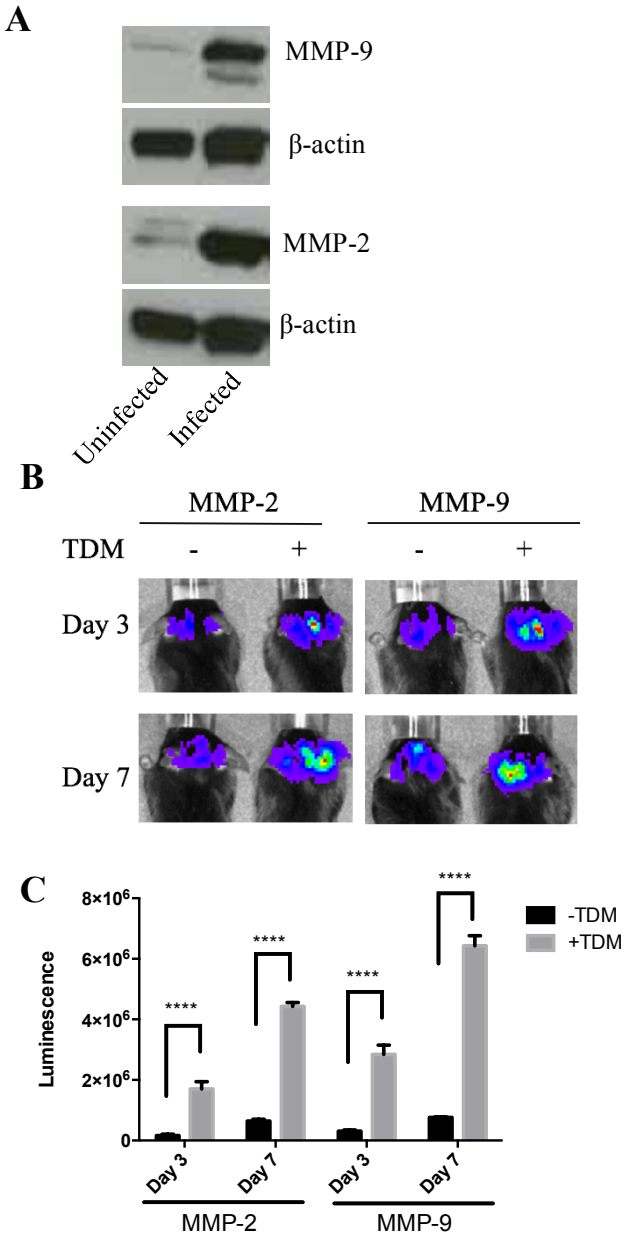

Figure 2.2 MMP-9 and MMP-2 level are up-regulated during murine Mtb infection or TDM induction.

(A): Protein level of MMP-9 and MMP-2 in uninfected and infected mice lung (n=3). Representative images were showed. **(B):** Representative images of luminescence

from MMP-9 or MMP-2 reporter cell lines within TDM granulomas in C57BL/6J mice. The same mice were imaged at Day 3 and Day 7 (n=5). Experiment performed twice with similar result. (**C):** Quantitative analysis of luminescent signal at Day 3 and Day 7 of MMP-2 and MMP-9 reporter cell lines within TDM granuloma (n=5). Data represented mean ± SD. ****: $p < 0.0001$, 2-way ANOVA with Šidák multiple comparison test.

2.3.2 The MMP inhibitor Marimastat impacts granuloma architecture and increases the potency of INH.

Marimastat is a broad spectrum MMP inhibitor that was developed as an anti-neoplastic drug candidate[42-44]. Treatment of mice with the drug induced morphological alterations in both subcutaneous TB granuloma models, including the TDM-bead Matrigel model and the Mtb-Matrigel subcutaneous challenge model (Figure 2.3A). The treatment appeared to result in higher cellular consolidation within the matrix. We probed the biological significance of this morphological change to disease progression through determination of both bacterial burden and histological change in mice challenged intranasally with Mtb. The design of the experiment is shown in Fig 2.3B. Mice were infected with Mtb then treated with PBS (control) or Marimastat from day 7 onwards. Mice were also treated with the frontline TB drug INH (+/- Marimastat) to explore the potential impact of MMP inhibition on drug efficacy. Mice were sacrificed at day 28 and process for both histology and bacterial counts.

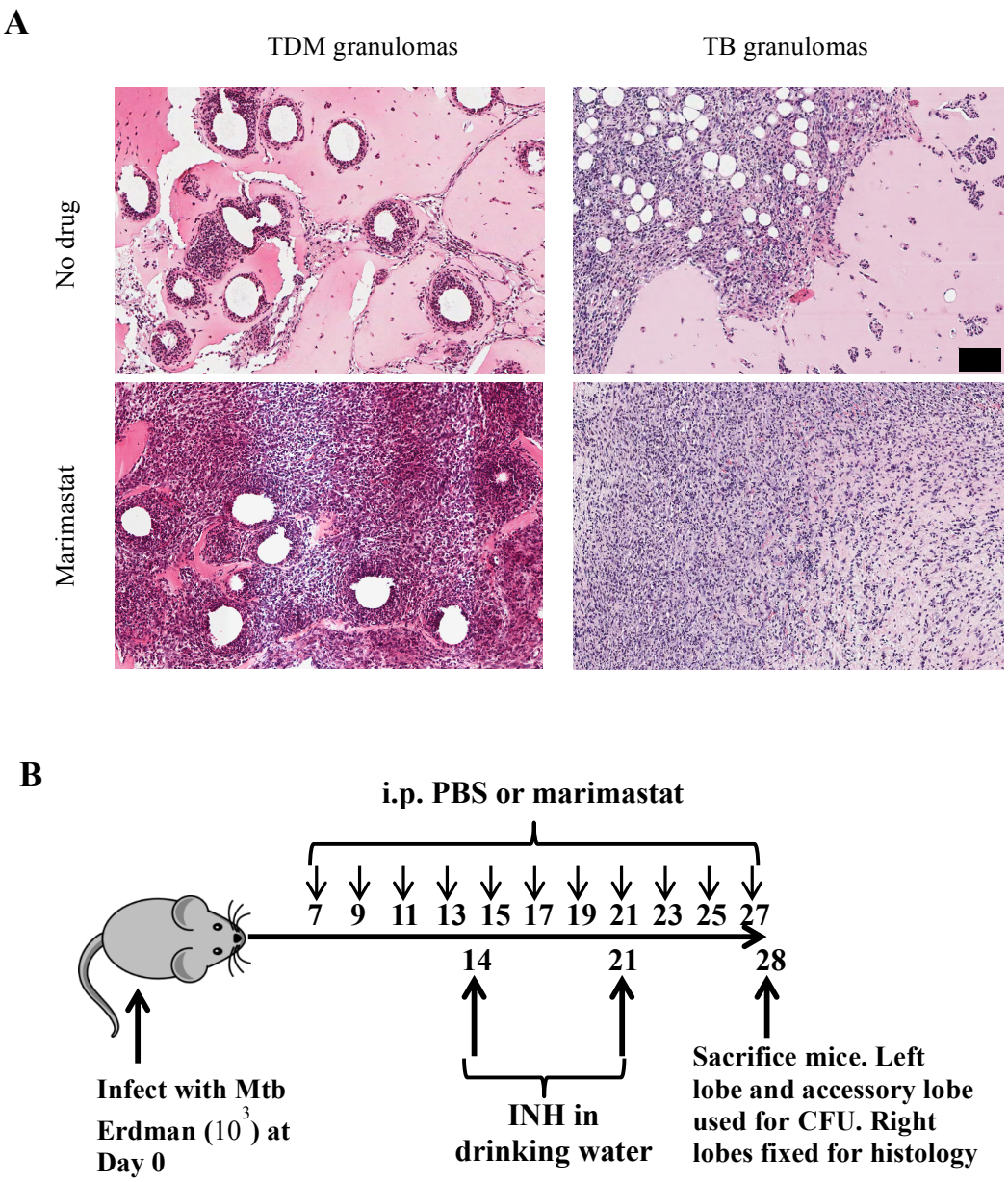

Figure 2.3 (**A**) MMP inhibitors increase cell infiltration in TDM granuloma and TB granuloma. Scale bar: 100μm. **(B)** Experimental setting of Marimastat's effect in lung infection model (n=5).

There was no statistically significant difference in bacterial load between the Marimastat and PBS groups at Day 14, Day 28 or Day 42 (Figure 2.4A), consistent with previous reports that inhibition of MMP activity did not impact bacterial burden[10, 26]. However, when INH was added into the drinking water, a synergistic effect was observed in the INH and Marimastat co-treated group (Figure 2.4A). INH alone reduced the bacteria load approximately ten-fold compared to the PBS control, while Marimastat and INH in combination reduced the bacterial load by another log over the INH only group (Figure 2.4A). This synergistic effect was significantly reduced but still observable by Day 42 (Figure 2.4A). The combination treatment also reduced size of the regions of cellular consolidation within the infected lung tissue, as shown by H&E staining (Figure 2.4B). This reduction is likely due to both MMP inhibition and the reduced inflammatory stimulation caused by the lower number of bacteria. The percentages of consolidated region within the whole tissue were measured and the percentages of consolidated region in PBS and Marimastat groups were comparable (Figure 2.4C). This percentage was decreased in the INH only group, and further reduced in the Marimastat and INH group (Figure 2.4C). This reduction correlates most closely with the CFU measurements.

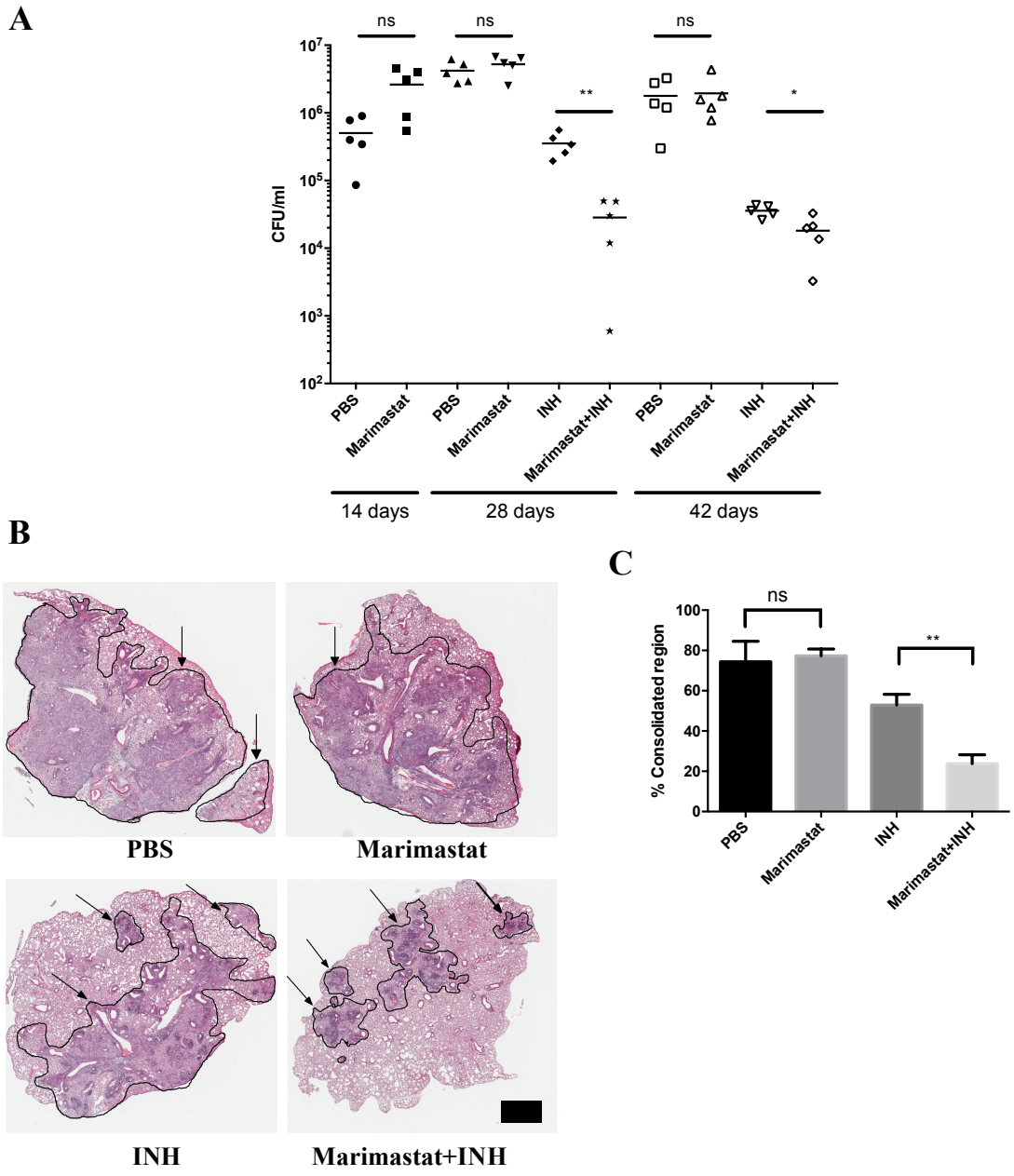

Figure 2.4 MMP inhibitors increase cell infiltration and facilitate INH killing of Mtb.

(A): CFU count of 2 groups (PBS and Marimastat) at Day 14, and 4 groups (PBS, Marimastat, INH and Mariamstat+INH) at Day 28 and Day 42 post infection. Each dot represented one mouse (n=5). Experiment was repeated 3 times with similar

observation. Data showed results from one representative experiment. **(B):** H&E stain of the 4 groups (PBS, Marimastat, INH and Mariamstat+INH) at Day 28 infection (n=5). Scale bar: 1mm. Arrow indicated consolidated region circled by black line. **(C):** Quantification of inflammatory region percentage within tissue of in all mice from different treatment groups (n=5). Data represented mean ± SD. **: $p < 0.01$, One-way ANOVA with Šidák multiple comparison test.

These data suggest that targeting MMP activities enhances the efficacy of INH against Mtb. To determine if this was due to activity at the level of the host cell or the host tissue environment we treated Mtb-infected BMDM with Marimastat in the presence and absence of INH. This tissue culture infection model did not recapitulate the synergistic effect of the two drugs combination (Figure 2.5), indicating that the synergy observed is dependent on the *in vivo* tissue environment.

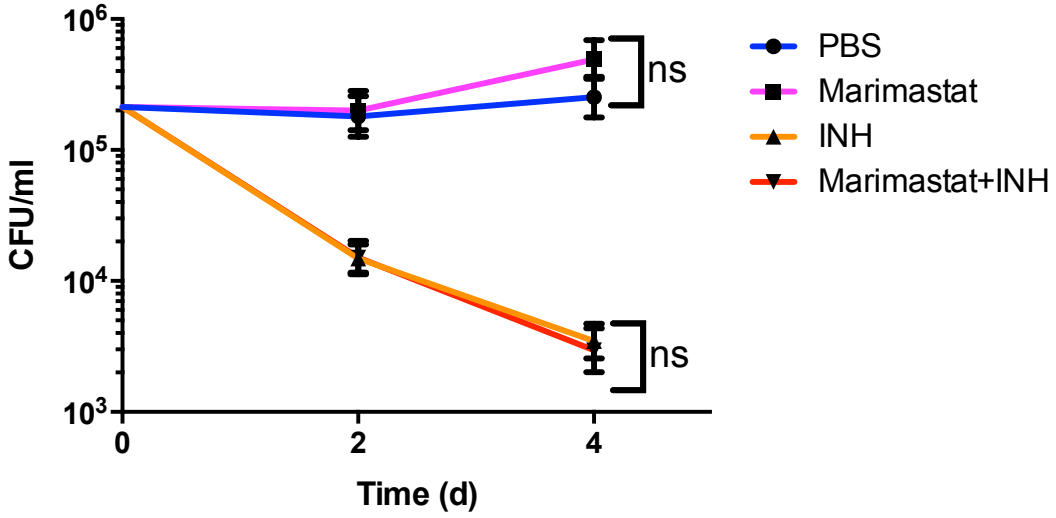

Figure 2.5 MMP inhibition does not synergize with frontline TB drug *in vitro*.

CFU count of BMDMs infected with Mtb and treated with PBS or Marimastat (20nM) for 2 or 4 days (n=5). Data represented mean ± SD. Two-way ANOVA with Šidák multiple comparison test.

2.3.3 The synergistic activities extend to both RIF and to other MMP inhibitors. Next, we investigated whether this synergetic effect could be observed with a different TB drug, RIF and/or with other MMP inhibitors. The combination of RIF and Marimastat decreased bacterial burden in comparison with RIF alone (Figure 2.6A), demonstrating that the ability of Marimastat to enhance anti-TB drug activity was not restricted to INH, and therefore unlikely to be linked to the specific mode of action of one anti-TB drug.

We then tested a panel of MMP inhibitors in combination with INH to determine if the synergy was Marimastat-specific. The panel of MMP inhibitors included (1) Batimastat, which shares a similar structure to Marimastat, but has lower water solubility, (2) Prinomastat, a structurally-unrelated broad spectrum MMP inhibitor, (3) Sb-3ct, a specific inhibitor of MMP-9 and MMP-2 and (4) MMP-9 inhibitor I, an inhibitor that exhibits much more specific activity against MMP-9[42]. In isolation, all these MMP inhibitors had minimal effect on bacterial burden. However, with the exception of Prinomastat, all the MMP inhibitors enhanced bacterial killing by INH (Figure 2.6B). Therefore, the synergistic effect between MMP inhibition and antibiotics is not limited to Marimastat and INH, but applied to other MMP inhibitors and other frontline TB drugs. Furthermore, this synergistic effect is likely due to inhibition of MMP-9/MMP-2.

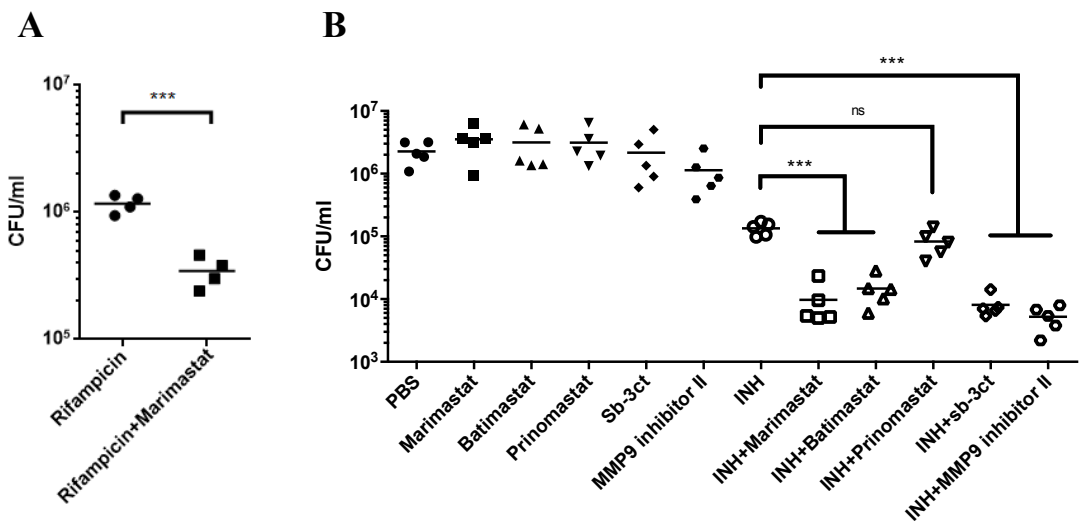

Figure 2.6 Other frontline TB drug (RIF) and other MMP inhibitors can induce synergistic effect to reduce Mtb burden.

(A): CFU count of lung tissue from Mtb-infected mice treated with Marimastat and RIF. Each dot represented one mouse (n=4). Data represented mean. ***: $p < 0.001$, Two-tailed Unpaired Student *t* test with Welch-correction. **(B):** CFU count of lung tissue from Mtb-infected mice treated with other MMP inhibitors and INH. Each dot represented one mouse (n=5). Data represented mean. ***: $p < 0.001$, One-way ANOVA with Šidák multiple comparison test.

2.3.4 Inhibition of MMP results in an increase in both collagen and Mannose Binding Lectin (MBL) within the infected tissue.

MMPs within the tissue have a wide range of substrates[12, 27, 43-46]. The most obvious target of these proteases is the extracellular matrix, including collagen. To verify the biological activity of Marimastat within the infection site we measured the levels of substrate within the tissue. The level of hydroxyproline, a modified amino acid specifically released from collagen degradation, was measured from infected mouse lung tissue. In the groups with Marimastat we observed a higher level of hydroxyproline, indicating higher collagen concentration (Figure 2.7A). Similar data were also generated in the TDM-Matrigel and the Mtb-Matrigel granuloma models (Figure 2.7B and C). However, interpretation of these data is complex because the fibrotic response itself is biologically-active[31, 32] and the outcome, greater collagen deposition, could be generated by other mechanisms in addition to reduced degradation of collagen by MMPs.

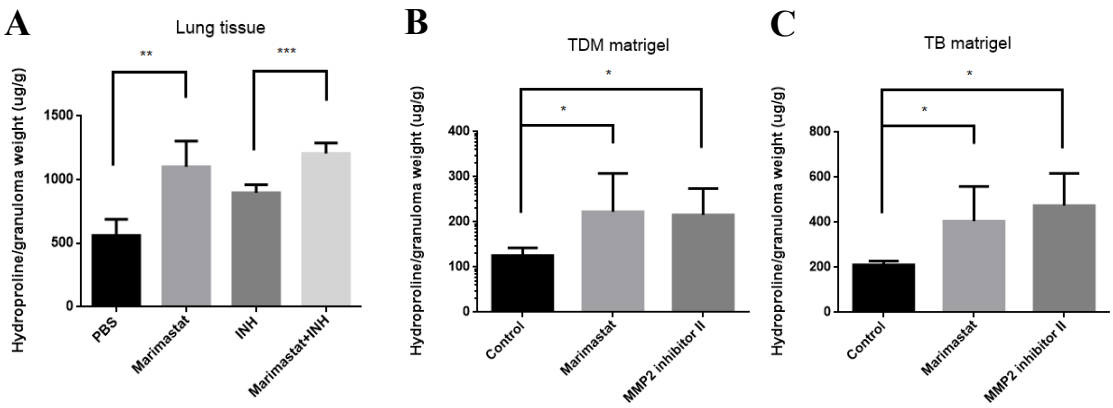

Figure 2.7 Inhibition of MMP results in an increase of collagen the infected tissue.

(A): 6-week-old Female C57BL/6J mice were infected with Erdman wildtype Mtb strain. Treatment of INH and Marimastat was indicated in Figure 2.3B. Lung tissue were collected and processed following method "Tissue collagen quantification" in the Method section. Hydroxyproline concentration in lung tissue from infected mice under different treatments (n=5). Data represented mean ± SD. **: $p < 0.01$, ***: $p < 0.001$, One-way ANOVA with Šidák multiple comparison test. **(B, C)**: 6-week-old Female C57BL/6J mice were injected with TDM matrigel or TB matrigel with or without MMP inhibitors (4μmol). TDM matrigel and TB matrigel was developed following the method "TDM granuloma model and the Mtb/Matrigel granuloma model" in the Method section. Matrigel tissue were collected and processed following method "Tissue collagen quantification" in the Method section. Hydroxyproline concentration in TDM matrigel (B) and TB matrigel (C) with Marimastat and MMP-2 inhibitor II treatment (n=5) from infected mice under different treatments (n=5). Data represented mean ± SD. *: $p < 0.05$, **: $p < 0.01$, ***: $p < 0.001$, One-way ANOVA with Šidák multiple comparison test.

Other known MMP substrates include the mannose-binding lectin (MBL), which has a collagen-like domain that is cleaved by MMP-2, MMP-9, and MMP-14[47]. MBL is an interesting immune modulator because it can recognize mycobacterial surface lipidoglycans[48-50], act as an opsonin, and activate the complement cascade[50, 51]. We examined the levels of MBL in the lung of Marimastat and INH treated, infected mice. Marimastat and INH combined treatment resulted in the highest MBL level (Figure 2.8A). The MBL level was relatively low in the Marimastat group compared to the Marimastat and INH group, which was due to higher MMP-2 and MMP-9 protein levels in the Marimastat group (Figure 2.8B). This may be a consequence of the larger number of bacteria present in the Marimastat group (Figure 2.4A), which could lead to MMP overproduction to compensate for the inhibition of Marimastat.

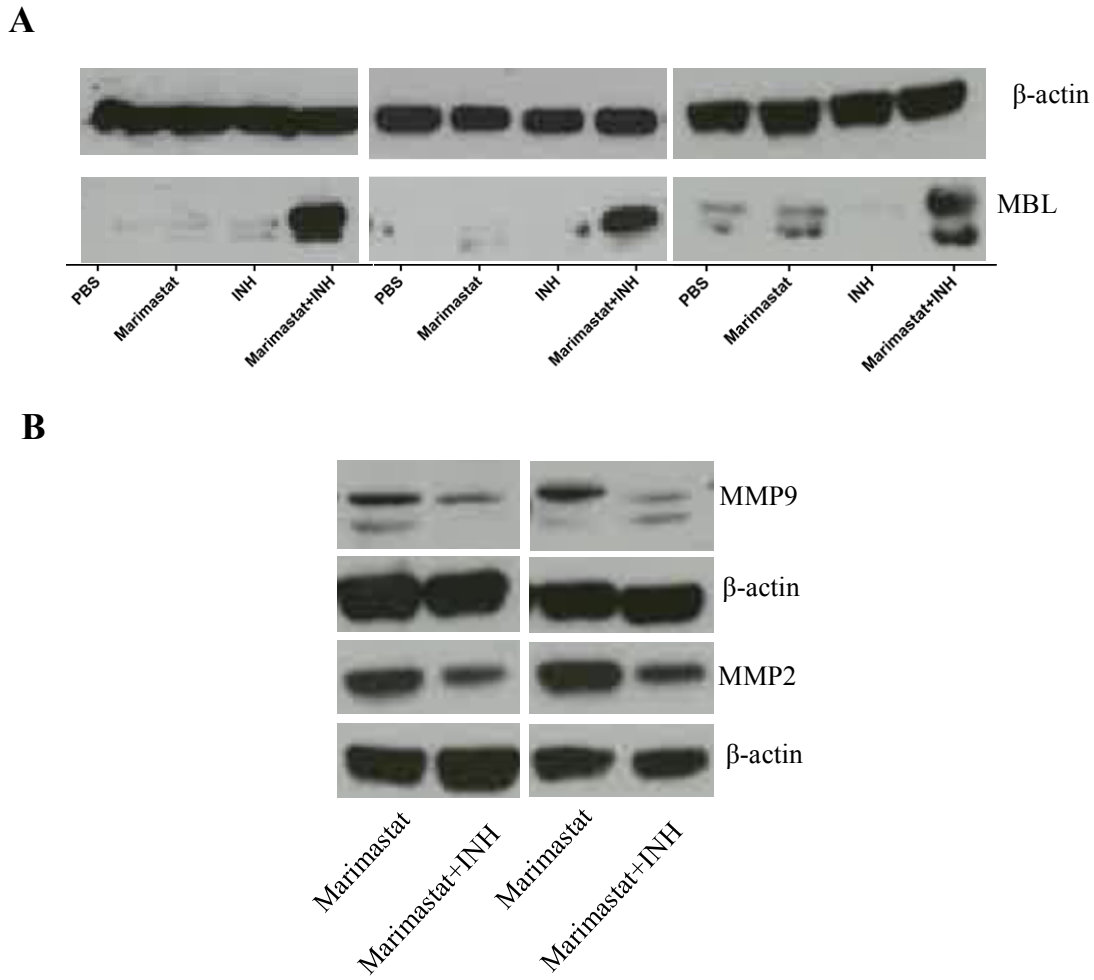

Figure 2.8 Inhibition of MMP results in an increase of Mannose Binding Lectin (MBL) within the infected tissue.

(A): Protein level of MBL in of Mtb infected mice under different treatments (n=5) in three separate experiments. (**B):** MMP-9 and MMP-2 protein level from lung lyse of infected mice with different treatments (n=5) in two separate experiments.

2.3.5 Increased blood vessel pericyte coverage by Marimastat treatment.

There is mounting evidence that MMPs have a strong effect on angiogenesis beyond ECM remodeling--MMPs can release ECM-bound angiogenic factors, detach pericytes from blood vessels, and degrade endothelial cell-cell adhesions[46, 52]. To test whether MMP inhibition impacts the vasculature at the infection site, we stained lung tissue of 4-week infected mice treated with PBS or Marimastat with CD31 for endothelial cells[53, 54]. We observed positive CD31 staining in sections from both PBS and Marimastat groups (Figure 2.9A, upper panel). Blinded histological analysis indicated that there was no significant difference in the number of CD31 positive blood vessels upon Marimastat treatment (Figure 2.9B).

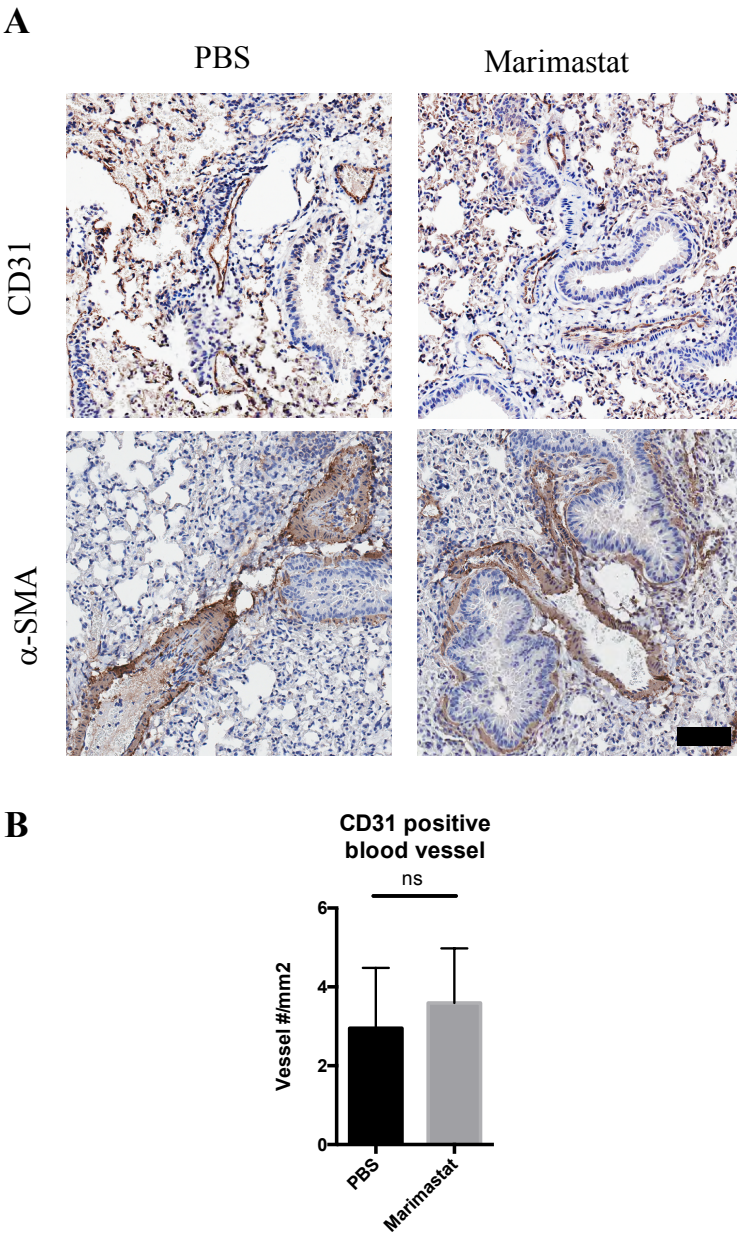

Figure 2.9 CD31 and α-SMA staining in the lung of infected mice treated with Marimastat.

(A): Mice infected with Mtb were treated with PBS (n=5) or Marimastat (n=5). Lung tissue from infected mice was stained for CD31 (upper panel) and α-SMA (lower panel). Scale bar: 80μm. **(B):** Quantification of CD31 positive blood vessel number.

We also stained tissue with alpha smooth muscle actin (α-SMA). α-SMA stains for pericytes which wrap around the endothelial layer to supply nutrients[53, 55], as well as for alpha smooth muscle cells around the bronchus, which can be easily distinguished from blood vessels by morphology (the bronchus has a single layer of columnar epithelial cells). Both the PBS group and Marimastat group had positive staining of α-SMA (Figure 2.9A, lower panel). Blinded histological analysis indicated that the percentage of positive α-SMA area was significantly higher in Marimastat group than that in PBS group (Figure 2.10A). Based on the positive staining of α-SMA, the blood vessel numbers from both groups were counted. The Marimastat group had significantly more α-SMA positive blood vessels than the PBS group (Figure 2.10B). This suggested that treatment with Marimastat increased the number of blood vessels covered by pericytes, while the total blood vessel number remained unchanged. Moreover, we counted the ✔-SMA positive blood vessels in the consolidated area (granuloma like structure) and the normal surrounding area separately. We found that the increase of pericyte coverage occurred in the surrounding area instead of in the consolidated area (Figure 2.10C and D). The numbers of blood vessels with positive α-SMA staining were not significantly different between the PBS and Marimastat treated groups at 2 weeks post infection (Figure 2.10F). As infection progressed to 4 weeks, the number of α-SMA positive blood vessels remained similar in the PBS control group, but was significantly increased by Marimastat treatment (Figure 2.10F), indicating MMP inhibition increases pericyte-covered blood vessels over time.

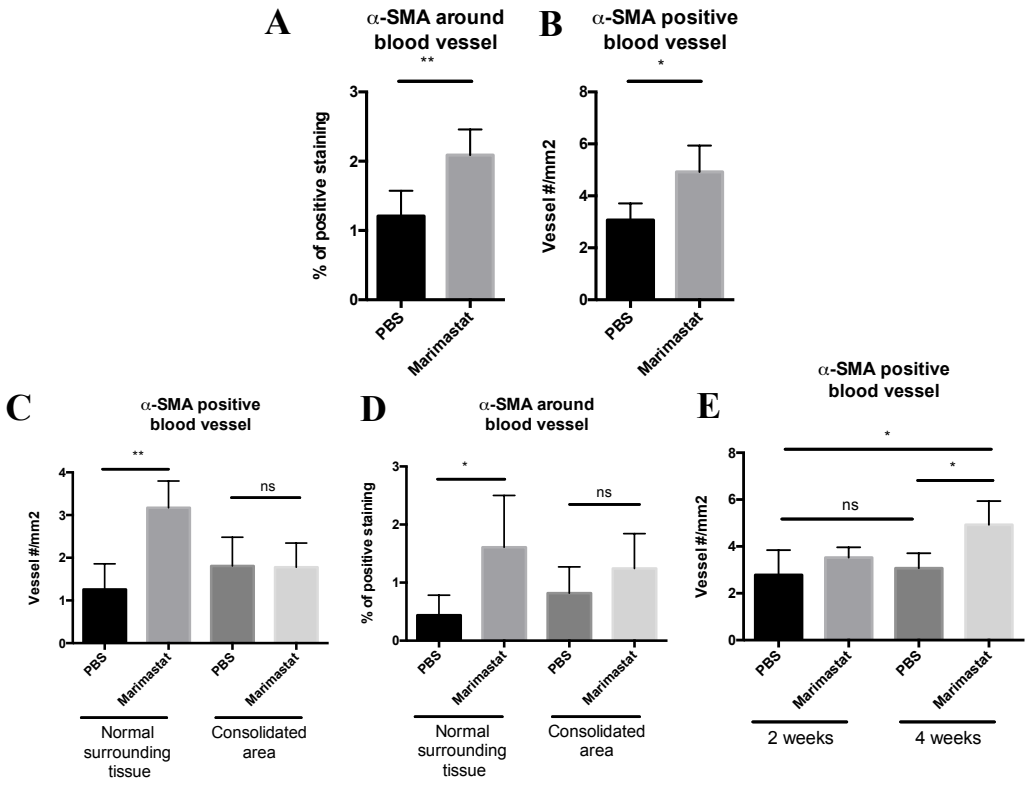

Figure 2.10 Quantification of α-SMA staining in the lung of infected mice treated with Marimastat.

(A, B): Quantification of percentage of α-SMA positive staining (A), and α-SMA positive blood vessel number (B) in PBS or Marimastat treated mice (n=5) 4-week post infection. Data represent mean ± SD. *: $p < 0.05$, **: $p < 0.01$, Two-tailed Unpaired Student *t* test with Welch-correction. **(C):** Quantification of α-SMA positive blood vessel number in consolidated area (granuloma like area) and surrounding normal tissue from PBS or Marimastat treated mice (n=5) 4-week post infection. (**D):** Quantification of percentage of α-SMA positive staining in consolidated area (granuloma like area) and surrounding normal tissue from PBS or Marimastat treated

mice (n=5) 4-week post infection. **(F)**: Quantification of α-SMA positive blood vessels number at 2-week and 4-week post infection from animal treated with PBS or Marimastat (n=5). Data represented mean ± SD. *: $p < 0.05$, **: $p < 0.01$. One-way ANOVA with Šidák multiple comparison test.

In summary, MMP inhibition reduced blood vessel abnormality by increasing pericyte coverage around the blood vessels. This increase of pericyte-covered blood vessel number and the improvement of blood vessel health could potentially enhance drug (such as INH) delivery or retention in the infected tissue environment.

2.3.6 Marimastat treatment reduces blood vessel leakage and increases drug delivery/retention in the lung.

Inflammation is known to increase vascular permeability[56-58] and we hypothesized that the increased pericyte coverage induced by Marimastat treatment might reflect a reversal of this permeability. To test the impact of Marimastat treatment on vascular permeability, we injected fluorescent dextran with different molecular weights to Mtb infected mice. Under normal, homeostatic conditions one would expect 10kDa dextran to passively diffuse out of the vasculature, while 70kDa dextran would be retained for longer. However, under inflammatory conditions, one would expect to see increased leakage of the 70kDa dextran[56]. Lung tissues from treated mice, infected or uninfected with Mtb, were fixed and stained for CD31 to mark the blood vessels, and imaged by a confocal microscope. Both PBS group and Marimastat group from infected mice showed positive staining of CD31 and fluorescent signal from the two dextran dyes (Figure 2.11A). We scored the 10kDa and 70kDa dextran signal that either co-localized with the CD31-positive blood vessels, or was present in the tissue outside the CD31-positive regions (Figure 2.11B and C). Compared to uninfected samples, Mtb-infected tissue had more 10kDa dextran outside blood vessels, indicating Mtb infection promotes neo-vascularization (Figure 2.11B). These new

blood vessels appeared to be leaky, as the levels of 70kDa dextran outside blood vessels were much higher in infected mice (treated with PBS) relative to the uninfected group (Figure 2.11C). Marimastat treatment reduced 70kDa dextran to a level similar to that of uninfected animals (Figure 2.11C), while further increased the 10kDa dextran level (Figure 2.11B). This suggests that Marimastat reduced blood vessel leakage and increased small molecule delivery in the lung, consistent with a "normalization" of the vasculature.

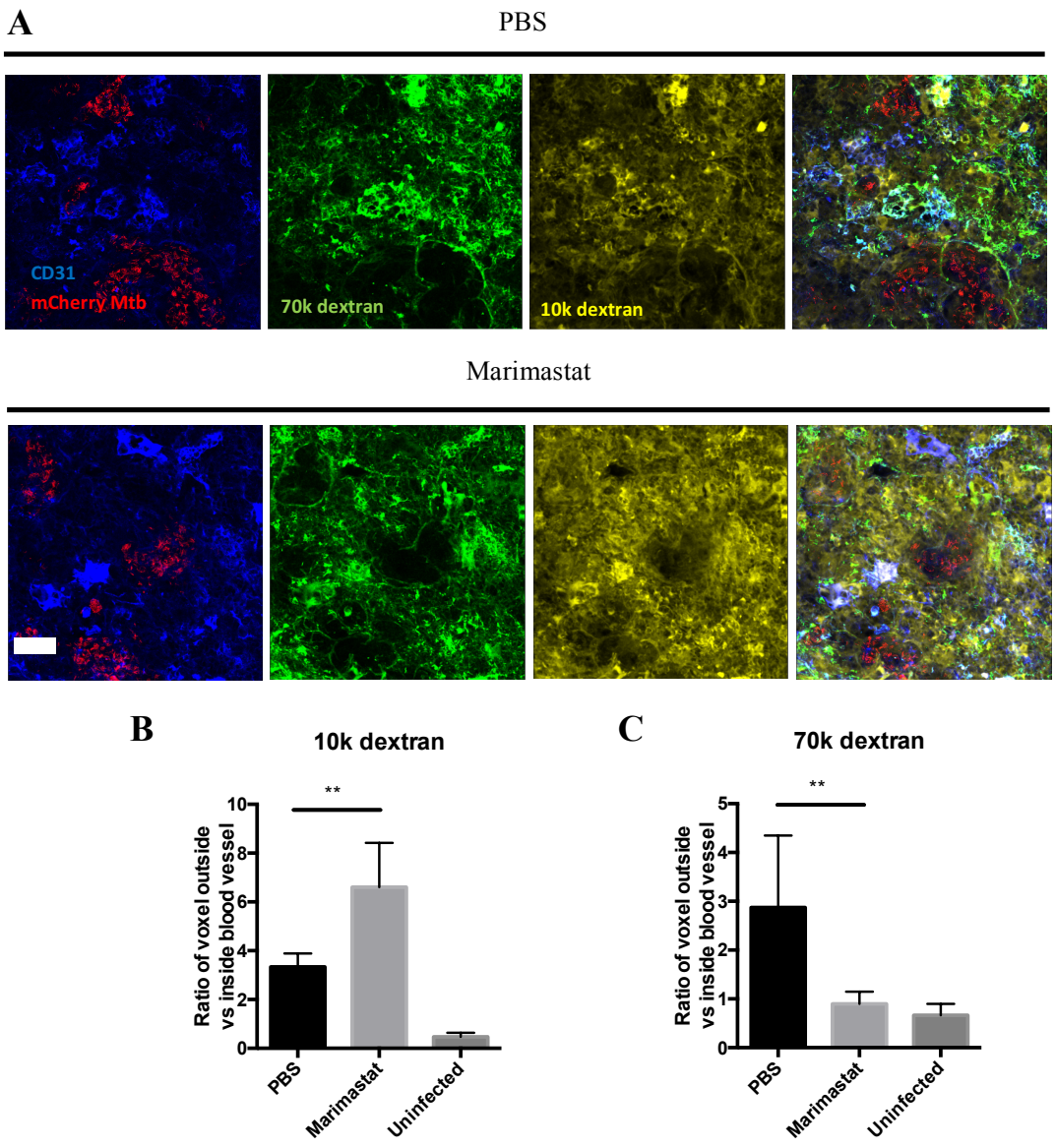

Figure 2.11 Leakage and delivery of blood vessels measured by fluorescent dextran.

(A): Mice infected with mCherry Mtb bacteria (red) were treated with PBS (n=3) or Marimastat (n=3). 70k dextran (green) and 10k dextran (yellow) were injected to mice

before euthanization. Lung tissue from infected mice was stained for CD31 (blue) to label the blood vessels. Both PBS and Marimastat groups had positive staining of CD31 and positive signal of 70k and 10k dextrans. Scale bar: 20μm. (**B):** Quantification of the ratio of 10k dextran outside vs inside of blood vessel (**C):** Quantification of the ratio of 70k dextran outside vs inside of blood vessel. Data represented mean ± SD. **: $p < 0.01$, One-way ANOVA with Šidák multiple comparison test.

The normalization of the vasculature in Mtb granulomas has been shown to improve small molecular delivery[53]. To determine whether or not Marimastat treatment could have a similar impact, we injected Evans blue dye intravenously into infected mice treated with or without Marimastat, and measured the dye retention in the lung tissue. We observed that there was an increase in Evans blue dye in the lungs of mice treated with Marimastat (Figure 2.12A), indicating that inhibition of MMP activity enhanced small molecule delivery and/or retention in the infected tissues. To further demonstrate this enhanced delivery and/or retention by MMP inhibition also applies to frontline TB drugs, we injected RIF and INH intravenously into infected mice treated with or without Marimastat. Intravenous injection of drugs minimizes inter-animal variation in absorption, which is a frequent confounding factor, particularly for RIF. Drug concentrations were measured in the harvested lung tissues at different time points by high-pressure liquid chromatography coupled to tandem mass spectrometry (HPLC-MS/MS) analysis, and normalized to the drug concentrations in the plasma [39]. 4h post drug injection, the Marimastat-treated group had significantly higher RIF and INH lung/plasma ratios than the PBS control group (Figure 2.12B and C), suggesting an enhanced drug delivery/retention by MMP inhibition. Although the drug concentrations decreased in the lung and plasma over time (Figure 2.12D-G), MMP inhibition maintained a relatively high INH concentration in the lung (Figure 2.12F). RIF concentration was not increased in the lung but decreased in the plasma upon MMP inhibition (Figure 2.12D and E), suggesting a faster turn-over rate of RIF. Taken together, these data indicated that inhibition of MMP activity enhanced frontline TB drug delivery and/or retention in the infected tissues through improving

blood vessel integrity.

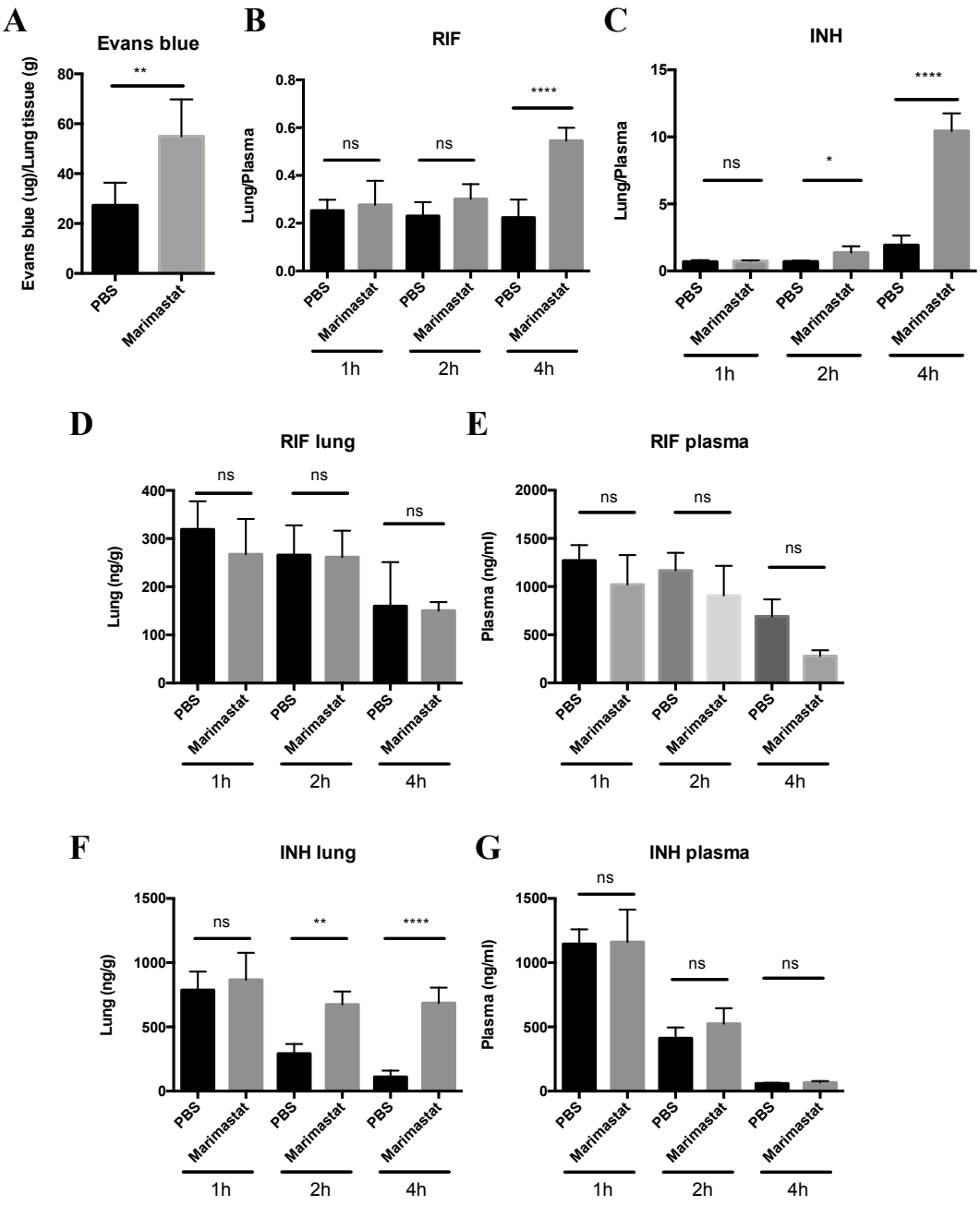

Figure 2.12 Delivery and/or retention of Evans blue dye or frontline TB drugs in infected animals treated with Marimastat.

(**A**): Mtb infected mice treated with or without Marimastat were injected intravenously with Evans blue dye before euthanization. Retention of Evans blue dye within the lung of infected mice treated with or without Marimastat. Data represented mean ± SD. **: $p < 0.01$, Two-tailed Unpaired Student *t* test with Welch-correction. Experiment was repeated twice. (**B** and **C**): Mtb infected mice treated with or without Marimastat were injected intravenously with RIF and INH before euthanization. At indicated time points, lung and blood samples were collected for drug measurement. The concentration of RIF (**B**) and INH (**C**) in the lung were normalized by drug concentration in the plasma. **(D-G)**: RIF and INH concentrations were measured in the lung (D, F) and the plasma (E, G). Data represented mean ± SD. *: $p < 0.05$, **: $p < 0.01$, ****: $p < 0.0001$, One-way ANOVA with Šidák multiple comparison test.

2.4 Discussion

Current therapeutic regimens for tuberculosis are cumbersome because of the need for multiple drugs (3-4) that have to be taken for 6-9 months. This places considerable strain on many healthcare systems, particularly those in under-resourced settings, and leads to ongoing problems of non-compliance and the emergence of drug-resistant Mtb strains. Given these challenges any strategy to increase the potency of our current anti-TB drugs could have tremendous benefit on tuberculosis control programs across the world. Here we show that small molecule MMP inhibitors increase the killing activity of the frontline anti-TB drugs INH and RIF. This enhanced killing was observed for several different MMP inhibitors suggesting that it is their anti-matrix metalloproteinase activity that confers their synergistic activity. We found that MMP inhibition improved blood vessel health, leading to increase of drug delivery and/or retention in the lung, which resulted in increased drug efficacy.

The majority of Mtb animal studies use the mouse as host. Different mouse strains and different infection methods created a number of Mtb murine models [59, 60]. However, mice infected with Mtb fail to form the well-defined and highly stratified granuloma structure, which is commonly seen in human TB patients [6, 7]. The granuloma structure developed in our murine model resembles an early stage human granuloma, where activated macrophages surround the infected cells with a layer of lymphocytes at the peripheral [59, 60]. Murine granulomas rarely progress to necrosis, which characterize late stage or disseminated human TB granulomas [6, 7]. Moreover, mice do not express MMP-1, which, along with other MMPs, is associated with tissue

destruction and transmission in disseminated human granuloma [23]. However, while there are limitations to murine models of Mtb pathogenesis, one cannot ignore the convenience of such a tractable experimental system if used appropriately. Different murine models are widely used to study essential bacterial genes or host immune response, because of their availability and well-characterized genetic variations. Recently, studies using resistant mouse strain infected with *M. marinum* [61], or susceptible mouse strain infected with Mtb [59, 60] observed granuloma-like structures with necrotic center in the lung, resembling the human granuloma. Moreover, murine models provide an *in vivo* platform to screen novel TB drugs for efficacy or synergy with frontline TB drugs, before advancing to costly non-human primate experiments or human clinical trials. We therefore believe that the mouse represents a valuable tool for discovery prior to downstream validation of ones finding in more restrictive platforms.

Treatment of Mtb-infected mice with Marimastat reduces extracellular matrix turnover and breakdown of the mannose-binding protein MBL. Histological analysis and vasculature-permeability experiments both indicate that the blood vessels in the TB granulomas were stabilized by Marimastat treatment. Healthy blood vessels, instead of leaky vessels, can improve the amount of drug, that is given orally, delivered to the lung. As a result, there is an improved tissue retention of small molecules and anti-TB drugs. Moreover, healthy blood vessels can potentially enhance drug accessibility to the bacteria at the center of a confined structure. Improvement of drug delivery through the normalization of blood vessels is widely accepted as a means of enhancing

the efficacy of anti-cancer drugs[62, 63]. Several phase III clinical studies have shown that combination of conventional chemotherapeutic drugs with FDA approved anti-angiogenesis drugs can significantly improve survival of patients with non-small lung cancer[64], breast cancer[65] and metastatic colorectal cancer[66, 67]. Moreover, the anti-VEGF drug, Bevacizumab, which is approved by FDA to treat metastatic colorectal cancer[68], also enhances small molecule delivery to tuberculosis granulomas in rabbits[53]. Additionally, Oehlers et al. showed that VEGF inhibitors can synergize with RIF to reduce bacterial burden of *M. marinum* in Zebrafish [69]. Based on our findings, it is reasonable to add doxycycline, an anti-mycobacteria antibiotic [70] and the only FDA-approved MMP inhibitor, to the current anti-TB drug regimens as an adjunctive drug. Specific MMP inhibitors like Marimastat were well-tolerated in animals and have been tested in clinical trials to target cancer metastasis [42, 71]. Respiratory dysfunction, a possible adverse effect considering increased fibrosis by MMP inhibition in the lung, was not identified in these clinical trials. Moreover, these side effects may be prevented by avoiding high-dose treatment [42, 71].

These data underline the importance of exploiting strategies that improve the efficacy of existing drugs as a readily tractable means of increasing the effectiveness of our anti-TB therapy. The possible addition of cheap, well-tolerated drugs such as MMP inhibitors to current multi-drug regimens is a practical and attractive means of increasing potency.

2.5 Reference

1. World Health Organization. Global tuberculosis report 2016. World Health Organization, 2016.

2. Centers for Disease Control and Prevention. Drug Resistant Tuberculosis: The Next Global Health Crisis? Centers for Disease Control and Prevention, 2015.

3. Manjelievskaia J, Erck D, Piracha S, Schrager L. Drug-resistant TB: deadly, costly and in need of a vaccine. Trans R Soc Trop Med Hyg. 2016;110(3):186-91. doi: 10.1093/trstmh/trw006. PubMed PMID: 26884499; PubMed Central PMCID: PMCPMC4755426.

4. Dye C, Williams BG. The population dynamics and control of tuberculosis. Science. 2010;328(5980):856-61. doi: 10.1126/science.1185449. PubMed PMID: 20466923.

5. Dye C, Glaziou P, Floyd K, Raviglione M. Prospects for tuberculosis elimination. Annu Rev Public Health. 2013;34:271-86. doi: 10.1146/annurev-publhealth-031912-114431. PubMed PMID: 23244049.

6. Russell DG. Who puts the tubercle in tuberculosis? Nat Rev Microbiol. 2007;5(1):39-47. doi: 10.1038/nrmicro1538. PubMed PMID: 17160001.

7. Russell DG, Cardona PJ, Kim MJ, Allain S, Altare F. Foamy macrophages and the progression of the human tuberculosis granuloma. Nat Immunol. 2009;10(9):943-8. doi: 10.1038/ni.1781. PubMed PMID: 19692995; PubMed Central PMCID: PMCPMC2759071.

8. Orme IM, Basaraba RJ. The formation of the granuloma in tuberculosis infection. Semin Immunol. 2014;26(6):601-9. doi: 10.1016/j.smim.2014.09.009.

PubMed PMID: 25453231.

9. Salgame P. MMPs in tuberculosis: granuloma creators and tissue destroyers. J Clin Invest. 2011;121(5):1686-8. doi: 10.1172/JCI57423. PubMed PMID: 21519148; PubMed Central PMCID: PMCPMC3083780.

10. Taylor JL, Hattle JM, Dreitz SA, Troudt JM, Izzo LS, Basaraba RJ, et al. Role for matrix metalloproteinase 9 in granuloma formation during pulmonary Mycobacterium tuberculosis infection. Infect Immun. 2006;74(11):6135-44. doi: 10.1128/IAI.02048-05. PubMed PMID: 16982845; PubMed Central PMCID: PMCPMC1695484.

11. Ong CW, Elkington PT, Friedland JS. Tuberculosis, pulmonary cavitation, and matrix metalloproteinases. Am J Respir Crit Care Med. 2014;190(1):9-18. doi: 10.1164/rccm.201311-2106PP. PubMed PMID: 24713029; PubMed Central PMCID: PMCPMC4226026.

12. Parks WC, Shapiro SD. Matrix metalloproteinases in lung biology. Respir Res. 2001;2(1):10-9. doi: 10.1186/rr33. PubMed PMID: 11686860; PubMed Central PMCID: PMCPMC59564.

13. Woessner JF, Jr. Role of matrix proteases in processing enamel proteins. Connect Tissue Res. 1998;39(1-3):69-73; discussion 141-9. PubMed PMID: 11062989.

14. Kim MJ, Wainwright HC, Locketz M, Bekker LG, Walther GB, Dittrich C, et al. Caseation of human tuberculosis granulomas correlates with elevated host lipid metabolism. EMBO Mol Med. 2010;2(7):258-74. doi: 10.1002/emmm.201000079. PubMed PMID: 20597103; PubMed Central PMCID: PMCPMC2913288.

15. Ong CW, Pabisiak PJ, Brilha S, Singh P, Roncaroli F, Elkington PT, et al. Complex regulation of neutrophil-derived MMP-9 secretion in central nervous system tuberculosis. J Neuroinflammation. 2017;14(1):31. doi: 10.1186/s12974-017-0801-1. PubMed PMID: 28173836; PubMed Central PMCID: PMCPMC5294728.

16. Elkington PT, Emerson JE, Lopez-Pascua LD, O'Kane CM, Horncastle DE, Boyle JJ, et al. Mycobacterium tuberculosis up-regulates matrix metalloproteinase-1 secretion from human airway epithelial cells via a p38 MAPK switch. J Immunol. 2005;175(8):5333-40. PubMed PMID: 16210639.

17. Elkington PT, Nuttall RK, Boyle JJ, O'Kane CM, Horncastle DE, Edwards DR, et al. Mycobacterium tuberculosis, but not vaccine BCG, specifically upregulates matrix metalloproteinase-1. Am J Respir Crit Care Med. 2005;172(12):1596-604. doi: 10.1164/rccm.200505-753OC. PubMed PMID: 16141443.

18. Rand L, Green JA, Saraiva L, Friedland JS, Elkington PT. Matrix metalloproteinase-1 is regulated in tuberculosis by a p38 MAPK-dependent, p-aminosalicylic acid-sensitive signaling cascade. J Immunol. 2009;182(9):5865-72. doi: 10.4049/jimmunol.0801935. PubMed PMID: 19380835.

19. Gong H, Rehman J, Tang H, Wary K, Mittal M, Chaturvedi P, et al. HIF2alpha signaling inhibits adherens junctional disruption in acute lung injury. J Clin Invest. 2015;125(2):652-64. doi: 10.1172/JCI77701. PubMed PMID: 25574837; PubMed Central PMCID: PMCPMC4319409.

20. Sathyamoorthy T, Tezera LB, Walker NF, Brilha S, Saraiva L, Mauri FA, et al. Membrane Type 1 Matrix Metalloproteinase Regulates Monocyte Migration and Collagen Destruction in Tuberculosis. J Immunol. 2015;195(3):882-91. doi:

10.4049/jimmunol.1403110. PubMed PMID: 26091717; PubMed Central PMCID: PMCPMC4505956.

21. Volkman HE, Pozos TC, Zheng J, Davis JM, Rawls JF, Ramakrishnan L. Tuberculous granuloma induction via interaction of a bacterial secreted protein with host epithelium. Science. 2010;327(5964):466-9. doi: 10.1126/science.1179663. PubMed PMID: 20007864; PubMed Central PMCID: PMCPMC3125975.

22. Brilha S, Sathyamoorthy T, Stuttaford LH, Walker NF, Wilkinson RJ, Singh S, et al. Early Secretory Antigenic Target-6 Drives Matrix Metalloproteinase-10 Gene Expression and Secretion in Tuberculosis. Am J Respir Cell Mol Biol. 2017;56(2):223-32. doi: 10.1165/rcmb.2016-0162OC. PubMed PMID: 27654284; PubMed Central PMCID: PMCPMC5359650.

23. Elkington P, Shiomi T, Breen R, Nuttall RK, Ugarte-Gil CA, Walker NF, et al. MMP-1 drives immunopathology in human tuberculosis and transgenic mice. J Clin Invest. 2011;121(5):1827-33. doi: 10.1172/JCI45666. PubMed PMID: 21519144; PubMed Central PMCID: PMCPMC3083790.

24. Brace PT, Tezera LB, Bielecka MK, Mellows T, Garay D, Tian S, et al. Mycobacterium tuberculosis subverts negative regulatory pathways in human macrophages to drive immunopathology. PLoS Pathog. 2017;13(6):e1006367. doi: 10.1371/journal.ppat.1006367. PubMed PMID: 28570642; PubMed Central PMCID: PMCPMC5453634.

25. Al Shammari B, Shiomi T, Tezera L, Bielecka MK, Workman V, Sathyamoorthy T, et al. The Extracellular Matrix Regulates Granuloma Necrosis in Tuberculosis. J Infect Dis. 2015;212(3):463-73. doi: 10.1093/infdis/jiv076. PubMed

PMID: 25676469; PubMed Central PMCID: PMCPMC4539912.

26. Hernandez-Pando R, Orozco H, Arriaga K, Pavon L, Rook G. Treatment with BB-94, a broad spectrum inhibitor of zinc-dependent metalloproteinases, causes deviation of the cytokine profile towards type-2 in experimental pulmonary tuberculosis in Balb/c mice. Int J Exp Pathol. 2000;81(3):199-209. PubMed PMID: 10971741; PubMed Central PMCID: PMCPMC2517727.

27. Izzo AA, Izzo LS, Kasimos J, Majka S. A matrix metalloproteinase inhibitor promotes granuloma formation during the early phase of Mycobacterium tuberculosis pulmonary infection. Tuberculosis (Edinb). 2004;84(6):387-96. doi: 10.1016/j.tube.2004.07.001. PubMed PMID: 15525562.

28. Zhang X, Goncalves R, Mosser DM. The isolation and characterization of murine macrophages. Curr Protoc Immunol. 2008;Chapter 14:Unit 14 1. doi: 10.1002/0471142735.im1401s83. PubMed PMID: 19016445; PubMed Central PMCID: PMCPMC2834554.

29. Weischenfeldt J, Porse B. Bone Marrow-Derived Macrophages (BMM): Isolation and Applications. CSH Protoc. 2008;2008:pdb prot5080. doi: 10.1101/pdb.prot5080. PubMed PMID: 21356739.

30. Rhoades E, Hsu F, Torrelles JB, Turk J, Chatterjee D, Russell DG. Identification and macrophage-activating activity of glycolipids released from intracellular Mycobacterium bovis BCG. Mol Microbiol. 2003;48(4):875-88. PubMed PMID: 12753183.

31. Sakamoto K, Kim MJ, Rhoades ER, Allavena RE, Ehrt S, Wainwright HC, et al. Mycobacterial trehalose dimycolate reprograms macrophage global gene

expression and activates matrix metalloproteinases. Infect Immun. 2013;81(3):764-76. doi: 10.1128/IAI.00906-12. PubMed PMID: 23264051; PubMed Central PMCID: PMCPMC3584883.

32. Sakamoto K, Geisel RE, Kim MJ, Wyatt BT, Sellers LB, Smiley ST, et al. Fibrinogen regulates the cytotoxicity of mycobacterial trehalose dimycolate but is not required for cell recruitment, cytokine response, or control of mycobacterial infection. Infect Immun. 2010;78(3):1004-11. doi: 10.1128/IAI.00451-09. PubMed PMID: 20028811; PubMed Central PMCID: PMCPMC2825938.

33. Tan S, Sukumar N, Abramovitch RB, Parish T, Russell DG. Mycobacterium tuberculosis responds to chloride and pH as synergistic cues to the immune status of its host cell. PLoS Pathog. 2013;9(4):e1003282. doi: 10.1371/journal.ppat.1003282. PubMed PMID: 23592993; PubMed Central PMCID: PMCPMC3616970.

34. Liu Y, Tan S, Huang L, Abramovitch RB, Rohde KH, Zimmerman MD, et al. Immune activation of the host cell induces drug tolerance in Mycobacterium tuberculosis both in vitro and in vivo. J Exp Med. 2016;213(5):809-25. doi: 10.1084/jem.20151248. PubMed PMID: 27114608; PubMed Central PMCID: PMCPMC4854729.

35. Kliment CR, Englert JM, Crum LP, Oury TD. A novel method for accurate collagen and biochemical assessment of pulmonary tissue utilizing one animal. Int J Clin Exp Pathol. 2011;4(4):349-55. PubMed PMID: 21577320; PubMed Central PMCID: PMCPMC3093059.

36. Chen H, Wu S, Lu R, Zhang YG, Zheng Y, Sun J. Pulmonary permeability assessed by fluorescent-labeled dextran instilled intranasally into mice with LPS-

induced acute lung injury. PLoS One. 2014;9(7):e101925. doi: 10.1371/journal.pone.0101925. PubMed PMID: 25007191; PubMed Central PMCID: PMCPMC4090205.

37. Ghosh CC, Mukherjee A, David S, Knaus UG, Stearns-Kurosawa DJ, Kurosawa S, et al. Impaired function of the Tie-2 receptor contributes to vascular leakage and lethality in anthrax. Proc Natl Acad Sci U S A. 2012;109(25):10024-9. doi: 10.1073/pnas.1120755109. PubMed PMID: 22665799; PubMed Central PMCID: PMCPMC3382507.

38. Radu M, Chernoff J. An in vivo assay to test blood vessel permeability. J Vis Exp. 2013;(73):e50062. doi: 10.3791/50062. PubMed PMID: 23524912; PubMed Central PMCID: PMCPMC3639515.

39. Zimmerman M, Lestner J, Prideaux B, O'Brien P, Dias-Freedman I, Chen C, et al. Ethambutol Partitioning in Tuberculous Pulmonary Lesions Explains Its Clinical Efficacy. Antimicrob Agents Chemother. 2017;61(9). doi: 10.1128/AAC.00924-17. PubMed PMID: 28696241; PubMed Central PMCID: PMCPMC5571334.

40. Geisel RE, Sakamoto K, Russell DG, Rhoades ER. In vivo activity of released cell wall lipids of Mycobacterium bovis bacillus Calmette-Guerin is due principally to trehalose mycolates. J Immunol. 2005;174(8):5007-15. PubMed PMID: 15814731.

41. Rhoades ER, Geisel RE, Butcher BA, McDonough S, Russell DG. Cell wall lipids from Mycobacterium bovis BCG are inflammatory when inoculated within a gel matrix: characterization of a new model of the granulomatous response to mycobacterial components. Tuberculosis (Edinb). 2005;85(3):159-76. doi: 10.1016/j.tube.2004.10.001. PubMed PMID: 15850754.

42. Vandenbroucke RE, Libert C. Is there new hope for therapeutic matrix metalloproteinase inhibition? Nat Rev Drug Discov. 2014;13(12):904-27. doi: 10.1038/nrd4390. PubMed PMID: 25376097.

43. Vanlaere I, Libert C. Matrix metalloproteinases as drug targets in infections caused by gram-negative bacteria and in septic shock. Clin Microbiol Rev. 2009;22(2):224-39, Table of Contents. doi: 10.1128/CMR.00047-08. PubMed PMID: 19366913; PubMed Central PMCID: PMCPMC2668236.

44. Khokha R, Murthy A, Weiss A. Metalloproteinases and their natural inhibitors in inflammation and immunity. Nat Rev Immunol. 2013;13(9):649-65. doi: 10.1038/nri3499. PubMed PMID: 23969736.

45. McQuibban GA, Gong JH, Wong JP, Wallace JL, Clark-Lewis I, Overall CM. Matrix metalloproteinase processing of monocyte chemoattractant proteins generates CC chemokine receptor antagonists with anti-inflammatory properties in vivo. Blood. 2002;100(4):1160-7. PubMed PMID: 12149192.

46. Rundhaug JE. Matrix metalloproteinases and angiogenesis. J Cell Mol Med. 2005;9(2):267-85. PubMed PMID: 15963249.

47. Butler GS, Sim D, Tam E, Devine D, Overall CM. Mannose-binding lectin (MBL) mutants are susceptible to matrix metalloproteinase proteolysis: potential role in human MBL deficiency. J Biol Chem. 2002;277(20):17511-9. doi: 10.1074/jbc.M201461200. PubMed PMID: 11891230.

48. Polotsky VY, Belisle JT, Mikusova K, Ezekowitz RA, Joiner KA. Interaction of human mannose-binding protein with Mycobacterium avium. J Infect Dis. 1997;175(5):1159-68. PubMed PMID: 9129080.

49. Weis WI, Drickamer K, Hendrickson WA. Structure of a C-type mannose-binding protein complexed with an oligosaccharide. Nature. 1992;360(6400):127-34. doi: 10.1038/360127a0. PubMed PMID: 1436090.

50. Ip WK, Takahashi K, Ezekowitz RA, Stuart LM. Mannose-binding lectin and innate immunity. Immunol Rev. 2009;230(1):9-21. doi: 10.1111/j.1600-065X.2009.00789.x. PubMed PMID: 19594626.

51. Parham P. The immune system. 3rd ed: Garland Science, Taylor & Francis Group; 2009.

52. Tang Y, Nakada MT, Kesavan P, McCabe F, Millar H, Rafferty P, et al. Extracellular matrix metalloproteinase inducer stimulates tumor angiogenesis by elevating vascular endothelial cell growth factor and matrix metalloproteinases. Cancer Res. 2005;65(8):3193-9. doi: 10.1158/0008-5472.CAN-04-3605. PubMed PMID: 15833850.

53. Datta M, Via LE, Kamoun WS, Liu C, Chen W, Seano G, et al. Anti-vascular endothelial growth factor treatment normalizes tuberculosis granuloma vasculature and improves small molecule delivery. Proc Natl Acad Sci U S A. 2015;112(6):1827-32. doi: 10.1073/pnas.1424563112. PubMed PMID: 25624495; PubMed Central PMCID: PMCPMC4330784.

54. Kusumbe AP, Ramasamy SK, Itkin T, Mae MA, Langen UH, Betsholtz C, et al. Age-dependent modulation of vascular niches for haematopoietic stem cells. Nature. 2016;532(7599):380-4. doi: 10.1038/nature17638. PubMed PMID: 27074508; PubMed Central PMCID: PMCPMC5035541.

55. Kim JH, Kim GH, Kim JW, Pyeon HJ, Lee JC, Lee G, et al. In Vivo

Angiogenic Capacity of Stem Cells from Human Exfoliated Deciduous Teeth with Human Umbilical Vein Endothelial Cells. Mol Cells. 2016;39(11):790-6. doi: 10.14348/molcells.2016.0131. PubMed PMID: 27871176; PubMed Central PMCID: PMCPMC5125934.

56. Egawa G, Nakamizo S, Natsuaki Y, Doi H, Miyachi Y, Kabashima K. Intravital analysis of vascular permeability in mice using two-photon microscopy. Sci Rep. 2013;3:1932. doi: 10.1038/srep01932. PubMed PMID: 23732999; PubMed Central PMCID: PMCPMC3671357.

57. Wilhelm DL. Mechanisms responsible for increased vascular permeability in acute inflammation. Agents Actions. 1973;3(5):297-306. PubMed PMID: 4785028.

58. Claesson-Welsh L. Vascular permeability--the essentials. Ups J Med Sci. 2015;120(3):135-43. doi: 10.3109/03009734.2015.1064501. PubMed PMID: 26220421; PubMed Central PMCID: PMCPMC4526869.

59. Beamer GL, Turner J. Murine models of susceptibility to tuberculosis. Arch Immunol Ther Exp (Warsz). 2005;53(6):469-83. PubMed PMID: 16407780.

60. Chackerian AA, Behar SM. Susceptibility to Mycobacterium tuberculosis: lessons from inbred strains of mice. Tuberculosis (Edinb). 2003;83(5):279-85. PubMed PMID: 12972341.

61. Lienard J, Carlsson F. Murine Mycobacterium marinum Infection as a Model for Tuberculosis. Methods Mol Biol. 2017;1535:301-15. doi: 10.1007/978-1-4939-6673-8_20. PubMed PMID: 27914088.

62. Ma J, Waxman DJ. Combination of antiangiogenesis with chemotherapy for more effective cancer treatment. Mol Cancer Ther. 2008;7(12):3670-84. doi:

10.1158/1535-7163.MCT-08-0715. PubMed PMID: 19074844; PubMed Central PMCID: PMCPMC2637411.

63. Huang Y, Goel S, Duda DG, Fukumura D, Jain RK. Vascular normalization as an emerging strategy to enhance cancer immunotherapy. Cancer Res. 2013;73(10):2943-8. doi: 10.1158/0008-5472.CAN-12-4354. PubMed PMID: 23440426; PubMed Central PMCID: PMCPMC3655127.

64. Sandler A, Gray R, Perry MC, Brahmer J, Schiller JH, Dowlati A, et al. Paclitaxel-carboplatin alone or with bevacizumab for non-small-cell lung cancer. N Engl J Med. 2006;355(24):2542-50. doi: 10.1056/NEJMoa061884. PubMed PMID: 17167137.

65. Miller K, Wang M, Gralow J, Dickler M, Cobleigh M, Perez EA, et al. Paclitaxel plus bevacizumab versus paclitaxel alone for metastatic breast cancer. N Engl J Med. 2007;357(26):2666-76. doi: 10.1056/NEJMoa072113. PubMed PMID: 18160686.

66. Giantonio BJ, Catalano PJ, Meropol NJ, O'Dwyer PJ, Mitchell EP, Alberts SR, et al. Bevacizumab in combination with oxaliplatin, fluorouracil, and leucovorin (FOLFOX4) for previously treated metastatic colorectal cancer: results from the Eastern Cooperative Oncology Group Study E3200. J Clin Oncol. 2007;25(12):1539-44. doi: 10.1200/JCO.2006.09.6305. PubMed PMID: 17442997.

67. Hurwitz H, Fehrenbacher L, Novotny W, Cartwright T, Hainsworth J, Heim W, et al. Bevacizumab plus irinotecan, fluorouracil, and leucovorin for metastatic colorectal cancer. N Engl J Med. 2004;350(23):2335-42. doi: 10.1056/NEJMoa032691. PubMed PMID: 15175435.

68. National Cancer Institute. Angiogensis inhibitors National Cancer Institute: National Cancer Institute.

69. Oehlers SH, Cronan MR, Scott NR, Thomas MI, Okuda KS, Walton EM, et al. Interception of host angiogenic signalling limits mycobacterial growth. Nature. 2015;517(7536):612-5. doi: 10.1038/nature13967. PubMed PMID: 25470057; PubMed Central PMCID: PMCPMC4312197.

70. Walker NF, Clark SO, Oni T, Andreu N, Tezera L, Singh S, et al. Doxycycline and HIV infection suppress tuberculosis-induced matrix metalloproteinases. Am J Respir Crit Care Med. 2012;185(9):989-97. doi: 10.1164/rccm.201110-1769OC. PubMed PMID: 22345579; PubMed Central PMCID: PMCPMC3359940.

71. Fisher JF, Mobashery S. Recent advances in MMP inhibitor design. Cancer Metastasis Rev. 2006;25(1):115-36. doi: 10.1007/s10555-006-7894-9. PubMed PMID: 16680577.

Chapter 3

Synthetic mRNA mediated immune cell recruitment and modulation

Abstract

Synthetic mRNA therapy is a recognized approach for avoiding the genomic integration that is often associated with DNA-based therapy, and the prolonged production of target proteins compared to recombinant protein therapy. Synthetic mRNA therapy has been explored in different disease models, which have focused mostly on expressing proteins with direct therapeutic effect or antigens to elicit an immune response. Moreover, current cell-based gene therapies require multiple procedures of retrieving and modifying autologous cells *ex vivo*. The potential of using synthetic mRNA to recruit and modify immune cells *in vivo* has not been well-studied. In this chapter, we demonstrate that synthetic mRNA encoding CCL2 or CCL3 are able to recruit certain populations of monocyte in a non-inflammatory manner. These recruited monocytes stayed in a neutral, non-programmed state, exhibiting neither bactericidal nor tissue-repairing phenotypes. Additional *Ifn-γ* mRNA or *Il-4* mRNA can polarize these cells to different phenotypes. Furthermore, the monocytes recruited by *Ccl3* and *Ifn-γ* mRNA were able to launch a rapid and robust superoxide burst compared to other mRNA combinations. Our study demonstrates that a synthetic mRNA based immune-modulation approach allows recruitment and modification of specific immune cell populations *in vivo*, providing an alternative route for immunotherapy.

3.1 Introduction

Synthetic mRNA therapy has been gaining interest in recent years, thanks to recent advances to enhance stability and reduce immunogenicity [1-5]. Because of its non-replicative nature, synthetic mRNA is simply a transient carrier of information, and will be degraded via metabolic pathways within a few days [2, 6]. Therefore, synthetic mRNA poses very little risk of genomic insertional mutagenesis, which is often a concern for DNA-based therapy [1, 2, 6, 7]. Moreover, synthetic mRNA therapy does not require nuclear delivery for transcription like DNA-based therapy [1, 2, 6, 7]. On the other hand, compared to recombinant protein, which usually has a shorter protein half-life within physiological environment (minutes to hours) [8, 9], synthetic mRNA can maintain protein expression at therapeutic level for a few days [2, 6]. Lastly, synthetic mRNA with chemical modification can provide a localized and intense expression of desired proteins in selected tissues or organs via systematic administration [1, 2, 9].

Preclinical studies using synthetic mRNA have been conducted in various fields including cancer immunotherapy [10-13], infectious disease vaccine delivery [14, 15] and protein-replacement therapy [16, 17]. Clinical trials involved HIV vaccine design [18, 19] , and treatment of cancers such as prostate cancer [20, 21], pancreatic cancer [22], colon cancer [23], melanoma [23]. However, these studies focus on expressing proteins that can recognize and eliminate malignant targets (virus, microbe or cancer cells) [12, 13, 16, 17, 21], or antigens that can trigger an antigen-specific immune attack [10, 11, 14, 15, 20, 22, 23]. Moreover, current cell-based gene therapies require

multiple steps of retrieving patients' own immune cells, modifying them *ex vivo* and transferring them back to patients. Using a cocktail of synthetic mRNAs expressing both cytokines/chemokines and stimulating signals (antigens or activation signals) can potentially reduce these steps into one simple injection. Therefore, it is of great value to investigate synthetic mRNA's ability to recruit and modify specific immune cell populations *in vivo*.

In this study, we explored a strategy to recruit and modulate host immune cells *in vivo* using synthetic encoding CCL2 or CCL3, which are known for their ability to recruit monocyte, memory T cells, neutrophils and natural killer (NK) cells in various diseases [24-28]. Monocytes recruited by our synthetic mRNA stayed in a neutral, non-programmed state, without adopting either a bactericidal or tissue-repairing phenotype. That is, these recruited monocytes were not activated in the peritoneum based on their MHC II expression, iNOS expression and reactive oxygen production. Additional mRNAs encoding IFN-γ and IL-4 further drove the recruited monocytes to different polarization states. *Ifn-γ* mRNA activated the recruited monocytes and the resident macrophages and drove them into a bactericidal state. Functionally, monocytes recruited by *Ccl3* and *Ifn-γ* mRNA were capable of eliciting a faster and stronger superoxide burst than those from other synthetic mRNA groups. Collectively, our results showed proof-of-principle that synthetic mRNA delivery enables recruitment and modification of specific immune cell populations *in vivo*, which may benefit a variety of immunotherapies.

3.2 Methods

a. Mouse and Cells

C57BL/6J mice, CD45.1^{+} mice (B6.SJL-Ptprc^{a} Pepc^{b}/BoyJ) were obtained from the Jackson Laboratory and housed under pathogen-free conditions. All experiments were approved by Cornell University Institutional Animal Care and Use Committee.

Hela cells, Vero cells and J774 cells were purchased from ATCC. Bone marrow derived macrophage (BMDM) were isolated from CD45.1^{+} or CD45.2^{+} mice, and maintained in DMEM (Corning Cellgro) containing 10% FBS (Thermo Scientific), 10% L929-cell conditioned media, 2 mM L-glutamine, 1 mM sodium pyruvate and antibiotics (penicillin/streptomycin) (Corning cellgro), at 37℃ in a 5% CO_2 incubator.

b. IVT mRNA synthesis

IVT mRNAs encoding for mouse CCL2 (NCBI: NM_011333), CCL3 (NCBI: NM_011337), IFN-γ (NCBI: NM_008337.4), and IL-4 (NCBI: NM_021283.2) were synthesized in lab from plasmids (Life Technologies) containing a T7 promoter followed by a Kozak consensus sequence, the gene sequence of interest, and the mouse alpha globin 3' untranslated region. A NotI restriction site was inserted following the mRNA sequence in order to allow overnight digestion to linearize plasmids, creating a 5' overhang for transcription. The digested DNA template was then purified and used to generate mRNA (Cellscript). A cap-1 structure and poly(A) tail were added enzymatically using the manufacturer's instructions, which increases their stability and expression efficiency. mRNAs were synthesized with a complete

substitution of uridine to N-1-methyl pseudouridine (Trilink), which has been shown to increase protein expression and decrease innate immune activation[5]. mRNA was treated with Antartic phosphatase (New England Biolabs) for 30 minutes to remove residual triphosphates before a final RNA purification step using a RNeasy midi kit (Qiagen). Finally, all mRNAs were quantified on a Nanodrop 2000 (Thermo Scientific) and stored frozen at –80°C.

c. Transfection with mRNA

5 x10^5 J774 or Vero cells seeded in 24 well plate, or 2 x10^6 BMDM cells seeded in 6 well plate were transfected with mRNA using Viromer Red transfection reagent following manufacture's procedure. The supernatant was collected for ELISA and the cell were collected for immunofluorescence or injection to animals.

d. Immunofluorescence

Cells were plated onto #1.5 glass coverslips the day before use. At the indicated time points, cells were fixed with 4% PFA for 10 min before permeabilization with 0.2% Triton X-100 for 5 min at room temperature (Sigma). Cells were then blocked in 10% Donkey Serum and 5% BSA for 30 min at 37 °C before incubation with primary anti-GFP antibody (8μg/mL, Life Technologies, a11122) for 30 min at 37 °C. Cells were then washed with PBS and incubated with AlexaFluor 488-conjugated secondary antibody (Jackson ImmunoResearch) for 30 min at 37 °C. Nuclei were stained with DAPI (Life Technologies) for 5 min and mounted onto glass slides with Prolong gold.

e. ELISA

$5x10^5$ J774 or Vero cells were plated into each well of a 24 well plate. After incubating overnight, cells were transfected with either 1μg of CCL2 or CCL3 mRNA or were incubated with 10μg/mL LPS or control media for 24 h. Cell supernatants were collected and centrifuged at 10^4 G for 10 min to clear the supernatant. Supernatants were diluted and tested by ELISA kits for mouse CCL2 (R&D, MJE00), CCL3 (R&D, MMA00), IFN-ɣ (R&D, MIF00) and IL-4 (R&D, M4000B).

f. Flow cytometry

For surface staining, cells were washed with PBS and blocked with PBS plus 5% FBS, 2.5% mouse serum and 0.5% anti FcϒIII/II (anti-CD16/32) for 15min. Cells were washed with PBS and incubated with viability dye (1:500, eBioscience) and antibodies (1:200) for 15min. Cells were washed with PBS and analyzed by LSR II (BD Biosciences). Flow cytometric data were further analyzed with FlowJo software (TreeStar).

For intracellular staining, cells were incubated with Brefeldin A (1:1000, eBioscience) in RPMI media plus10%FBS in 37℃ for 4-5h. Then cells were washed, blocked and stained according to the Intracellular Staining protocol (eBioscience). Cells were washed with PBS and analyzed by BD LSR II.

Antibodies used in this paper include Ly6C-APC Cy7, Ly6C-APC, F4/80-PE, F4/80-e450, Ly6G 1A8-PE Cy7, Ly6G 1A8-FITC (BD), CD45.2-APC, CD45.2-AF700,

CD45.1-PE, CD45.1-AF700, CD3-e450, NK1.1-AF780, CD11b-PerCP Cy5.5 (BD), CD206-PE, Arginase1-PE (R & D), Anti-mouse Relm-alpha antibody (PeproTech). Antibodies were from eBioscience unless stated otherwise.

g. Statistics

Two-tailed Unpaired Student t test with Welch-correction and One-way ANOVA with Turkey multiple comparison tests were conducted in Prism (GraphPad). All experiments were repeated at least twice. Number of mice used in each experiment is indicated in figures.

3.3 Results

3.3.1 Expression of CCL2 and CCL3 *in vitro* using synthetic mRNA.

mRNAs were synthesized through *in vitro* transcription with a complete substitution of uridine to N-1-methyl pseudouridine, to increase protein expression and reduce innate immune activation [5]. These mRNAs were then chemically modified extensively including 5' capping, coding region optimization, and 3' poly(A) tail elongation (see Methods and Materials for detailed procedure). Delivery of synthetic mRNA encoding the green fluorescent protein (*Gfp*) to Hela cells showed GFP expression as early as 5h post-transfection (Figure 3.1A). The GFP signal peaked between 8h and 24h post-transfection, and lasted for 72 hours (Figure 3.1A). Interestingly, we found that difficult cell types such as macrophage were very effective at expressing foreign genes when delivered in the form of synthetic mRNA. Macrophage-like cell line, J774, was transfected with this *Gfp* mRNA and approximately 70% of the cells were expressing the GFP protein 24 hours post-transfection (Figure 3.1B).

To explore the potential for manipulating tissue responses through cell recruitment and reprogramming we expressed CCL2 (MCP1) and CCL3 (MIP1α) using synthetic mRNA. CCL2 and CCL3 are able to recruit different immune cells including monocyte, memory T cell, neutrophil and natural killer (NK) cell [24-28]. We transfected the J774 cells with *Ccl2* or *Ccl3* synthetic mRNAs and detected CCL2 or CCL3 proteins by ELISA in the supernatant 24h post-transfection (Figure 3.1C). This data indicated the mRNAs were successfully translated and the corresponding

proteins being secreted. We focused on *Ccl3* synthetic mRNA due to its more robust and effective expression over *Ccl2* synthetic mRNA (Figure 3.1C).

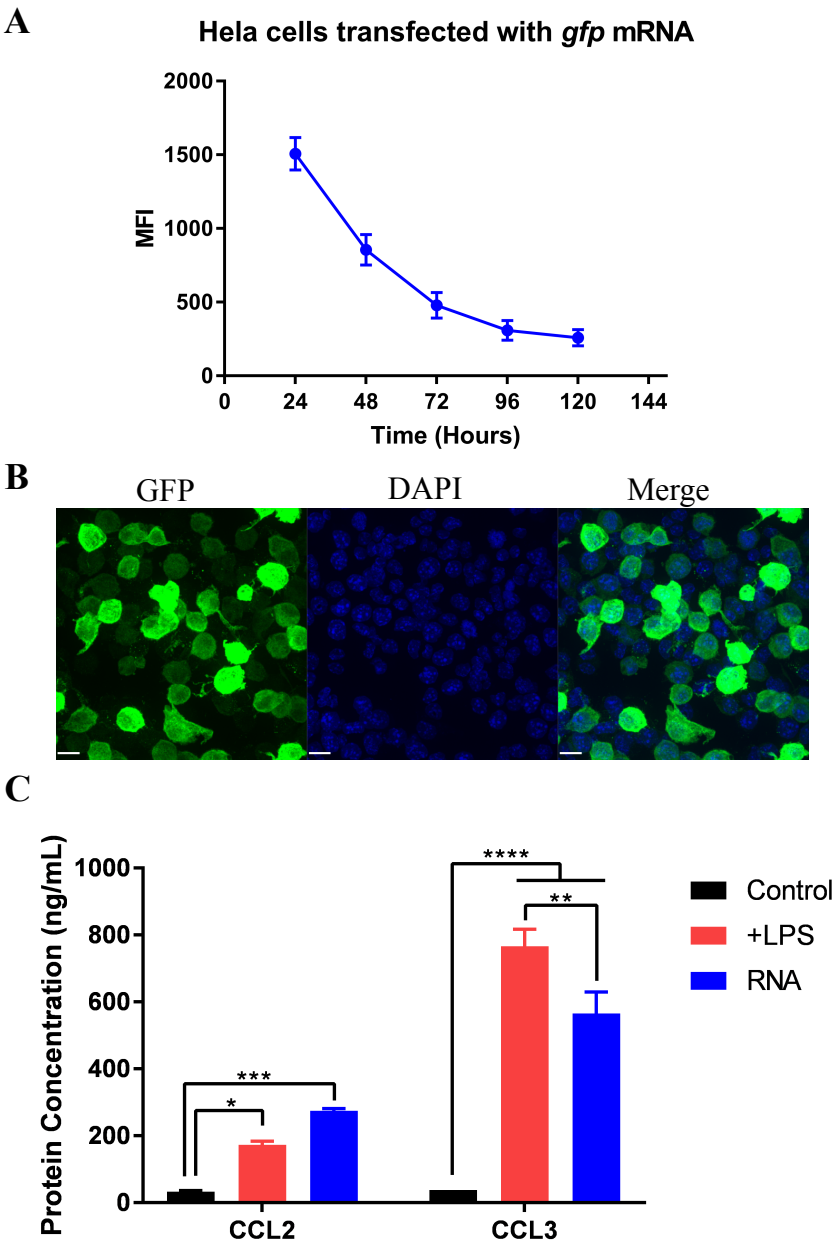

Figure 3.1 J774 cells transfected with *Gfp*, *Ccl2* or *Ccl3* synthetic mRNA express GFP, CCL2 or CCL3, respectively.

A: GFP fluorescence in transfected cells starts diminishing after 24 hours. HeLa cells were transfected with 250ng of *Gfp* mRNA and prepared for flow cytometry at the indicated time points. Points represented the geometric mean fluorescence intensity of

at least 10^4 cells per time point. Error bars represented robust coefficient of variance. Experiment was performed in duplicate. **B:** Cells were transfected with 1μg of *Gfp* mRNA and fixed 24 hours post-transfection. Cells were stained for GFP (green) and nuclei were stained with DAPI (blue). Scale bar represents 12μm. **C:** Concentration of CCL2 or CCL3 was measured by ELISA in cleared J774 supernatants after transfection with either 1μg of *Ccl2* or *Ccl3* mRNA (blue) or incubation with or without 10μg/mL LPS for 24 h. Scale bars represent standard deviation. Data represents mean of two independent experiments. Statistical significance was measured by two-way ANOVA. *: $p<0.05$. **: $p<0.01$. ***: $p<0.001$. ****: $p<0.0001$.

3.3.2 Expression of functionally-active CCL3 in primary Bone Marrow-Derived Macrophages.

To demonstrate that the CCL3-encoding synthetic mRNAs expressed functionally-active proteins we transfected bone marrow derived macrophages (BMDMs) with *Ccl3* mRNA and injected these cells to mice intraperitoneally (Figure 3.2A). Peritoneal cells were collected 16h later and analyzed by flow cytometry. CCL3 expression was detected in cell culture of BMDM transfected with *Ccl3* mRNA, as well as in peritoneal fluid from mice injected with these *Ccl3* transfected BMDM (Figure 3.2B). The gating strategy is illustrated in Figure 3.2C.

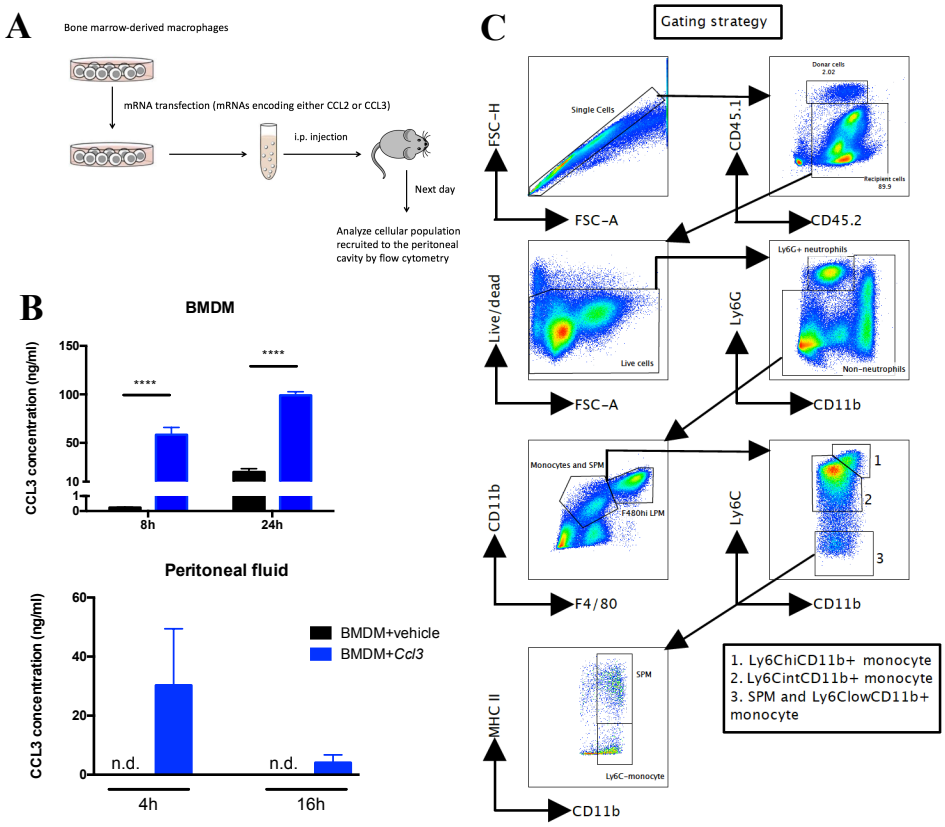

Figure 3.2 *Ccl3* synthetic mRNA transfected BMDMs secrete CCL3 in BMDM culture and peritoneal fluid.

A: Experiment setup. In brief, we transfected synthetic mRNAs encoding either CCL2 or CCL3 into bone marrow-derived macrophage (BMDM) generated from $CD45.1^+$ congenic mice. 8h after transfection, the cells were harvested, washed with PBS, and injected intraperitoneally into $CD45.2^+$ congenic mice. 16h later, we collected the cells from peritoneal cavity and analyzed them by flow cytometry. The use of the congenic $CD45.1^+/CD45.2^+$ mouse strains enabled us to discriminate between the donor BMDM transfected with the chemokine mRNAs and the resident tissue macrophages. **B:** Demonstration of CCL3 production in supernatant of BMDMS transfected with *Ccl3* mRNA, as well as in peritoneal fluid from mice injected with these BMDMs. **C:**

Flow cytometry analysis gating strategy, in which we identified neutrophils ($Ly6G^{+}CD11b^{+}$), large peritoneal macrophages (LPM, $F4/80^{high}CD11b^{+}$), $Ly6C^{high}$ monocyte ($F4/80^{low}Ly6C^{high}CD11b^{+}$), $Ly6C^{int}$ monocyte ($F4/80^{low}Ly6C^{int}CD11b^{+}$), $Ly6C^{low}$ monocyte ($F4/80^{low}Ly6C^{low}CD11b^{+}$MHC II^{-}) and small peritoneal macrophage (SPM, $F4/80^{low}Ly6C^{low}CD11b^{+}$MHC II^{+}).

Interestingly, in the mice injected with BMDM transfected with *Ccl3* synthetic mRNA, we observed significant recruitment of a monocyte-like cell subset (Figure 3.3A and B), expressing high level of Ly6C and low level of F4/80 (Figure 3.3C and D). Additionally, monocytes that express intermediate level of Ly6C ($F4/80^{low}Ly6C^{int}CD11b^{+}$), were significantly increased in these mice. These monocyte subsets can be distinguished from resident peritoneal macrophages, which express high levels of F4/80 (Figure 3.3D). We also observed marked decrease of large peritoneal macrophage number after injection of BMDM transfected with *Ccl3* synthetic mRNA (Figure 3.3A and B), with their F4/80 expression also decreased (Figure 3.3E). This disappearance of peritoneal macrophage effect has been previously documented as the macrophage disappearance reaction (MDR) upon inflammation such as injection of thioglycolate broth, LPS or bacteria[29-31]. The number of total cell, small peritoneal macrophage (SPM) or $Ly6C^{low}$ monocyte recovered from the peritoneal cavity does not differ between mice injected with and without *Ccl3* transfected BMDM (Figure 3.3F).

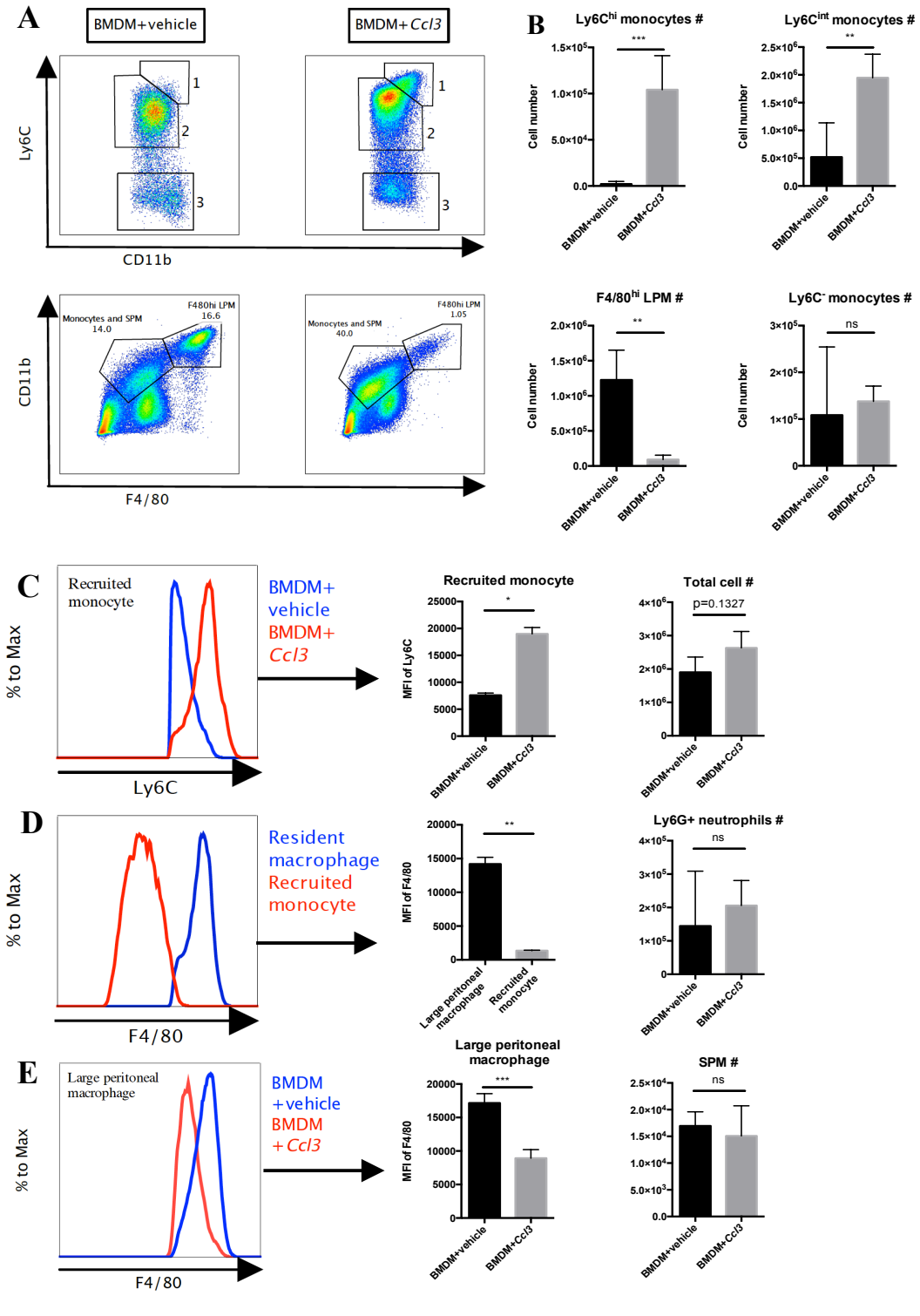
A
BMDM+vehicle
BMDM+Ccl3
Ly6C
CD11b
1
2
3
CD11b
F4/80
Monocytes and SPM
14.0
F480hi LPM
16.6
Monocytes and SPM
40.0
F480hi LPM
1.05
B
Ly6Chi monocytes #
Ly6Cint monocytes #
F4/80hi LPM #
Ly6C- monocytes #
Cell number
BMDM+vehicle
BMDM+Ccl3
***
**
ns
C
Recruited monocyte
% to Max
Ly6C
BMDM+ vehicle
BMDM+ Ccl3
Recruited monocyte
MFI of Ly6C
Total cell #
p=0.1327
D
Resident macrophage
Recruited monocyte
F4/80
MFI of F4/80
Large peritoneal macrophage
Recruited monocyte
Ly6G+ neutrophils #
E
Large peritoneal macrophage
BMDM +vehicle
BMDM +Ccl3
Large peritoneal macrophage
SPM #

Figure 3.3 *Ccl3* synthetic mRNA transfected BMDM can change cell population in the peritoneum.

A: *Ccl3* synthetic mRNA transfected BMDM recruited a population of $Ly6C^{hi}CD11b^{+}$ monocyte (Gate 1), increased the number of $Ly6C^{int}CD11b^{+}$ monocyte (Gate 2), and decreased the number of $F4/80^{hi}$ large peritoneal macrophage. Experiments were repeated 3 times. Data showed representative flow plot from one experiment. **B:** The numbers of $Ly6C^{hi}$ and $Ly6C^{int}CD11b^{+}$ monocytes, $F4/80^{hi}$ large peritoneal macrophage and $Ly6G^{+}$ neutrophil were quantified. Data represent mean ± SD. ns: $p>0.05$, **: $p < 0.01$, ***: $p < 0.001$, Unpaired t test with Wench correction. **C:** Ly6C expression of recruited monocytes from vehicle only group (blue) and *Ccl3* group (red). **D:** F4/80 expression of the large peritoneal macrophage (blue) and recruited monocytes (red) from *Ccl3* group. **E:** F4/80 expression of recruited monocytes from vehicle only group (blue) and *Ccl3* group (red). The MFI of Ly6C and F4/80 were quantified in the right. Experiment was repeated three times. Data represent mean ± SD. ns: $p>0.05$, *: $p < 0.05$, **: $p < 0.01$, Unpaired t test with Wench correction. **F.** Number of total peritoneal cells, $Ly6C^{-}$ monocytes and small peritoneal macrophages from vehicle only group and *Ccl3* group. Experiment was repeated three times. Data represent mean ± SD. ns: $p>0.05$, Unpaired t test with Wench correction.

Studies injecting recombinant CCL3 (rCCL3) into peritoneal cavity showed recruitment of neutrophils started as early as at 2h, and reached its peak at 4h, then declined at 8h [32]. Monocyte was also observed recruited after injection of rCCL3 using air pouch animal model [33]. We compared effects of rCCL3 and BMDM transfected with *Ccl3* mRNA in the peritoneum at 4h and 16h (Figure 3.4). We found that at 4h there was a significant recruitment of neutrophils after rCCL3 injection, which is consistent with previous reports. However, injection of vehicle-transfected BMDMs recruited similar number of neutrophils with injection of rCCL3 (Figure 3.4A), which was consequence of basal expression of CCL3 in those vehicle-transfected BMDMs (Figure 3.2B). More importantly, injection of *Ccl3* mRNA transfected BMDMs recruited far more neutrophils (Figure 3.4A). These observations indicate that our method of using synthetic mRNA to modulate immune environment has different outcome with one using recombinant proteins.

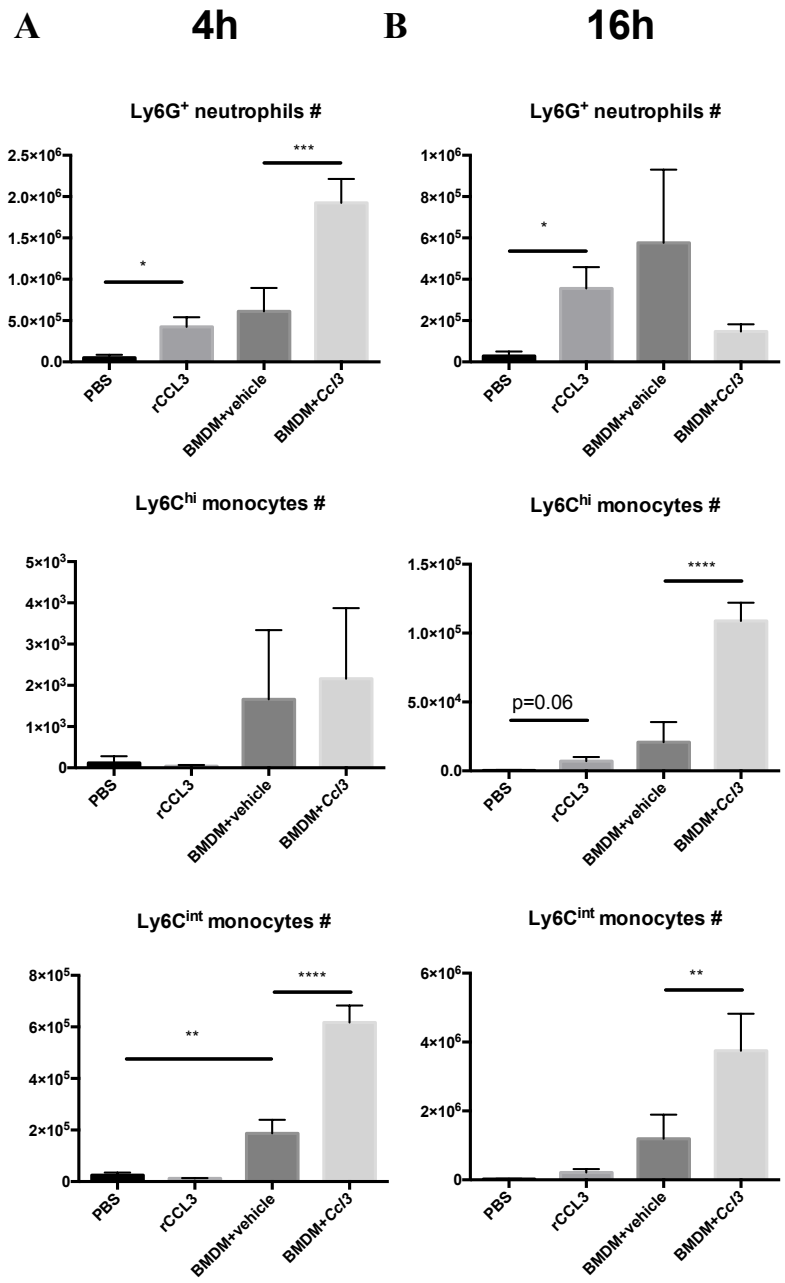

Figure 3.4 Different cell populations from mice injected with recombinant CCL3 or BMDM transfected with *Ccl3* mRNA.

Cell number of Ly6C^{hi} monocytes, Ly6C^{int} monocytes and Ly6G^{+} neutrophils injecting recombinant CCL3 and BMDM transfected with *Ccl3* mRNA at 4h (A) and 16h (B) post injection. Experiment was repeated two times. Data represent mean ±

SD. ns: $p>0.05$, *: $p < 0.05$, **: $p < 0.01$, ***: $p < 0.001$, ****: $p < 0.0001$, One-way ANOVA with Tukey's multiple comparison test.

3.3.3 Monocytes are recruited through blood stream to the peritoneal cavity in a "Neutral" State.

Upon acute inflammation or pathogen infection, monocytes are recruited via the blood stream to peripheral tissues, in response to various inflammatory cytokines including CCL2 and CCL3[27, 34, 35]. To demonstrate that the increased $Ly6C^+$ monocyte populations were indeed recruited to the peritoneum through blood stream, we used congenic marker CD45 to differentiate the cell identity of donor and recipient cells. CD45 have two functional identical alleles, CD45.1 and CD45.2. We isolated monocytes from $CD45.1^+$ mice and injected them intravenously to $CD45.2^+$ mice that were given BMDM transfected with or without *Ccl3* mRNA. We observed more $CD45.1^+$ cells in the peritoneum of mice given *Ccl3* transfected BMDMs (Figure 3.5). This indicated the $Ly6C^+$ monocytes were able to follow the CCL3 signal from the peritoneum and eventually reach the peritoneum through blood stream.

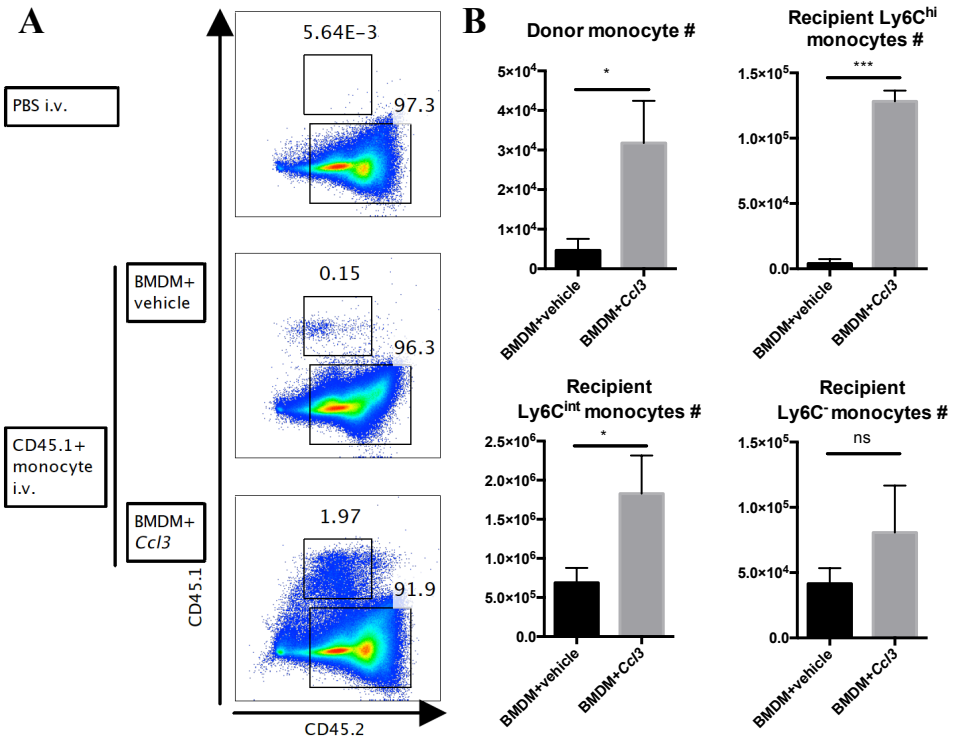

Figure 3.5 Monocytes are recruited through the blood stream to the peritoneum.

A: Representative flow plots showing monocytes isolated from CD45.1^{+} mice and intravenously transfer to CD45.2^{+} mice. CD45.2^{+} mice were intraperitoneally injected with BMDMs transfected with or without *ccl3* mRNA before CD45.1^{+} monocytes infusion. Experiments were repeated 2 times. **B:** The number of donor CD45.1^{+} monocytes, Ly6C^{hi}, Ly6C^{int} and Ly6C^{low} monocytes were quantified. Data represent mean ± SD. ns: p>0.05, *: p < 0.05, ***: p < 0.001, Unpaired t test with Wench correction.

In the acute inflammatory challenge models, such as thioglycolate broth induction, the monocytes are recruited in combination with other inflammatory cytokines and chemokines that drive the cells into an inflammatory, or M1 activation state [27, 36-40]. We wanted to determine whether the monocytes recruited by CCL2 or CCL3 alone without inflammatory stimuli, were similarly activated or whether these cells were recruited in a neutral, or "non-programmed" state.

We examined the levels of expression of iNOS and RELM-α proteins to determine whether the recruited monocytes elicited through ectopic expression of CCL3 in BMDMs were being driven towards either a classically-activated (M1) or alternatively-activated (M2) phenotype. Intriguingly, we found that the very few monocytes recruited through CCL3 activity express either iNOS or Relm-α (Figure 3.6A, B, upper panels). This suggests that in a sterile environment, absent additional signals or stimuli, the recruited cells adopt neither bactericidal nor tissue-repairing phenotype, but remain neutral. The data suggest that CCL3 is responsible for immune cell recruitment, but without additional signals, is not involved in the reprogramming of these recruited cells. We also examined the levels of surface expression of MHC II, CD80 and CD86 on recruited monocytes, as well as resident macrophages and neutrophils. Again the ectopic expression of *Ccl3* mRNA in donor BMDMs did not increase the expression of three markers on the cell types examined, with the exception of a slight increase in CD80 expression on recruited monocytes (Figure 3.7).

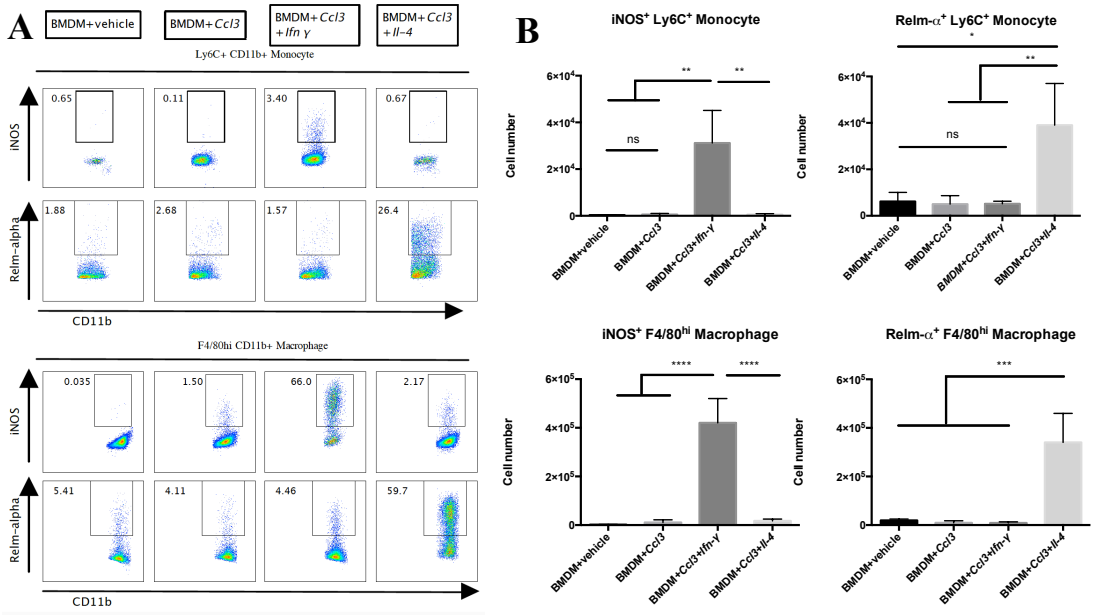

Figure 3.6 Co-transfection of interferon gamma (*Ifn-γ*) or *Il-4* synthetic mRNA with *Ccl3* mRNA drives large peritoneal macrophage and recruited monocyte to different behaviors.

A: Representative flow plots showing the expression of iNOS and Relm-α in recruited monocytes ($Ly6C^+CD11b^+$, upper panel) and large peritoneal macrophage ($F4/80^{hi}CD11b^+$, lower panel) under induction of *Ccl3* mRNA with *Ifn-γ* or *Il-4* mRNA. **B:** The cell number of $iNOS^+$ or Relm-α^+ recruited monocyte and $F4/80^{hi}$ macrophage were quantified. Experiment was repeated three times with similar result. Data represent mean ± SD. *: $p < 0.05$, **: $p < 0.01$, ***: $p < 0.001$, ****: $p < 0.0001$, One-way ANOVA with Tukey's multiple comparison test.

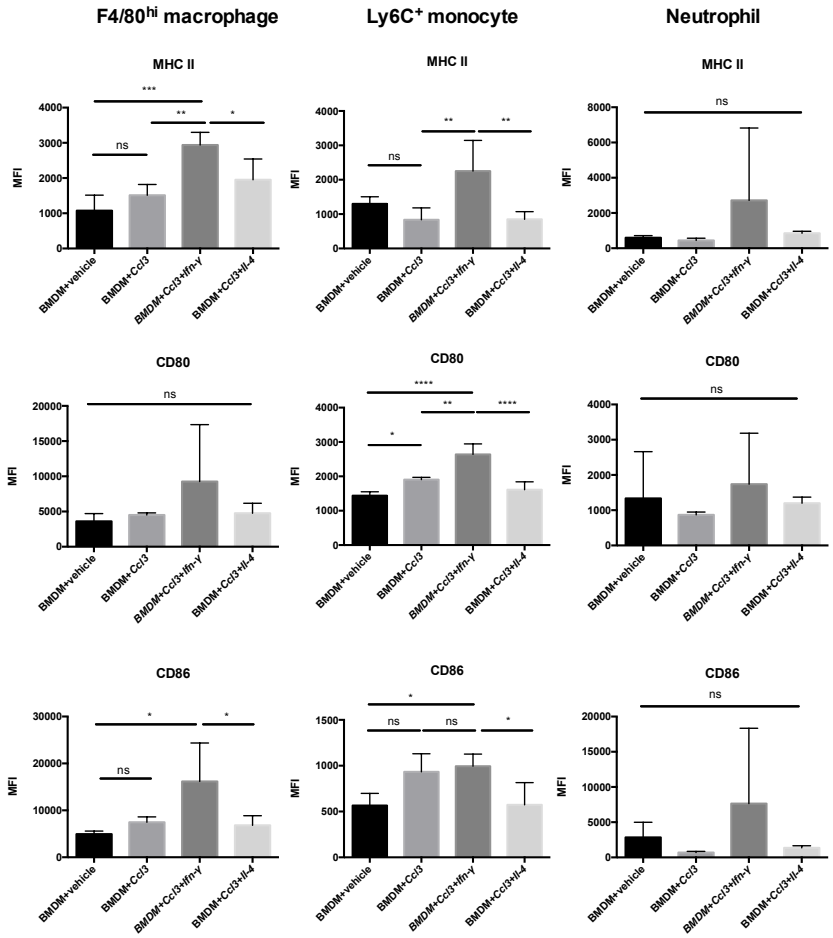

Figure 3.7 Activation status of F4/80^{hi} macrophage, Ly6C^{+} monocyte and neutrophil.

Activation markers (MHC II, CD80 and CD86) expression in resident macrophage (F4/80^{hi} macrophage), recruited monocyte (Ly6C^{+} monocyte) and neutrophil (Ly6G^{+}). Experiment was repeated two times. Data represent mean ± SD. ns: $p>0.05$, *: $p < 0.05$, **: $p < 0.01$, ***: $p < 0.001$, ****: $p < 0.0001$, One-way ANOVA with Tukey's multiple comparison test.

3.3.4 Recruited Monocytes can be Re-Programmed by Co-Expression of Additional Synthetic mRNAs.

We asked whether it were feasible to differentiate these neutral monocytes toward different phenotypes or polarization states. We designed and synthesized two synthetic mRNAs that encoded *Ifn-γ* and *Il-4* transcripts, respectively. The functionality of the mRNAs was validated through the detection of IFN-γ and IL-4 in the supernatant following their transfection into Vero cells (Figure 3.8A). The *Ifn-γ* and *Il-4* mRNAs were mixed individually with *Ccl3* mRNA, transfected into $CD45.1^+$ BMDM, and injected into $CD45.2^+$ mice peritoneum. We detected the expression of IFN-γ and IL-4 in the peritoneal fluid (Figure 3.8B) as well as IFN-γ produced by $CD45.1^+$ BMDM actively (Figure 3.8C). As one would have anticipated, there was a marked increase of iNOS positive monocytes recruited in response to synthetic mRNAs encoding *Ccl3* and *Ifn-γ* (approximately 30-fold above the controls), (Figure 3.6A and B, upper panels). While the number of Relm-α positive monocytes recruited by the *Ccl3* and *Il-4* mRNA combination increased significantly (approximately 20-fold above the controls), (Figure 3.6A and B, upper panels).

As a collateral effect of the IFN-γ and IL-4 expression in the peritoneum, the resident macrophage ($F4/80^{high}CD11b^+$) adopted the microbicidal and tissue-repairing phenotype in a more intense manner. The iNOS positive resident macrophages increased about 50 folds in response to synthetic mRNAs encoding *Ccl3* and *Ifn-γ* above the controls (Figure 3.6A and B, lower panels). On the other hand, the number of Relm-α positive resident macrophages increased about 40 folds in the mice

receiving *Ccl3* and *Il-4* mRNA combination above the controls (Figure 3.6A and B, lower panels).

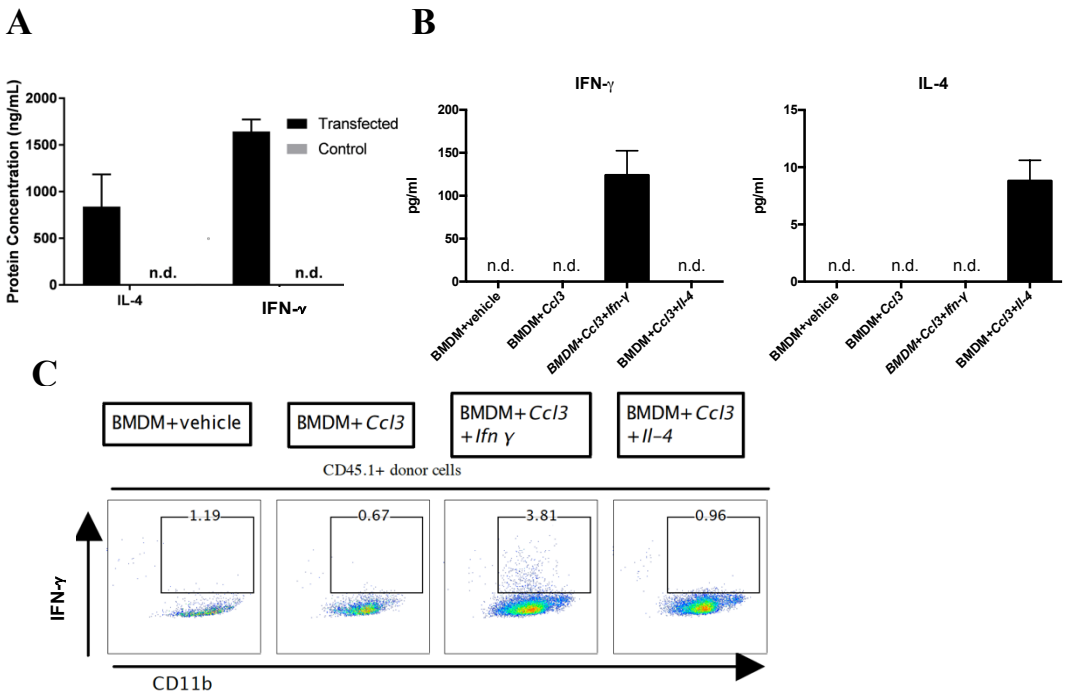

Figure 3.8 Expression of IFN-γ and IL-4 in Vero cells, peritoneal fluid and CD45.1$^+$ cells recovered from peritoneum.

A: Concentration of IFN-γ and IL-4 was measured by ELISA in cleared Vero supernatants after transfection with either 1µg of *Ifn-γ* and *Il-4* mRNA or control media for 24 h. No protein was detected in untreated samples (n.d.). Scale bars represent standard deviation. Data represents mean of two independent experiments. Cells transfected with *Ifn-γ* and *Il-4* mRNA (black bars) produced significantly more proteins than those with empty vehicle (grey bars). **B:** Concentration of IFN-γ and IL-4 in peritoneal fluid from mice injected with different mRNA transfected BMDMs. Experiment was repeated two times. Data represent mean ± SD. **C:** Representative flow plots showing detection of IFN-γ production from *Ccl3*+*Ifn-γ* group but not from other groups. Experiment was repeated two times.

Further characterization of the peritoneal cells demonstrated that resident macrophages and recruited monocytes from mice receiving BMDMs transfected with *Ccl3* and *Ifn-γ* mRNA up-regulated their MHC II expression, but not with the neutrophils (Figure 3.7). Surface expression of CD80 was increased on recruited monocytes, but not on resident macrophages or neutrophils (Figure 3.7). In contrast, there was no marked change in the surface expression of these markers in the peritoneal cell from mice receiving *Ccl3* and *Il-4* mRNAs (Figure 3.7).

3.3.5 Functional demonstration of phagocyte activation.

Reactive oxygen species production can be utilized as an indicator of cell activation status. VanderVen et al. previously used superoxide burst reporter beads to demonstrate that activating BMDM with recombinant IFN-γ can enhance reactive oxygen species production [41]. These beads are covalently modified with Oxyburst-SE albumin and a calibration fluorochrome, and designed to detect oxidative burst within phagosomes. We confirmed IFN-γ's ability to activate BMDM to produce more reactive oxygen species, and further demonstrated that adding recombinant IL-4 to BMDM culture can limit oxidative radical production, compared to resting BMDM (Figure 3.9A).

To verify the activation status of those cells recruited by BMDMs receiving *Ccl3* and *Ifn-γ*, we harvested peritoneal cells from mice that had received synthetic mRNA transfected BMDMs, and added these Oxyburst reporter beads after short-term culture. Peritoneal cells from mice injected with *Ccl3* transfected BMDM showed no

difference with those from control mice, in terms of reactive oxygen species production. Interestingly, corresponding to the oxidative species production from BMDM treated with recombinant IFN-γ or IL-4, peritoneal cells from mice injected with *Ccl3* and *Ifn-γ* mRNA transfected BMDM exhibited increased production of oxidative radical, while peritoneal cells from mice injected with *Ccl3* and *Il-4* mRNA transfected BMDM showed reduced reactive oxygen species production (Figure 3.9B).

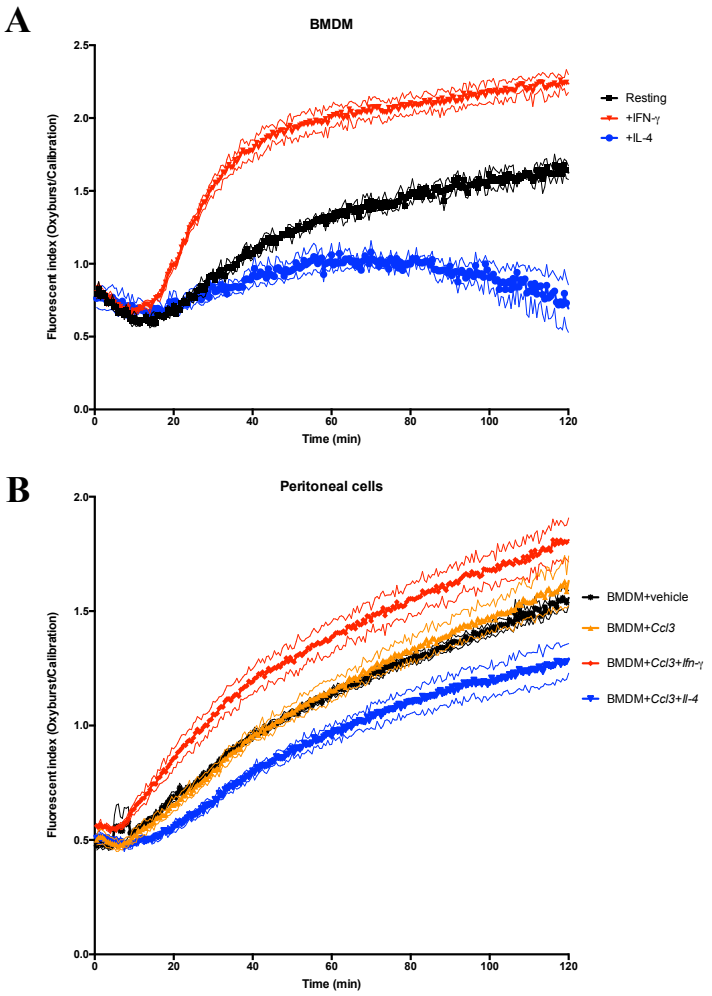

Figure 3.9 Phagocytosis of Oxyburst beads and generation of Oxyburst signal by BMDM and peritoneal cells under different conditions.

A: Kinetics of Oxyburst response of BMDMs treated with or without recombinant IFN-γ and IL-4. Experiment was repeated three times. **B.** Kinetics of Oxyburst response of peritoneal cells from mice (n=3) injected with different mRNA transfected BMDMs. Experiment was repeated twice.

To further segregate different cell populations' ability to produce oxidative species, we used flow cytometry to analyze the peritoneal cells that were incubated with reporter beads and fixed at different time points. We gated on the $Ly6C^{+}$ recruited monocytes and quantified both the number of cells registering a superoxide burst, as well as the mean fluorescence index (MFI) of Oxyburst signal in the bead-containing phagocytes (Figure 3.10A). The number of cells registering a superoxide burst differed kinetically, with those cells from the mice that had received BMDMs transfected with *Ccl3* and *Ifn-γ* mRNAs exhibiting the most robust superoxide burst response (Figure 3.10B). In addition, the magnitude of the MFI of the superoxide burst/Oxyburst signal in the cells from those mice that had received the *Ccl3* and *Ifn-γ* mRNAs exceeds the signal measured in the cells from other synthetic mRNA groups (Figure 3.10B).

The data confirmed our hypothesis that CCL3 recruits monocytes in a relatively neutral state, but that co-expression of other synthetic mRNAs can effectively reprogram these cells to adopt other physiologically significant phenotypes relevant to either microbicidal responses or wound healing.

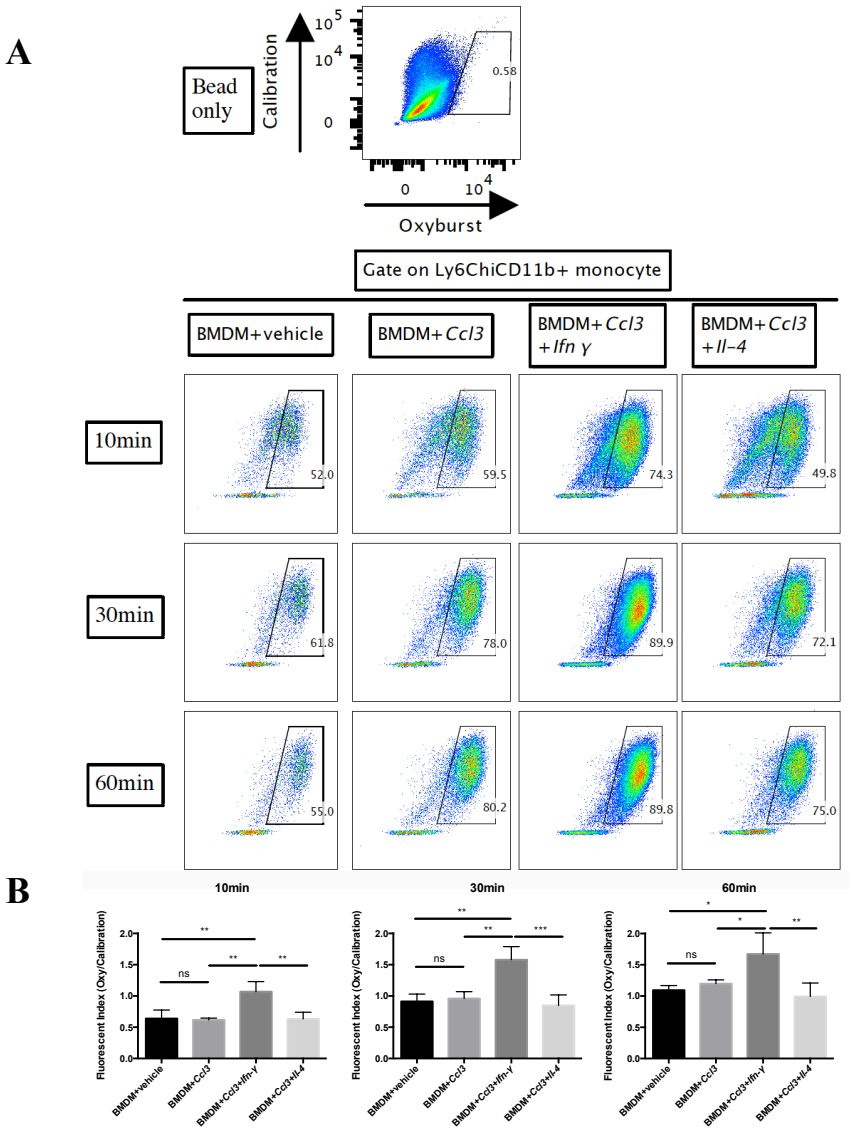

Figure 3.10 Phagocytosis of Oxyburst beads and generation of Oxyburst signal by recruited monocytes increased over time, and these effects are more profound in monocytes exposed to *Ifn-γ* mRNA.

A: Peritoneal cells from mice (n=3) injected with different mRNA transfected BMDMs were analyzed by flow cytometry. Representative flow plots showing the gating of positive Oxyburst signal. Oxyburst beads without cells were served as a negative control (upper panel). The lower panel were gated on recruited monocytes

(Ly6C^{+}CD11b^{+}) of 4 groups incubated with Oxyburst beads at different times (10min, 30min and 60min). Experiment was repeated three times. **B:** Quantification of fluorescent index of mean Oxyburst fluorescent intensity. The mean Oxyburst fluorescent intensity of all the recruited monocytes that were positive for calibration flour were calculated. The number was divided by the mean calibration fluorescent intensity to get the fluorescent index. Experiment was repeated three times with similar result. Data represent mean ± SD. *: $p < 0.05$, **: $p < 0.01$, ***: $p < 0.001$, One-way ANOVA with Tukey's multiple comparison test.

3.3.6 Naked mRNA complexed with Viromer Red can induce similar monocytes recruitment.

We wonder whether naked mRNA without BMDM as a mediator, can exhibit similar phenotypes we observed above. We injected uncoated, naked mRNA, or vehicle coated mRNA directly to the peritoneum. Injections of uncoated *Ccl3* mRNA neither significantly increased the recruitment of the Ly6C^{hi} or Ly6C^{int} monocytes nor induced peritoneal macrophage disappearance (Figure 3.11 A-C). However, intraperitoneal injection of vehicle-coated *Ccl3* mRNA was sufficient to induce Ly6^{hi} and Ly6^{int} monocytes recruitments and macrophage disappearance (Figure 3.11 A-C). These data suggest that delivery of naked mRNA without vehicle coating is not sufficient to change the cell populations. It is possible that most of the mRNA was not taken-up by peritoneal cells efficiently without transfection reagent. On the other hand, vehicle-coated mRNA can actively pass the cell membrane of peritoneal cells and initiate production of desired proteins.

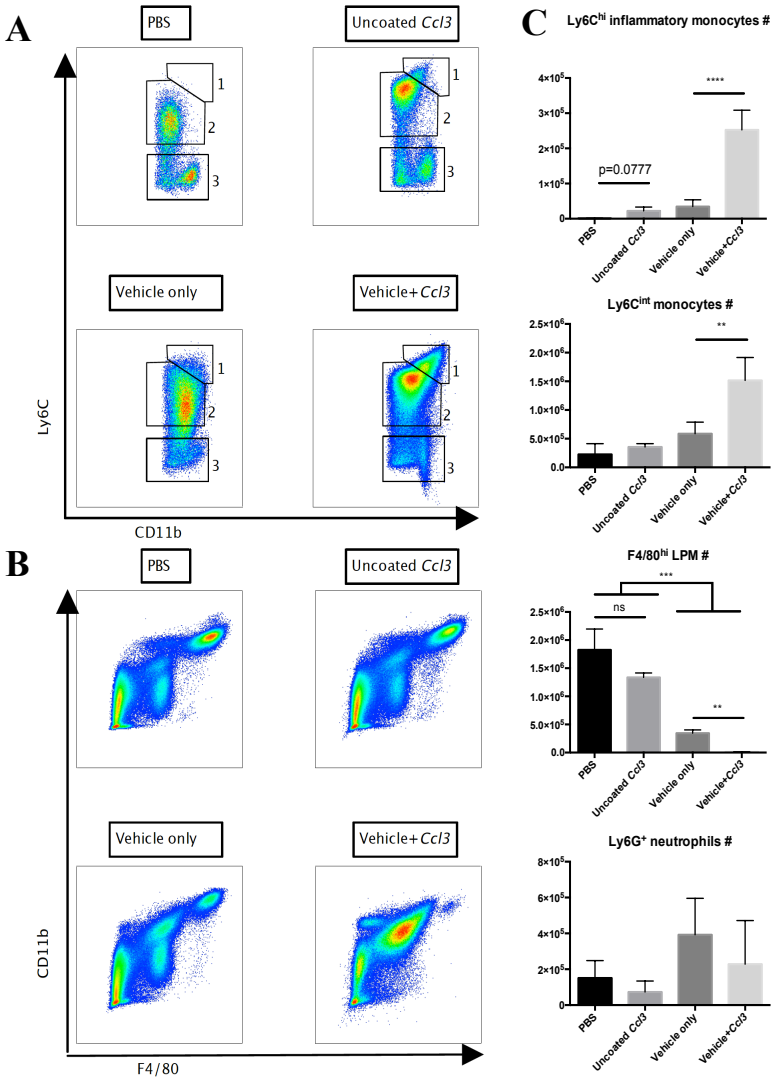

Figure 3.11 mRNA coated with Viromer Red can recruit similar populations of monocytes as mRNA-transfected BMDMs do.

A: Representative flow plots showing injection of naked, uncoated *Ccl3* mRNA can recruit some Ly6C^{hi} monocytes, but didn't increase number of Ly6C^{int} monocytes. On the other hand, injection of vehicle-coated *Ccl3* mRNA significantly recruited Ly6C^{hi} monocytes and increased number of Ly6C^{int} monocytes. **B:** Representative flow plots showing injection of vehicle-coated *Ccl3* mRNA significantly reduced F4/80^{hi} large

peritoneal macrophage, similarly as injection of BMDM transfected with *Ccl3* mRNA, while injection of naked *Ccl3* mRNA did not. **C:** The numbers of Ly6C^{hi} and Ly6C^{int} monocytes, F4/80^{hi} large peritoneal macrophage and Ly6G^{+} neutrophil were quantified. Experiment was repeated two times. Data represent mean ± SD. ns: $p>0.05$, **: $p < 0.01$, ***: $p < 0.001$, ****: $p < 0.0001$, One-way ANOVA with Tukey's multiple comparison test.

Next, we wonder whether these vehicle-coated mRNAs are able to differentiate the recruited monocytes as the transfected BMDMs did. We injected vehicle-coated mRNAs encoding IFN-γ and IL-4 into the peritoneum with *Gfp* mRNA as control. We found that additional *Ifn-γ* and *Il-4* mRNAs were able to induce the most iNOS and RELM-α expression in the $Ly6C^+$ recruited monocytes, respectively (Figure 3.12 A). Moreover, mice receiving extra *Ifn-γ* and *Il-4* mRNAs had the highest $iNOS^+$ and RELM-α^+ cell number (Figure 3.12 B). These data suggest that mRNAs complexed with vehicle are able to modify the recruited monocytes without BMDM as a cell mediator, demonstrating the potential of using mRNAs to recruit and modify immune cells in vivo, without *ex vivo* modification of autologous cells.

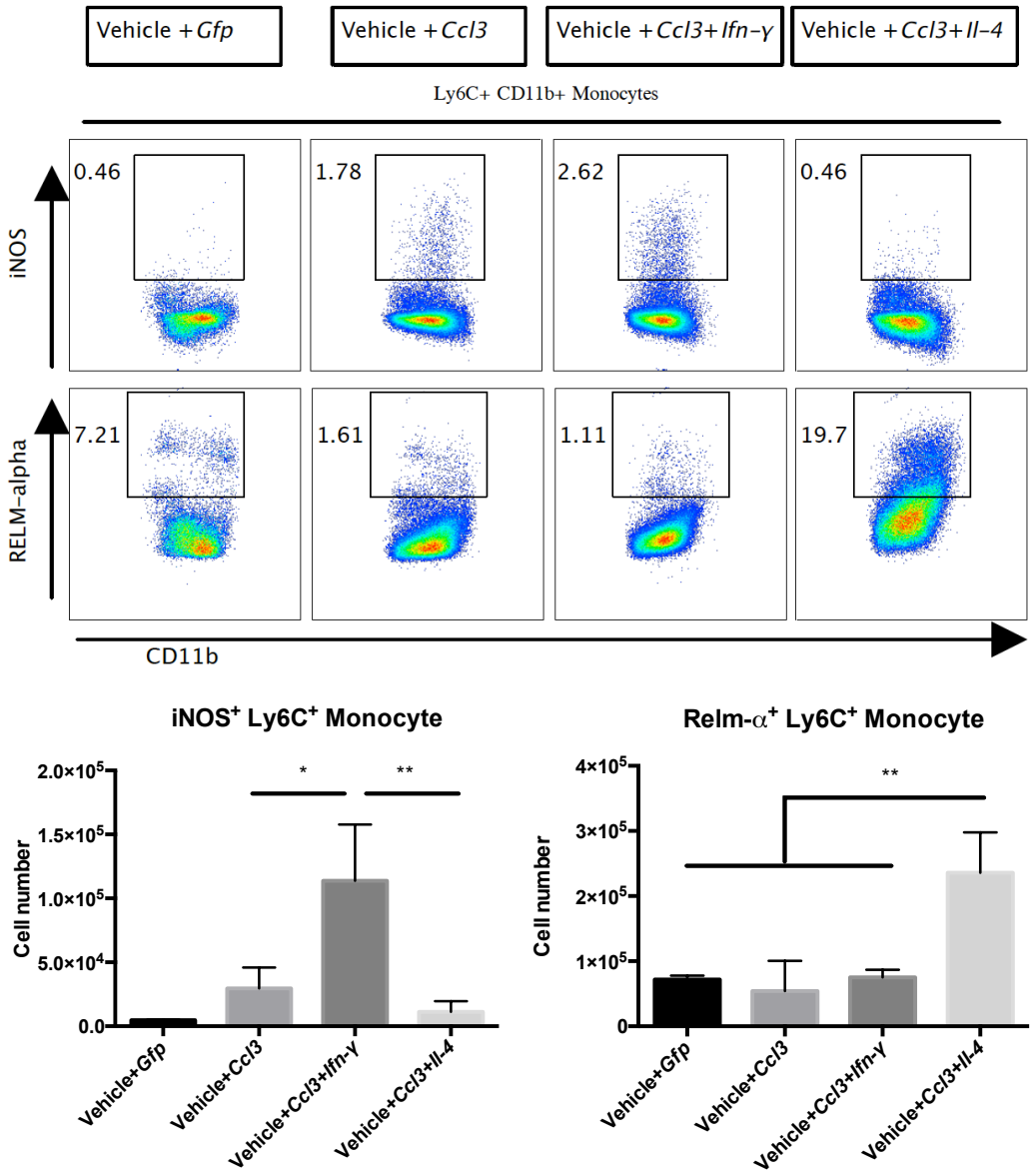

Figure 3.12 mRNA coated with Viromer Red can differentiate monocytes towards different activation status as mRNA-transfected BMDMs do.

A: Representative flow plots showing iNOS and RELM-α expression in recruited monocytes from mice injected with vehicle-coated mRNAs. **B:** Quantification of the cell numbers of iNOS$^+$ and RELM-α$^+$ monocytes from mice injected with vehicle-coated mRNAs. Experiment was repeated two times. Data represent mean ± SD. ns:

p>0.05, **: p < 0.01, One-way ANOVA with Tukey's multiple comparison test.

3.4 Discussion

Synthetic mRNA therapy is a promising therapeutic approach to deliver proteins of interest *in vivo* [1, 2, 6, 7]. It avoids the risk of genomic insertional mutagenesis often associated with DNA-based therapy, and bypasses nuclear delivery for expression [1, 2, 6, 7]. Compared to traditional recombinant protein therapy, synthetic mRNA can maintain expression of desired protein at therapeutic level for a longer time period, which can reduce the required frequency of administration [2, 6]. Moreover, mRNA transfected cells can actively migrate to targeted tissue or organ and provide a localized and intense release of proteins of interest [1, 2, 9]. Indeed, synthetic mRNA therapy has been investigated in preclinical and clinical studies covering several different disease fields [2, 8, 9]. However, these studies mostly used synthetic mRNA to express proteins with direct therapeutic effect or antigens to trigger an antigen specific immune response. The potential of using synthetic mRNA in cell based therapies to recruit cells of interest and modify them locally *in vivo*, is not well studied.

Our findings demonstrated that *Ccl2* and *Ccl3* synthetic mRNA transfected BMDMs were able to recruit a certain population of monocyte in a non-inflammatory manner. Instead of polarizing to either a bactericidal or a tissue-repairing phenotype, these recruited cells stayed in a neutral, or non-programmed state. These recruited monocytes remained inactivated as they migrated, according to their MHC II and iNOS expression, as well as their reactive oxygen production. The addition of either *Ifn-γ* mRNA and *Il-4* mRNA successfully drove these recruited monocytes to different polarization states. Those monocytes recruited by *Ccl3* and *Ifn-γ* mRNA mounted the

most rapid and strongest superoxide burst compared to other mRNA groups (Figure 3.11). Taking together, our data prove the concept of using synthetic mRNA to recruit and modify specific immune cell populations in a targetted and localized manner.

CCL3 is known to recruit neutrophils as well as monocytes/macrophages [26, 42-45]. We observed a neutrophil infiltration both 4h and 16h after injecting recombinant CCL3. BMDMs transfected with *Ccl3* synthetic mRNA recruit neutrophils at 4hr post injection but not at 16hr post injection. Additionally, we observed a robust recruitment of monocytes after giving *Ccl3* transfected BMDMs. The differences between using rCCL3 and *Ccl3* transfected BMDMs could be due to the difference between delivery of a "bolus" of protein versus sustained production of the protein at lower levels in the peritoneum. It is also possible that the BMDMs play an active part in amplifying the inflammation by synthesizing other cytokines besides CCL3.

Several studies have suggested CCL3's ability to activate immune cells [28, 44, 46]. However, we didn't observe a significant change on MHC II or iNOS expression in peritoneal immune cells with *Ccl3* mRNA. One possible explanation for this contradiction is that the studies showing CCL3's activation property were mostly carried *in vitro* [28, 44, 46]. Moreover, *in vivo* evidence supporting CCL3's ability to activate immune cells in a non-inflammatory environment is lacking. The majority of *in vivo* studies with CCL3 involved certain disease models. Our results showed that in a sterile environment, CCL3 only functions as a cell-recruitment chemokine without activating immune cells.

A rich body of literature has demonstrated the efficacy of synthetic mRNA in multiple disease models such as different kinds of cancers [20-23], infectious diseases like tuberculosis or ADIS [15, 18-23], cardiovascular disease [8, 9, 47], asthma [17]. These studies transfected patients' immune cells with mRNA expressing antigens or effective proteins. Transfected cells were then infused back to patients. However, this method requires multiple invasive procedures and a period of time (one week) for *ex vivo* modification. Our findings provide an alternative that can potentially combine these procedures into one single step, by using synthetic mRNA to recruit specific immune cell populations and modify them locally with one single dose of mRNAs. Our study can have a great impact on a variety of immunotherapies delivering *ex vivo* modified autologous cells by providing a simpler and more efficient avenue.

3.5 Reference

1. Kuhn AN, Beibetaert T, Simon P, Vallazza B, Buck J, Davies BP, et al. mRNA as a versatile tool for exogenous protein expression. Curr Gene Ther. 2012;12(5):347-61. PubMed PMID: 22827224.

2. Sahin U, Kariko K, Tureci O. mRNA-based therapeutics--developing a new class of drugs. Nat Rev Drug Discov. 2014;13(10):759-80. doi: 10.1038/nrd4278. PubMed PMID: 25233993.

3. Kormann MS, Hasenpusch G, Aneja MK, Nica G, Flemmer AW, Herber-Jonat S, et al. Expression of therapeutic proteins after delivery of chemically modified mRNA in mice. Nat Biotechnol. 2011;29(2):154-7. doi: 10.1038/nbt.1733. PubMed PMID: 21217696.

4. Anderson BR, Muramatsu H, Jha BK, Silverman RH, Weissman D, Kariko K. Nucleoside modifications in RNA limit activation of 2'-5'-oligoadenylate synthetase and increase resistance to cleavage by RNase L. Nucleic Acids Res. 2011;39(21):9329-38. doi: 10.1093/nar/gkr586. PubMed PMID: 21813458; PubMed Central PMCID: PMCPMC3241635.

5. Andries O, Mc Cafferty S, De Smedt SC, Weiss R, Sanders NN, Kitada T. N(1)-methylpseudouridine-incorporated mRNA outperforms pseudouridine-incorporated mRNA by providing enhanced protein expression and reduced immunogenicity in mammalian cell lines and mice. J Control Release. 2015;217:337-44. doi: 10.1016/j.jconrel.2015.08.051. PubMed PMID: 26342664.

6. Schlake T, Thess A, Fotin-Mleczek M, Kallen KJ. Developing mRNA-vaccine

technologies. RNA Biol. 2012;9(11):1319-30. doi: 10.4161/rna.22269. PubMed PMID: 23064118; PubMed Central PMCID: PMCPMC3597572.

7. Kirschman JL, Bhosle S, Vanover D, Blanchard EL, Loomis KH, Zurla C, et al. Characterizing exogenous mRNA delivery, trafficking, cytoplasmic release and RNA-protein correlations at the level of single cells. Nucleic Acids Res. 2017. doi: 10.1093/nar/gkx290. PubMed PMID: 28449134.

8. Hadas Y, Katz MG, Bridges CR, Zangi L. Modified mRNA as a therapeutic tool to induce cardiac regeneration in ischemic heart disease. Wiley Interdiscip Rev Syst Biol Med. 2017;9(1). doi: 10.1002/wsbm.1367. PubMed PMID: 27911047.

9. Chien KR, Zangi L, Lui KO. Synthetic chemically modified mRNA (modRNA): toward a new technology platform for cardiovascular biology and medicine. Cold Spring Harb Perspect Med. 2014;5(1):a014035. doi: 10.1101/cshperspect.a014035. PubMed PMID: 25301935; PubMed Central PMCID: PMCPMC4292072.

10. Zhou WZ, Hoon DS, Huang SK, Fujii S, Hashimoto K, Morishita R, et al. RNA melanoma vaccine: induction of antitumor immunity by human glycoprotein 100 mRNA immunization. Hum Gene Ther. 1999;10(16):2719-24. doi: 10.1089/10430349950016762. PubMed PMID: 10566900.

11. Fotin-Mleczek M, Duchardt KM, Lorenz C, Pfeiffer R, Ojkic-Zrna S, Probst J, et al. Messenger RNA-based vaccines with dual activity induce balanced TLR-7 dependent adaptive immune responses and provide antitumor activity. J Immunother. 2011;34(1):1-15. doi: 10.1097/CJI.0b013e3181f7dbe8. PubMed PMID: 21150709.

12. Yoon SH, Lee JM, Cho HI, Kim EK, Kim HS, Park MY, et al. Adoptive

immunotherapy using human peripheral blood lymphocytes transferred with RNA encoding Her-2/neu-specific chimeric immune receptor in ovarian cancer xenograft model. Cancer Gene Ther. 2009;16(6):489-97. doi: 10.1038/cgt.2008.98. PubMed PMID: 19096447.

13. Barrett DM, Zhao Y, Liu X, Jiang S, Carpenito C, Kalos M, et al. Treatment of advanced leukemia in mice with mRNA engineered T cells. Hum Gene Ther. 2011;22(12):1575-86. doi: 10.1089/hum.2011.070. PubMed PMID: 21838572; PubMed Central PMCID: PMCPMC3237694.

14. Martinon F, Krishnan S, Lenzen G, Magne R, Gomard E, Guillet JG, et al. Induction of virus-specific cytotoxic T lymphocytes in vivo by liposome-entrapped mRNA. Eur J Immunol. 1993;23(7):1719-22. doi: 10.1002/eji.1830230749. PubMed PMID: 8325342.

15. Lorenzi JC, Trombone AP, Rocha CD, Almeida LP, Lousada RL, Malardo T, et al. Intranasal vaccination with messenger RNA as a new approach in gene therapy: use against tuberculosis. BMC Biotechnol. 2010;10:77. doi: 10.1186/1472-6750-10-77. PubMed PMID: 20961459; PubMed Central PMCID: PMCPMC2972232.

16. Creusot RJ, Chang P, Healey DG, Tcherepanova IY, Nicolette CA, Fathman CG. A short pulse of IL-4 delivered by DCs electroporated with modified mRNA can both prevent and treat autoimmune diabetes in NOD mice. Mol Ther. 2010;18(12):2112-20. doi: 10.1038/mt.2010.146. PubMed PMID: 20628358; PubMed Central PMCID: PMCPMC2997578.

17. Mays LE, Ammon-Treiber S, Mothes B, Alkhaled M, Rottenberger J, Muller-Hermelink ES, et al. Modified Foxp3 mRNA protects against asthma through an IL-

10-dependent mechanism. J Clin Invest. 2013;123(3):1216-28. doi: 10.1172/JCI65351. PubMed PMID: 23391720; PubMed Central PMCID: PMCPMC3582134.

18. Allard SD, De Keersmaecker B, de Goede AL, Verschuren EJ, Koetsveld J, Reedijk ML, et al. A phase I/IIa immunotherapy trial of HIV-1-infected patients with Tat, Rev and Nef expressing dendritic cells followed by treatment interruption. Clin Immunol. 2012;142(3):252-68. doi: 10.1016/j.clim.2011.10.010. PubMed PMID: 22177848.

19. Van Gulck E, Vlieghe E, Vekemans M, Van Tendeloo VF, Van De Velde A, Smits E, et al. mRNA-based dendritic cell vaccination induces potent antiviral T-cell responses in HIV-1-infected patients. AIDS. 2012;26(4):F1-12. doi: 10.1097/QAD.0b013e32834f33e8. PubMed PMID: 22156965.

20. Heiser A, Coleman D, Dannull J, Yancey D, Maurice MA, Lallas CD, et al. Autologous dendritic cells transfected with prostate-specific antigen RNA stimulate CTL responses against metastatic prostate tumors. J Clin Invest. 2002;109(3):409-17. doi: 10.1172/JCI14364. PubMed PMID: 11828001; PubMed Central PMCID: PMCPMC150859.

21. Su Z, Dannull J, Yang BK, Dahm P, Coleman D, Yancey D, et al. Telomerase mRNA-transfected dendritic cells stimulate antigen-specific CD8+ and CD4+ T cell responses in patients with metastatic prostate cancer. J Immunol. 2005;174(6):3798-807. PubMed PMID: 15749921.

22. Morse MA, Nair SK, Boczkowski D, Tyler D, Hurwitz HI, Proia A, et al. The feasibility and safety of immunotherapy with dendritic cells loaded with CEA mRNA

following neoadjuvant chemoradiotherapy and resection of pancreatic cancer. Int J Gastrointest Cancer. 2002;32(1):1-6. doi: 10.1385/IJGC:32:1:1. PubMed PMID: 12630764.

23. Morse MA, Nair SK, Mosca PJ, Hobeika AC, Clay TM, Deng Y, et al. Immunotherapy with autologous, human dendritic cells transfected with carcinoembryonic antigen mRNA. Cancer Invest. 2003;21(3):341-9. PubMed PMID: 12901279.

24. Yoshimura T. The production of monocyte chemoattractant protein-1 (MCP-1)/CCL2 in tumor microenvironments. Cytokine. 2017. doi: 10.1016/j.cyto.2017.02.001. PubMed PMID: 28189389.

25. Yoshimura T, Robinson EA, Tanaka S, Appella E, Kuratsu J, Leonard EJ. Purification and amino acid analysis of two human glioma-derived monocyte chemoattractants. J Exp Med. 1989;169(4):1449-59. PubMed PMID: 2926329; PubMed Central PMCID: PMCPMC2189237.

26. Maurer M, von Stebut E. Macrophage inflammatory protein-1. Int J Biochem Cell Biol. 2004;36(10):1882-6. doi: 10.1016/j.biocel.2003.10.019. PubMed PMID: 15203102.

27. Shi C, Pamer EG. Monocyte recruitment during infection and inflammation. Nat Rev Immunol. 2011;11(11):762-74. doi: 10.1038/nri3070. PubMed PMID: 21984070; PubMed Central PMCID: PMCPMC3947780.

28. Wolpe SD, Davatelis G, Sherry B, Beutler B, Hesse DG, Nguyen HT, et al. Macrophages secrete a novel heparin-binding protein with inflammatory and neutrophil chemokinetic properties. J Exp Med. 1988;167(2):570-81. PubMed PMID:

3279154; PubMed Central PMCID: PMCPMC2188834.

29. Barth MW, Hendrzak JA, Melnicoff MJ, Morahan PS. Review of the macrophage disappearance reaction. J Leukoc Biol. 1995;57(3):361-7. PubMed PMID: 7884305.

30. Shannon BT, Love SH. Additional evidence for the role of hyaluronic acid in the macrophage disappearance reaction. Immunol Commun. 1980;9(8):735-46. PubMed PMID: 7016740.

31. Tomazic V, Bigazzi PE, Rose NR. The macrophage disappearance reaction (mdr) as an in vivo test of delayed hypersensitivity in mice. Immunol Commun. 1977;6(1):49-62. PubMed PMID: 324893.

32. Ramos CD, Canetti C, Souto JT, Silva JS, Hogaboam CM, Ferreira SH, et al. MIP-1alpha[CCL3] acting on the CCR1 receptor mediates neutrophil migration in immune inflammation via sequential release of TNF-alpha and LTB4. J Leukoc Biol. 2005;78(1):167-77. doi: 10.1189/jlb.0404237. PubMed PMID: 15831559.

33. Bouma G, Nikolic T, Coppens JM, van Helden-Meeuwsen CG, Leenen PJ, Drexhage HA, et al. NOD mice have a severely impaired ability to recruit leukocytes into sites of inflammation. Eur J Immunol. 2005;35(1):225-35. doi: 10.1002/eji.200425513. PubMed PMID: 15593124.

34. Serbina NV, Jia T, Hohl TM, Pamer EG. Monocyte-mediated defense against microbial pathogens. Annu Rev Immunol. 2008;26:421-52. doi: 10.1146/annurev.immunol.26.021607.090326. PubMed PMID: 18303997; PubMed Central PMCID: PMCPMC2921669.

35. Xiong H, Pamer EG. Monocytes and infection: modulator, messenger and

effector. Immunobiology. 2015;220(2):210-4. doi: 10.1016/j.imbio.2014.08.007. PubMed PMID: 25214476; PubMed Central PMCID: PMCPMC4404758.

36. Mantovani A, Sica A, Sozzani S, Allavena P, Vecchi A, Locati M. The chemokine system in diverse forms of macrophage activation and polarization. Trends Immunol. 2004;25(12):677-86. doi: 10.1016/j.it.2004.09.015. PubMed PMID: 15530839.

37. Zhou D, Huang C, Lin Z, Zhan S, Kong L, Fang C, et al. Macrophage polarization and function with emphasis on the evolving roles of coordinated regulation of cellular signaling pathways. Cell Signal. 2014;26(2):192-7. doi: 10.1016/j.cellsig.2013.11.004. PubMed PMID: 24219909.

38. Striz I, Brabcova E, Kolesar L, Sekerkova A. Cytokine networking of innate immunity cells: a potential target of therapy. Clin Sci (Lond). 2014;126(9):593-612. doi: 10.1042/CS20130497. PubMed PMID: 24450743.

39. Rhee I. Diverse macrophages polarization in tumor microenvironment. Arch Pharm Res. 2016;39(11):1588-96. doi: 10.1007/s12272-016-0820-y. PubMed PMID: 27562774.

40. Cassetta L, Cassol E, Poli G. Macrophage polarization in health and disease. ScientificWorldJournal. 2011;11:2391-402. doi: 10.1100/2011/213962. PubMed PMID: 22194670; PubMed Central PMCID: PMCPMC3236674.

41. VanderVen BC, Yates RM, Russell DG. Intraphagosomal measurement of the magnitude and duration of the oxidative burst. Traffic. 2009;10(4):372-8. doi: 10.1111/j.1600-0854.2009.00877.x. PubMed PMID: 19183302; PubMed Central PMCID: PMCPMC2736473.

42. Xue ML, Thakur A, Cole N, Lloyd A, Stapleton F, Wakefield D, et al. A critical role for CCL2 and CCL3 chemokines in the regulation of polymorphonuclear neutrophils recruitment during corneal infection in mice. Immunol Cell Biol. 2007;85(7):525-31. doi: 10.1038/sj.icb.7100082. PubMed PMID: 17579602.

43. Bonville CA, Percopo CM, Dyer KD, Gao J, Prussin C, Foster B, et al. Interferon-gamma coordinates CCL3-mediated neutrophil recruitment in vivo. BMC Immunol. 2009;10:14. doi: 10.1186/1471-2172-10-14. PubMed PMID: 19298652; PubMed Central PMCID: PMCPMC2662797.

44. Fahey TJ, 3rd, Tracey KJ, Tekamp-Olson P, Cousens LS, Jones WG, Shires GT, et al. Macrophage inflammatory protein 1 modulates macrophage function. J Immunol. 1992;148(9):2764-9. PubMed PMID: 1573267.

45. Terpos E, Politou M, Viniou N, Rahemtulla A. Significance of macrophage inflammatory protein-1 alpha (MIP-1alpha) in multiple myeloma. Leuk Lymphoma. 2005;46(12):1699-707. doi: 10.1080/10428190500175049. PubMed PMID: 16263571.

46. Takahashi H, Tashiro T, Miyazaki M, Kobayashi M, Pollard RB, Suzuki F. An essential role of macrophage inflammatory protein 1alpha/CCL3 on the expression of host's innate immunities against infectious complications. J Leukoc Biol. 2002;72(6):1190-7. PubMed PMID: 12488501.

47. Yang R, Ogasawara AK, Zioncheck TF, Ren Z, He GW, DeGuzman GG, et al. Exaggerated hypotensive effect of vascular endothelial growth factor in spontaneously hypertensive rats. Hypertension. 2002;39(3):815-20. PubMed PMID: 11897770.

Chapter 4

Concluding Remarks

Mycobacterium tuberculosis (Mtb) continues to be the leading cause of death from a single infectious agent worldwide, leading to 1.8 million deaths in 2015. The long treatment required (6-9 months), with all of its incumbent problems, can promote the emergence of multidrug-resistant (MDR) TB strains, so strategies to shorten the treatment duration are in dire need. Mtb's success as a pathogen hinges on its ability to modulate the host tissue, characterized by extracellular matrix (ECM) remodeling and leaky vascularization. The matrix metalloproteinase (MMP) enzymes are the major drivers to this remodeling process thanks to their ability to degrade ECM such as collagen, elastin, fibronectin and proteoglycans[1-3]. Increased level of MMP-2 and MMP-9 were found in human TB granuloma and murine infected lesion. Disruption of MMP up-regulation may deter Mtb progression. However, studies using MMP inhibitors to perturb Mtb infection *in vivo* have generated conflicting data. Thus, it is of value to further study the impact of MMP inhibition on disease progression and on granuloma architecture. In Chapter 2, we reported that inhibition of matrix metalloproteinases (MMPs) significantly enhances the potency of frontline TB antibiotics in a murine infection model. Inhibition of MMP activity is demonstrated by increased level of collagen and mannose binding lectin (MBL), both of which are subjected to MMP cleavage. MMP inhibition increases pericyte coverage in the normal surrounding area of the lung, therefore improving relative proportion of healthy blood vessels versus leaky dysfunctional vessels. This improvement of healthy

blood vessels enhances delivery and/or retention of frontline TB drugs such as INH and RIF. Our findings highlight the potential of targeting Mtb-induced host tissue remodeling to enhance the efficacy of current frontline antibiotics. It also suggests an alternative therapeutic strategy to repair the leaky blood vessels in TB granulomas to enhance drug delivery. Repurposing of MMP inhibitors may hold the key to shortening TB treatments and combating the emergence of MDR strains.

To develop potential treatment strategies, we explored a novel method to modulate host immune environment using synthetic mRNA. Synthetic mRNA for gene therapy poses very little risk of genomic insertional mutagenesis because of its non-replicative nature [4, 5]. Recent advances to enhance synthetic mRNA stability enable prolonged production of target proteins for a few days [4, 5]. Preclinical and clinical studies using synthetic mRNA have demonstrated its potentials in various disease treatments. However, these studies focused on expressing proteins that recognized and eliminated malignant targets (virus, microbe or cancer cells) [6-10], or antigens that can trigger an antigen-specific immune attack [11-17]. Moreover, current cell-based gene therapies require multiple steps of retrieving patients' immune cells and modifying them *ex vivo*. A cocktail of synthetic mRNAs expressing both cytokines/chemokines and stimulating signals (antigens or activation signals) may potentially reduce these steps into one. Therefore, it is of value to investigate synthetic mRNA's ability to recruit and modify specific immune cell populations *in vivo*. In Chapter 3, we used synthetic mRNA encoding CCL2 or CCL3, to recruit and modulate host immune cells *in vivo*. CCL2 and CCL3 are known for their ability to recruit a variety of immune cells including

monocyte, memory T cells, neutrophils and natural killer (NK) cells in different disease models [18-22]. We found that our synthetic mRNA recruited a population of monocytes, which stayed in a neutral, non-programmed state, without adopting either a bactericidal or tissue-repairing phenotype. These recruited monocytes were not activated based on their expression of activation markers, iNOS expression and reactive oxygen production. Additional mRNAs encoding IFN-γ and IL-4 drove these recruited monocytes to different polarization states. Combination of *Ccl3* and *Ifn-γ* mRNA activated the recruited monocytes and the resident macrophages, allowing them to launch a faster and stronger superoxide burst. Whilst the combination of *ccl3* and *il-4* mRNA drove the recruited monocytes and the resident macrophages to a tissue-repairing phenotype. Collectively, our findings showed that synthetic mRNA enables recruitment and modification of specific immune cell populations *in vivo*, which may benefit a variety of immunotherapies.

While the findings of both studies have great potential, the results need to be viewed as preliminary. Our findings need to be further validated in other animal models and clinical trials before they can be translated into therapies. Regarding our findings of using MMP inhibitors to enhance frontline TB drug efficacy, future work can investigate the drug distribution in different regions of the lung after MMP inhibition. Accessibility of TB drugs to the bacteria within the granuloma is usually limited due to reduced blood vessels inside the granuloma. It would be very informative to learn if drugs were able to penetrate in the granuloma-like structure or stay in the normal surrounding tissue. Laser microscopy dissection can be used to obtain tissue from

different regions of the infected lung and perform mass spectrometry. Moreover, future work can investigate the mechanism of the synergistic effect with more details. For example, how MMP inhibition increases pericyte coverage. One possible theory is MMP inhibitors limit degradation of collagen IV, which is an important component of blood vessel. Uneven collagen IV coverage will result in pericyte detachment and blood vessel leakage [23]. Western blot and immunohistochemistry can be utilized to quantify collagen IV around blood vessels. Mice with conditional knockout of collagen IV and complement of exogenous collagen IV in these mice, can be used to study whether collagen IV is essential in this synergistic effect. For our findings of using synthetic mRNA to modulate immune environment, future work can investigate changes of lymphocyte populations in the peritoneum when different synthetic mRNAs are injected.

In summary, this dissertation presents two methods to modulate host immune environment, in order to develop new treatment strategies against Mtb infection. Our findings of using MMP inhibitors to improve TB drug efficacy demonstrated that modulating important host environmental factors such as blood vessel growth and extracellular matrix deposition, can be an alternative therapeutic strategy for TB treatment. On the other hand, our findings of using synthetic mRNA to recruit and modify host immune cell populations demonstrated that modulating immune cell populations with synthetic mRNA may serve as an efficient therapeutic strategy for a variety of diseases. These two studies showed the potential of modulating host cellular or environmental components to develop novel therapeutic strategies for tuberculosis.

Reference:

1. Salgame P. MMPs in tuberculosis: granuloma creators and tissue destroyers. J Clin Invest. 2011;121(5):1686-8. doi: 10.1172/JCI57423. PubMed PMID: 21519148; PubMed Central PMCID: PMCPMC3083780.

2. Taylor JL, Hattle JM, Dreitz SA, Troudt JM, Izzo LS, Basaraba RJ, et al. Role for matrix metalloproteinase 9 in granuloma formation during pulmonary Mycobacterium tuberculosis infection. Infect Immun. 2006;74(11):6135-44. doi: 10.1128/IAI.02048-05. PubMed PMID: 16982845; PubMed Central PMCID: PMCPMC1695484.

3. Ong CW, Elkington PT, Friedland JS. Tuberculosis, pulmonary cavitation, and matrix metalloproteinases. Am J Respir Crit Care Med. 2014;190(1):9-18. doi: 10.1164/rccm.201311-2106PP. PubMed PMID: 24713029; PubMed Central PMCID: PMCPMC4226026.

4. Sahin U, Kariko K, Tureci O. mRNA-based therapeutics--developing a new class of drugs. Nat Rev Drug Discov. 2014;13(10):759-80. doi: 10.1038/nrd4278. PubMed PMID: 25233993.

5. Schlake T, Thess A, Fotin-Mleczek M, Kallen KJ. Developing mRNA-vaccine technologies. RNA Biol. 2012;9(11):1319-30. doi: 10.4161/rna.22269. PubMed PMID: 23064118; PubMed Central PMCID: PMCPMC3597572.

6. Yoon SH, Lee JM, Cho HI, Kim EK, Kim HS, Park MY, et al. Adoptive immunotherapy using human peripheral blood lymphocytes transferred with RNA encoding Her-2/neu-specific chimeric immune receptor in ovarian cancer xenograft

model. Cancer Gene Ther. 2009;16(6):489-97. doi: 10.1038/cgt.2008.98. PubMed PMID: 19096447.

7. Mays LE, Ammon-Treiber S, Mothes B, Alkhaled M, Rottenberger J, Muller-Hermelink ES, et al. Modified Foxp3 mRNA protects against asthma through an IL-10-dependent mechanism. J Clin Invest. 2013;123(3):1216-28. doi: 10.1172/JCI65351. PubMed PMID: 23391720; PubMed Central PMCID: PMCPMC3582134.

8. Creusot RJ, Chang P, Healey DG, Tcherepanova IY, Nicolette CA, Fathman CG. A short pulse of IL-4 delivered by DCs electroporated with modified mRNA can both prevent and treat autoimmune diabetes in NOD mice. Mol Ther. 2010;18(12):2112-20. doi: 10.1038/mt.2010.146. PubMed PMID: 20628358; PubMed Central PMCID: PMCPMC2997578.

9. Su Z, Dannull J, Yang BK, Dahm P, Coleman D, Yancey D, et al. Telomerase mRNA-transfected dendritic cells stimulate antigen-specific CD8+ and CD4+ T cell responses in patients with metastatic prostate cancer. J Immunol. 2005;174(6):3798-807. PubMed PMID: 15749921.

10. Barrett DM, Zhao Y, Liu X, Jiang S, Carpenito C, Kalos M, et al. Treatment of advanced leukemia in mice with mRNA engineered T cells. Hum Gene Ther. 2011;22(12):1575-86. doi: 10.1089/hum.2011.070. PubMed PMID: 21838572; PubMed Central PMCID: PMCPMC3237694.

11. Heiser A, Coleman D, Dannull J, Yancey D, Maurice MA, Lallas CD, et al. Autologous dendritic cells transfected with prostate-specific antigen RNA stimulate CTL responses against metastatic prostate tumors. J Clin Invest. 2002;109(3):409-17.

doi: 10.1172/JCI14364. PubMed PMID: 11828001; PubMed Central PMCID: PMCPMC150859.

12. Morse MA, Nair SK, Boczkowski D, Tyler D, Hurwitz HI, Proia A, et al. The feasibility and safety of immunotherapy with dendritic cells loaded with CEA mRNA following neoadjuvant chemoradiotherapy and resection of pancreatic cancer. Int J Gastrointest Cancer. 2002;32(1):1-6. doi: 10.1385/IJGC:32:1:1. PubMed PMID: 12630764.

13. Morse MA, Nair SK, Mosca PJ, Hobeika AC, Clay TM, Deng Y, et al. Immunotherapy with autologous, human dendritic cells transfected with carcinoembryonic antigen mRNA. Cancer Invest. 2003;21(3):341-9. PubMed PMID: 12901279.

14. Martinon F, Krishnan S, Lenzen G, Magne R, Gomard E, Guillet JG, et al. Induction of virus-specific cytotoxic T lymphocytes in vivo by liposome-entrapped mRNA. Eur J Immunol. 1993;23(7):1719-22. doi: 10.1002/eji.1830230749. PubMed PMID: 8325342.

15. Lorenzi JC, Trombone AP, Rocha CD, Almeida LP, Lousada RL, Malardo T, et al. Intranasal vaccination with messenger RNA as a new approach in gene therapy: use against tuberculosis. BMC Biotechnol. 2010;10:77. doi: 10.1186/1472-6750-10-77. PubMed PMID: 20961459; PubMed Central PMCID: PMCPMC2972232.

16. Fotin-Mleczek M, Duchardt KM, Lorenz C, Pfeiffer R, Ojkic-Zrna S, Probst J, et al. Messenger RNA-based vaccines with dual activity induce balanced TLR-7 dependent adaptive immune responses and provide antitumor activity. J Immunother. 2011;34(1):1-15. doi: 10.1097/CJI.0b013e3181f7dbe8. PubMed PMID: 21150709.

17. Zhou WZ, Hoon DS, Huang SK, Fujii S, Hashimoto K, Morishita R, et al. RNA melanoma vaccine: induction of antitumor immunity by human glycoprotein 100 mRNA immunization. Hum Gene Ther. 1999;10(16):2719-24. doi: 10.1089/10430349950016762. PubMed PMID: 10566900.

18. Yoshimura T. The production of monocyte chemoattractant protein-1 (MCP-1)/CCL2 in tumor microenvironments. Cytokine. 2017. doi: 10.1016/j.cyto.2017.02.001. PubMed PMID: 28189389.

19. Yoshimura T, Robinson EA, Tanaka S, Appella E, Kuratsu J, Leonard EJ. Purification and amino acid analysis of two human glioma-derived monocyte chemoattractants. J Exp Med. 1989;169(4):1449-59. PubMed PMID: 2926329; PubMed Central PMCID: PMCPMC2189237.

20. Maurer M, von Stebut E. Macrophage inflammatory protein-1. Int J Biochem Cell Biol. 2004;36(10):1882-6. doi: 10.1016/j.biocel.2003.10.019. PubMed PMID: 15203102.

21. Shi C, Pamer EG. Monocyte recruitment during infection and inflammation. Nat Rev Immunol. 2011;11(11):762-74. doi: 10.1038/nri3070. PubMed PMID: 21984070; PubMed Central PMCID: PMCPMC3947780.

22. Wolpe SD, Davatelis G, Sherry B, Beutler B, Hesse DG, Nguyen HT, et al. Macrophages secrete a novel heparin-binding protein with inflammatory and neutrophil chemokinetic properties. J Exp Med. 1988;167(2):570-81. PubMed PMID: 3279154; PubMed Central PMCID: PMCPMC2188834.

23. Baluk P, Hashizume H, McDonald DM. Cellular abnormalities of blood vessels as targets in cancer. Curr Opin Genet Dev. 2005;15(1):102-11. Epub

2005/01/22. doi: 10.1016/j.gde.2004.12.005. PubMed PMID: 15661540.

Appendix

1. Marimastat treatment associated with higher bacterial stress

To assess the effect of treatment on bacterial stress, we used the HspX Erdman Mtb strain (*hspX*'::GFP, *smyc*'::mCherry) to evaluate the stress level of bacteria, which is constitutively labeled with mCherry fluorescence and turns on GFP expression when sensing hypoxia and nitric oxide (NO) stress through the *hspX* promoter [1]. The mice were infected with the HspX Erdman strain at Day 0, treated with marimastat at Day 5 and INH at Day 10, and euthanized at Day 16. After fixation at 4% PFA overnight, lung sections were cut and stained for DAPI and phalloidin and then imaged by confocal microscopy. In all different treatment group, we observed GFP expressing bacteria (Figure 5.1A). GFP signal indicating hypoxia and NO stress in each cell was quantified and normalized to the size of the bacteria indicated by their mCherry signal. We found that, however, with or without INH treatment, the HspX bacteria were expressing higher level of GFP when mice were treated with marimastat (Figures 5.1B). This suggests that the bacteria were experiencing higher level of stress when marimastat was present during mice infection.

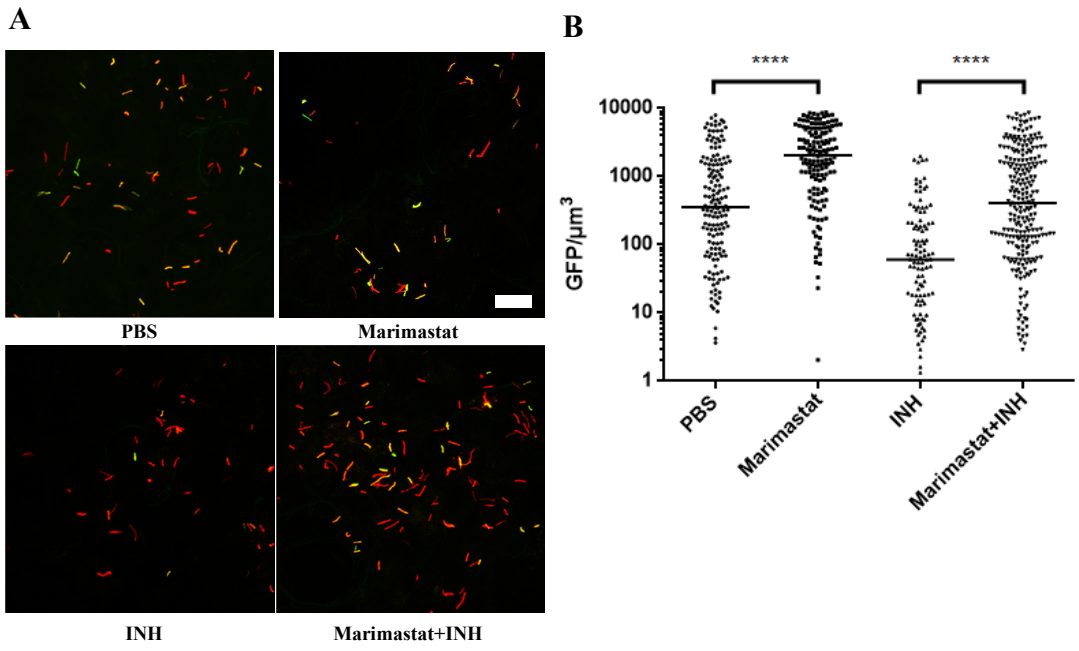

Figure 5.1 Mtb experienced higher level of stress in the lung of infected mice treated with marimastat.

A: HspX reporter bacteria in lung sections from infected mice under different treatments. Scale bar: 20µm. **B**: Quantification of GFP signal (normalized by bacteria volume) of HspX bacteria from A. Data represent median. ****: $p < 0.0001$, Mann-Whitney nonparametric test.

2. MBL has minimal effect on synergy of Marimastat and INH *in vivo*.

To validate the hypothesis that MBL contributes to the synergetic killing, we infected MBL knockout mice (B6129S4MBL1^{kata}MBL2^{kata}) with Mtb bacteria and provided the same drug treatment regime as we did to the C57BL/6J mice[2-4]. The bacterial burden in the PBS groups, Marimastat groups and INH groups of C57BL/6J and MBL knockout mice were comparable (Figure 5.2). MBL knockout mice under combined treatment of marimastat and INH have more bacterial burden compared to that of the INH only group. However, the effect seems to be somewhat modest—MBL in C57BL/6J mice increased INH killing of Mtb by about 20% killing compared with the MBL knockout mice. It is possible that the MBL knockout mice might have developed compensatory mechanisms, which is common in constitutive knockout models. However, bacterial burden in the Marimastat+INH group is still lower than the INH only group in the MBL knockout mice (Figure 5.2), suggesting that MBL does not account for the synergistic effect entirely.

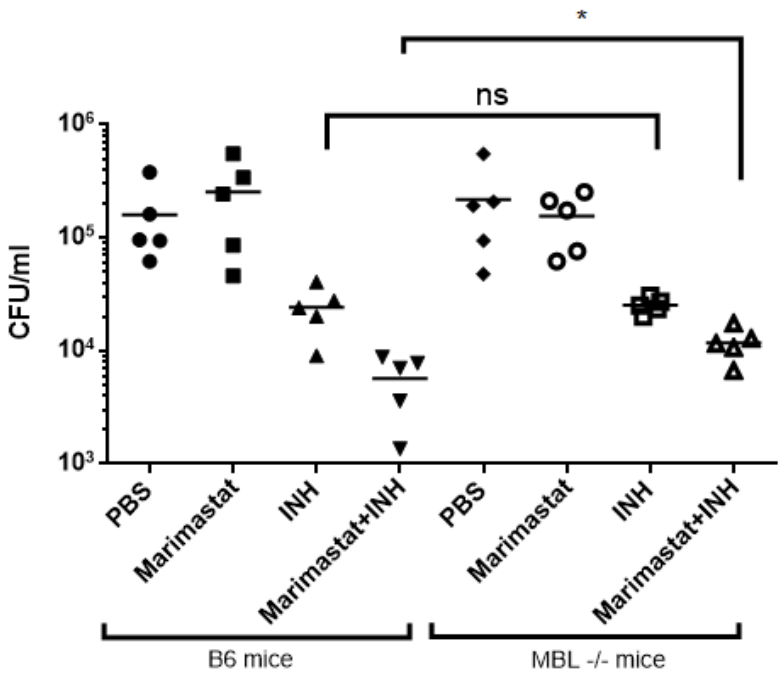

Figure 5.2 CFU count of lung tissue from Mtb-infected B6 mice and MBL knockout mice treated with marimastat and INH. Data represent mean. *: $p < 0.05$, One-way ANOVA with Šidák multiple comparison test.

3. Nanoparticles extravasate from blood vessel into mouse granulomas-like lesions.

Unpublished data from Griffiths's lab showed that nanoparticles (NPs) were able to diffuse out of blood vessel and reach the tissue where Mtb reside in zebrafish infection model. To further investigate whether this observation can be translated in mouse infection model, we injected PEGylated 100nm, far red-labeled liposomes or 173 nm polymeric micelles intravenously into mice infected with *M. tuberculosis*. Animals were sacrificed 24 hours post injection and lung tissues were sectioned for confocal microscopy. Both types of NP accumulated strongly in the consolidated area in the lung (granuloma like structure) enriched with Mtb, while few NP were found in areas without the bacteria (Fig 7A-D). Quantification of the fluorescence signal in different areas confirmed that the amount of Liposomes and polymeric micelles in granuloma like structure was about 20 and 5 times higher, respectively, than that found in normal surrounding tissues of the lung (Fig 7E). These data indicated the NP can actively extravasate out of blood vessels and accumulate around the tissue where the bacteria reside, instead of the normal surrounding tissue without bacteria. Moreover, we found that in the granuloma-like structure, the bacteria accumulate at the center while the fluorescent NP locate only at the peripheral of the structure, indicating the blood vessels did not reach the center of these lesion. This observation is consistent with current opinion of human granuloma structure, that at the late stage of granuloma development, the vasculature collapes at the center of granuloma, rendering the blood supply to the bacteria or the cells.

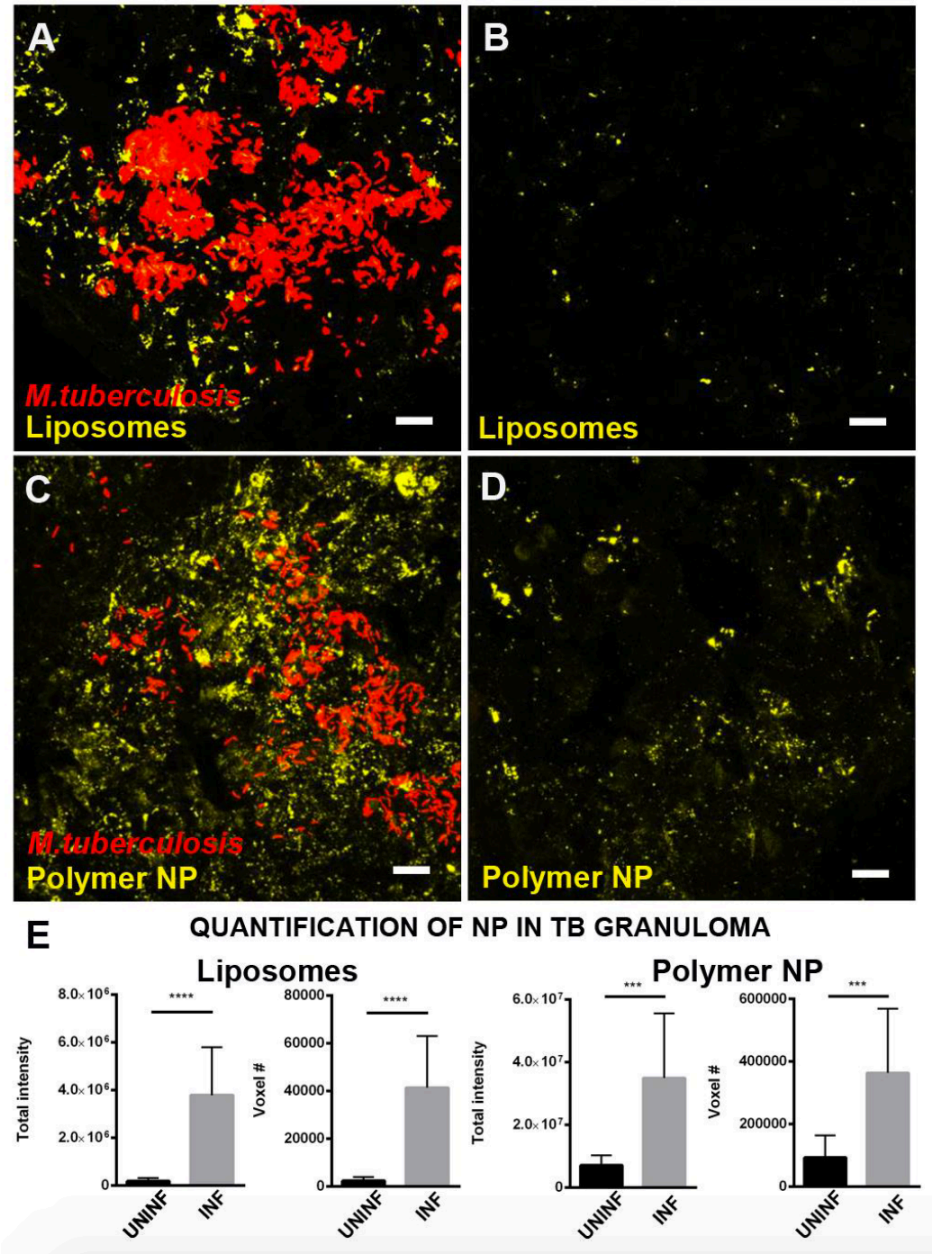

Figure 5.3 Liposomes and polymeric NP accumulate in the consolidated tissue in the lung of Mtb infected mouse.

Accumulation of liposomes **(A and B)** or polymeric NP **(C and D)** in sections of infected lung tissue. A and C are images from sections enriched with Mtb, while B and D are images from normal surrounding area without presence of the bacteria. **(E)**:

quantitation of the total fluorescent intensity and voxel number of the liposomes (left panel) or polymeric nanoparticles (right panel). Data represent mean ± SD. ***: $p < 0.001$, ****: $p < 0.0001$ Unpaired t test with Wench correction.

Reference

1. Sukumar N, Tan S, Aldridge BB, Russell DG. Exploitation of Mycobacterium tuberculosis reporter strains to probe the impact of vaccination at sites of infection. PLoS Pathog. 2014;10(9):e1004394. doi: 10.1371/journal.ppat.1004394. PubMed PMID: 25233380; PubMed Central PMCID: PMCPMC4169503.

2. Moller-Kristensen M, Ip WK, Shi L, Gowda LD, Hamblin MR, Thiel S, et al. Deficiency of mannose-binding lectin greatly increases susceptibility to postburn infection with Pseudomonas aeruginosa. J Immunol. 2006;176(3):1769-75. PubMed PMID: 16424207; PubMed Central PMCID: PMCPMC3071691.

3. Shi L, Takahashi K, Dundee J, Shahroor-Karni S, Thiel S, Jensenius JC, et al. Mannose-binding lectin-deficient mice are susceptible to infection with Staphylococcus aureus. J Exp Med. 2004;199(10):1379-90. doi: 10.1084/jem.20032207. PubMed PMID: 15148336; PubMed Central PMCID: PMCPMC2211809.

4. Ip WK, Takahashi K, Ezekowitz RA, Stuart LM. Mannose-binding lectin and innate immunity. Immunol Rev. 2009;230(1):9-21. doi: 10.1111/j.1600-065X.2009.00789.x. PubMed PMID: 19594626.